

Ministry of Higher Education and Scientific Research
University of Baghdad
College of Education for Pure Science, Ibn Al-Haitham
Department of physics



Structural and Optical Characteristics of PbO/Ag and PbO/Cu Nano-particles

A Thesis Submitted to

The Council of the College of Education for Pure Science, Ibn Al-Haitham
University of Baghdad in a Partial Fulfillment of the Requirements for the
Degree of Master of Education

Presented By:

Mohamed Ahmed Karem

Supervised by

Assist.Prof.Dr.Raghad subhi AL Khafaji

بِسْمِ اللَّهِ الرَّحْمَنِ الرَّحِيمِ

وَقُلْ رَبِّ أَنْزِلْنِي مُنْزَلًا

مُبَارَكًا وَأَنْتَ خَيْرُ الْمُنْزِلِينَ

صَدَقَ اللَّهُ الْعَلِيِّ الْعَظِيمِ

سورة المؤمنون الآية (٢٩)

Supervisor Certification

I certify that this thesis entitled, "Optical and Microstructure Properties a(Ceramic_Metal) Composites NPs" was prepared by Mohamed Ahmed Karem under my supervision at the Physics Department in the College of education for pure science (Ibn Al-Haitham), University of Baghdad as partial requirement for the degree of Master in Physical of Science.

Signature:



Name: Assist. Prof. Dr. Raghad subhi ALkhafaji

Date: 17/9/2018

Recommendation the head of the Department of Physics:

In view of the available recommendations, I forward this thesis for debate by the examination committee.

Signature: S.A. MAKI

Name: Dr. Samir A. Maki

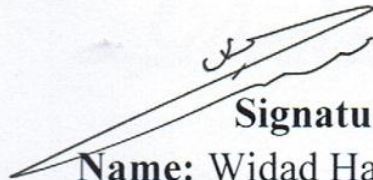
Title: professor

Address: Chairman of the Department of Physics, College of Education for pure science (Ibn Al-Haitham), University of Baghdad.

Date: 17/9/2018

Certification

We certify that we have read this thesis, entitled " **Structural and Optical Characteristics of PbO/Ag and PbO/Cu Nano-particles**" And as examination committee, we examined the student "**Mohamed Ahmed Karem** "on its contents, and that in our opinion it is adequate for the partial fulfillment of requirements for the Degree of Master in science of Physics.



Signature

Name: Widad Hamdi Jassim

Title: Prof. Dr.

(Chairman)

Date: 24/4/ 2019

Signature



Name: Thamir Abdul-Jabbar Jumah

Title: Assist. Prof. Dr.

(Member)

Date: 24/4/ 2019



Signature

Name: Farouq Ibrahim Hussain

Title: Assist. Prof. Dr.

(Member)

Date: 24/4/ 2019



Signature

Name: Raghad Subhi AL-Khafaji

Title: Assist. Prof. Dr.

(Supervisor)

Date: 30/4/ 2019

Signature:



Name: Dr. Hasan Ahmed Hasan

Title: Professor

Address: The Dean of College of Education for Pure Science Ibn Al-Haitham /University of Baghdad.

Date: 5/5/ 2019

DEDICATION

Dedicated To

My Father

My Mother

My wife

My Brothers

And My Sister

For their Kindness,

Attention and encouragement.

Acknowledgments

*Thanks to God "Allah" who helped me to accomplish this work,
which I hope, will serve our community.*

I am grateful to the College of Education for Pure science /(Ibn Al-Haitham) university of Baghdad and special thanks to the head of physics department **Dr.Samir A.Maki** for their help in completing my studies.

I would like to express my deep gratitude and appreciation to my supervisor **Assist. Prof. Dr. Raghad Subhi ALkafaji** for suggesting the topic of the thesis, continuous advice and their guidance throughout this work.

I would like to thank Dr. kazem Abdel ALwahed(Bagdad University College of the Science) was given the Opportunity to work in the laboratory, Dr. Hasan Nasser Hashem(AL-Nahrain University College of the Science)for his help in this study andMr.Hadi Jabbar Majbal(Ibn-ALHaytham College/Physics department).

I would like to thank (Hasan , Mustafa, Mohammed, Badran, Mousa and Maithm)

In the way to the completion of this Thesis, my teachers, colleagues, and all friends contributed in different ways. At this moment, I am very thankful to all of them.

Finally, my special thanks, great appreciation and sincere gratitude goes to my family for all their patience, great efforts and facilities offered to make this thesis possible.

Abstract

A homogenous colloidal composed of PbO/Cu and PbO/Ag were prepared pulsed laser ablation technique (PLAL) ,through a prepare of mixtures of Pb:Cu and Pb:Ag with different concentration (15,20,30,50,75 and 85wt%).The resultants powders were pressed as a pellet of dimensions() used a targets. ND-YAG pulsed laser of wavelength (1064) and pulse duration 6ns at a condition of 300pulses associated with energy 400J.The resultant powders of PbO/Cu and PbO/Ag were subjected to XRD and uv-vis techniques for studying both structural and optical property .TEM and SEM techniques were used for studying the size, shape and morphology of the prepared powders. The absorbance is found increased and take maximum values at the wavelength of (220-230)nm due to surface Plasmon resonance of each colloidal. The absorbance peaks are found tend to red shift near to the infrared region. In addition, the extinction coefficient display and enhanced value with increasing the doping concentration of both Cu and Ag increased too. The energy gap suffer some reduced and reached to (3.291 eV) for 75wt% Cu with PbO and (2.63eV) for 20wt% Ag with PbO.

List of Contents

page	Contents	No.
	Chapter One :Introduction	1
1	Introduction	1.1
3	Nanotechnology	1.2
5	Historical Review	1.3
10	Aims of the Study	1.4
	Chapter Two	
11	Introduction	2.1
11	Nano materials	2.2
13	Classification of Nano materials	2.3
13	Zero-Dimensional (0-D) Nanostructures	2.3.1
13	One-Dimensional (1-D) Nanostructures	2.3.2
13	Two-Dimensional (2-D) Nanostructures	2.3.3
14	Three Dimensions (3-D) System	2.3.4
14	Laser Ablation in Liquid	2.4
16	Mechanisms of Laser Ablation Technique and Nanoparticles Formation	2.5
16	General Considerations of Laser Ablation of Materials	2.5.1
17	Steps of the Formation of NPs by Laser Ablation Technique	2.5.2
20	Mechanisms of Formation NPs in Two Cases of	2.5.3

	Nanosecond	
20	Laser ablation via Nanosecond Laser Irradiation	2.5.4
23	Fundamental Mechanisms of PLAL Technique	2.6
20	General Arrangement of PLAL Technique	2.6.1
20	Mechanisms of PLAL Technique	2.6.2
23	Laser-Assisted Size Control (Fragmentation Process)	2.6.3
23	PLAL Parameters	2.7
25	Laser Parameters	2.7.1
25	Liquids Properties	2.7.2
26	Target Properties	2.7.3
27	Advantages and Disadvantages of PLAL Technique	2.8
29	Characterization of Started Materials	2.9
29	Properties of lead Oxide (PbO) Material	2.9.1
29	Optical Properties of Copper (Cu)	2.9.2
30	Optical Properties of Sliver	2.9.3
30	The optical Properties	2.10
30	Absorbance	2.10.1
31	Transmittance	2.10.2
33	Reflection	2.10.3

33	Absorption Coefficient	2.10.4
34	Optical Energy Gap	2.10.5
34	Extinction Coefficient	2.10.6
35	Refractive Index	2.10.7
35	Indexing X.ray Diffraction	2.11
36	Procedure for Indexing non Cubic XRD Patterns	2.12
39	Quality of Refinement (Reliabilty Factor)	2.13
40	Debye Scherrer formula	2.14
	Chapter Three	
41	Laser Ablation in Solution System	3.1
42	Material Preparations	3.2
42	Preparation of PbCuO Ag NPs	3.2.1
45	Characteristic Of PbOCu\ PbOAg NPs	3.3
45	X-Ray Diffraction Technique	3.3.1
45	Morphological	3.3.2
48	Optical Analysis	3.3.3
49	XRD Characterization of selected materials	3.4
49	XRD of PbO (lead oxide)	3.4.1
50	XRD of Copper(Cu)	3.4.2
51	XRD of Sliver (Ag)	4.3.3
	Chapter Four	
52		4.1

	Introduction	
52	X-ray Diffraction of PbO / Cu and Pb/Ag Nanoparticles	4.2
53	Indexing of X-ray Diffraction Patterns	4.3
61	Morphology of PbO/Cu and PbO/Ag Nanoparticles	4.4
61	Scanning Electron Microscopy (SEM)	4.4.1
67	Transmission Electron Microscopy (TEM)	4.4.2
71	The Optical Properties	4.5
89	Conclusion	4.6
90	Suggestion for Future Works	4.7

List of figures

Figures	page
Figure 2.1 Classification of nanomaterials according to 0-D, 1-D, 2-D, and 3-D.	14
Figure 2.2: A schematic Diagram of Physical Mechanism of the Formation of the NPs, A/Generation Process, b- Transformation Process and c - Condensation Process	19
Figure 2.3: Mechanisms of laser Ablation Techniques in: (a) Nanosecond –Pulsed laser Ablation	22
Figure 2-4: (a) A general Schematic Diagram of the Experiment procedure of PLAL. (b) A Combination of Constituents and Interactions in PLAL	24
Figure (2-5) Beam that is Incident Reflected, Absorbed, and Transmitted	32
Figure (3.1) this flow chart	41
Figure(3.2) Pulsed Laser Depositing (PLD)	43
Figure(.3.3) Images of Prepared Nanoparticles Colloidal for (a)PbOCu and(b) PbOAg	44
Figure(3.4)Schematic of Experiment Setup Applied for the Synthesis of Pbo/Cu and PbO\Ag	45
Figure(3.5) Scanning Electron Microscopy (SEM)	46
Figure(3.6) Translation Electron Microscopy(TEM)	37
Figure (3.7) UV-Visible.	48
Figure(3.8) Show Structure and Peaks of lead oxide	49

Figure(3.9)Show Structure and Peaks of Cupper	50
Figure(3.10) Show Structure and Peaks of Ag	51
Fig.(4. 1) XRD Pattern for Prepared	56
Fig.(4. 2) XRD Pattern for Prepared PbO/Ag Film	56
Fig.(4.3) Riveted Method XRD 85%Ag	59
Fig.(4.4) Riveted Method XRD 85%Cu	60
Fig.4.5 Statistical area distribution of synthesized nanoparticales from SEM	64
Fig4.6 EDX spectrums for pure (a)PbO, (b)Pb/Ag and (c)PbO/Cu.	65
Fig4.7 SEM Images for Prepared PbO , PbO/Cu and PbO/Ag nanoparticles	66
Fig.4.8 Histogram Particle Size Distribution of 85%Ag	69
Fig.4.9 Histogram Particle Size Distribution of 85%Cu	69
Fig.4.10 TEM Images for Prepared Nanoparticles for PbO/85%Cu and PbO/85%Ag nanoparticles.	70
Fig.4.11. Absorption Spectrum of PbOCu Nanoparticles with Different Cu Doped Produced in Aqueous Solution of DI Water	75
Fig.4.12. Absorption spectra of PbOAg Nanoparticles with Different Ag Doped Produced in Aqueous Solution of DI Water	76

Fig.4.13. Extinction Coefficient (k) of PbOCu Nanoparticles with Different Cu Doped in Aqueous Solution of DIW	77
Fig.4.13 Extinction Coefficient (k) of PbOAg Nanoparticles with Different Cu Doped in Aqueous Solution of DIW	78
Fig.4.14. Refractive Index (n) of PbOCu Nanoparticles Colloidal with Different Cu Doped Produced in Aqueous Solution of DIW	79
Fig.4.15. Refractive Index(n) of PbOAg Nanoparticles Colloidal with Different Ag Doped Produced in Aqueous Solution of DI Water	80
Fig.4.16.shows the allowed transition of the direct energy gap of the of 100% pbO	82
Fig.4.17.shows the allowed transition of the direct energy gap of the of 15% Cu	82
Fig.4.18.shows the allowed transition of the direct energy gap of the of 20% Cu	83
Fig.4.19.shows the allowed transition of the direct energy gap of the of 30% Cu	83
Fig.4.20.shows the allowed transition of the direct energy gap of the of 50% Cu	84
Fig.4.21.shows the allowed transition of the direct energy gap of the of 75% Cu	84
Fig.4.22.shows the allowed transition of the direct energy gap of the of 85% Cu	85
Fig.4.23.shows the allowed transition of the direct energy gap of the of 15% Ag	85
Fig.4.24.shows the allowed transition of the direct energy gap of the of 20% Ag	86
Fig.4.25.shows the allowed transition of the direct energy gap of the of 30% Ag	86
Fig.4.26.shows the allowed transition of the direct energy gap of the of 50% Ag	87
Fig.4.27.shows the allowed transition of the direct energy gap of the of 75% Ag	87

Fig.4.28.shows the allowed transition of the direct energy gap of the of 85% Ag

88

List of Symbol and Abbreviation

Symbol	Description
V	Unit Cell Volume
(hkl)	Miller Indices
a and c	Lattice Constants
Θ	Incident Angle of Ray
d(hkl)	Inter Planer Distance (hkl)
λ	Wave Length of XRD
XRD	X_ray Diffraction
CNT	Classical Nucleation Theory
DIW	Deionized Water
DLS	Dynamic Laser Scattering
fs	Femtosecond
PbO	Lead Oxide
Cu	Copper
Ag	Silver
Nd-YAG	Neodymium yttrium Aluminum Garnet
NPs	Nanoparticles
ns	Nanosecond
PLA	Pulsed Laser Ablation
PLAL	Pulsed Laser Ablation in Liquid Media
PLLD	Pulsed _Laser Induced Liquid _Deposition
PRR	Pulse Repetition Rate
ps	Picosecond
SPR	Surface Plasmon Resonance
EDX	Energy Dispersive X_ray
SEM	Scanning Electron Microscope
SHC	Second Harmonic Generation
TEM	Transmission Electron Microscope
TTM	Two Temperature Model
UV-VIS	Ultraviolet_Visible
Eg	Energy Gap
α	Absorption Coefficient
k	Extinction Coefficient
n	Refractive Index

List of Table

Table No.	Table Caption	Page NO.
4.1	Structural parameters for the synthesized thin films PbOCu and PbOAg at different Cu and Ag concentration.	57
4.2	Crystallite Size of thin films PbOCu and PbOAg detected from SEM and TEM techniques	57
4.3	Reliability factor for PbOCu and PbOAg thin films obtained from reitvld	58
4.4	Allowed direct energy gap $E_g(\text{ev})$ for prepared thin films.	81

Chapter one

Introduction

1.1 Introduction:

Nano science defines a set of technologies and developments based on physical, chemical, and biological phenomena that existing at the Nano scale range of approximately (1-100) nanometer [1]. The properties and the behaviors of nanomaterial differ from those with macro or bulk materials [2]. The transition from micro to nano scale in the materials leads to a significant change in their properties. The major change is the increasing in their surface area to volume ratio. Thus large portions of the surface atoms accumulated with ultra-fine size and shape effects resulting in the formation of the nanoparticles that exhibit different properties from those for the bulk nature [3].

In general, there are two approaches used to fabricate Nano materials which named as top-down and bottom-up. In the top-down approach the nanoparticles are etching to smaller structures from larger ones. On the other hand, bottom-up approach refers to the build-up of a material from the bottom: atom-by atom, molecule-by-molecule, or cluster-by-cluster [4].

The most efficient physical methods for the fabrication of nanostructure are the laser ablation, and it is a typical example of the top-down approach in the fabrication of nanoparticles. Laser ablation is the process of ablated material from a solid surface by irradiating it with a laser beam [5].

The laser ablation of a material from the target leads to form Nano clusters that deposition on a substrate yielding a nanostructure film or when the Nano clusters can released into the liquid forming a colloidal nanoparticles solution, Also the difference may occurs between these processes when the plasma begins to expand ,which occurs freely in

vacuum but is confined by liquid layer, the liquid delays the expansions of the plasma leading to high plasma pressure and temperature, which allows to formation of novel materials [6].

The mechanism of laser- ablation of the particles from a target starts when the laser beam irradiates at the interface between the solid and the liquid. Through the liquid, a plasma plume is formed at the interface, and confined by the surrounding liquid during each pulse.

The confined plasma expands adiabatically at a supersonic velocity, creating a shock front that in turn induces an elevated pressure and increase the plasmas temperature. Such a transient pressure in front of the plasma plume impinges the ablated species of metallic ions, atoms and clusters into the confined liquid, and the chemical reactions between the ablated species and the liquid occur, resulting in nucleation of oxides and/or hydroxides, depending on the type of liquid. It is believed that in the case of PLAL the shock wave plays a self-limiting role for the generation of NPs and alters the efficiency of the process [7, 8]. PLAL has been demonstrated that the size of the synthesized material can be controlled by changing the laser parameters including: laser fluencies, wavelength, and pulse laser duration or by changing the type of the surfactant solution. The reason mentioned before in which are parameters effect of the stability and size of the resulted NPs.

Ablation process that used ultra-short laser beam makes it suitable to produce very gentle material removal converting a bulk material into nanoparticles in gases and liquids media without changing its stoichiometry [9].

Moreover, the limited heating effect resulted from the interaction of ultra-short pulses with the matter led to faster cooling of the ablated

particles and prevented their aggregation. The ablation process occurs from both melted and vaped phases, leading to the emission of particulate and liquid micro-droplets[10].

The long lasting material emission and longer pulse duration lead to laser-vapor interaction that limiting the control of the properties of the ablated particles[11]. Scientists believe that nanotechnology will solve a range of challenges facing humanity such as disease, clean water for all, as well as cheap space trips that are not affected by radiation.

The origin of the word "Nano" is derived from the Greek word "Nano", a Greek word meaning dwarf and meant, everything is small and here means the technique of nanoparticles or nanotechnology micro or miniature technology. Nano science is the study of the basic principles of molecules and compounds that are not more than 100 nanometers. Valona is the most accurate metric unit known to date. It is one billionth of a meter, ten times the atomic measurement unit known as angstrom. The nanometer is defined as part of Billionth of a meter, and a fraction of a thousand micrometers. To bring this definition closer to reality, the diameter of the head hair is approximately 75,000 nm, and the red blood cell is up to 2,000 nm. The Nan science is the boundary between the world of atoms and molecules and the world of macro[12] .

1.2. Nano technology

The technological breakthrough was the unique feature of the 20th century, which we called a few years ago. The experts agreed that the most important technological development in the latter half of this century was the invention of silicon or transistor electronics and

electronic laboratories. Their development led to the emergence of solid to a technical revolution in all areas such as communications, computer, medicine and others[13]. Until 1950 there was only white and black television, and there were only ten computers in the world. There were no mobile phones, no digital clocks or the Internet. All these inventions are due to the small segments, whose increased demand has led to lower prices for easy access to all the consumer electronics that surround us today. Over the past few years, a new term has emerged that has put its weight on the world and has become the focus of attention. The term is "nanotechnology."

This promising technique promises a huge deep in all branches of science and engineering, and think it will over shadow all areas of modern medicine, global economy, international relations and even the everyday life of the ordinary person. It will simply enable us to do anything we imagine by lining the molecules of matter together Imagine a supercomputer that can be injected into the blood or ingested to treat blood clots, tumors and incurable diseases[14].

Nanotechnology is a field of applied science and technology covering a wide range of topics. The standardization of the main subject is to control any order of magnitude smaller than the micrometer, as well as manufacturing the same hardware along this schedule table [15]. It is a highly interdisciplinary field, taking advantage of areas such as macromolecular physics and extended physics. There is a lot of speculation about what new science and technology might produce from these research lines. Some people see nanotechnology marketing a term that describes existing research lines applied to a micron-wide sub-scale[16]. Despite the simplicity of what this definition, Nan scale includes various areas of investigation. Nanotechnology permeates many

fields, including the genetics of science, chemistry, biology and applied physics. It can be considered an extension of science on the list, appreciating either the reworking of existing science using the latest or most modern means[17]. There are two main approaches that use nanotechnology: it is the "base" that is the building materials and tools of molecules that combine chemical elements using the principles of molecular recognition; the other "top-to-bottom" that is opposed is a larger Nano-building than sub-atomic entities. The momentum of nano science terms from the new interest of science adding a new generation of analytical tools such as atomic force microscopy and scanning microscopy. Common and duplicate processes such as electron beam and lithography these two instruments are deliberate manipulation, nanostructures and this in turn led to monitoring phenomena. The nano scale also describes the emerging technical developments associated with sub - dimensional microscopy[19]. Despite the great promise of numerous nano scale techniques such as point size and nano metric, real applications that have emerged from the laboratory to the market are mainly using the advantages of nano party colloidal not in most of the form, such as suntan lotion, cosmetics, protective coatings and stain-resistant clothing[20].

1.3. Historical review:

Tabor(1974)[21] made a comparison between polythene that prepared with and without lead oxide fillings in terms of friction, wear and tear. The fillings significantly reduce the corrosion but not the high density polythene friction found under the conditions it is observed that any such reduction in low-density polythene. With high-density

polythene, improved corrosion is limited to high speeds and relatively soft steel facades.

Mustafa Amer Hassan(2012) [22] prepared pure and doped copper oxide thin films by chemical spray pyrolysis. The films were doped with Manganese (Mn) at 2 and 4 wt%. X-ray diffraction pattern shows that all prepared films have two strong peaks located around 35.74° and 38.95° which correspond to the $(\bar{1}11)$ and (111) reflection planes respectively, similar to those for CuO. The absorption coefficient was calculated from the transmission spectra in the range of (450-950) nm, and it was increased with increasing the doping concentration. Similarly, the allowed direct optical band gap energy has been increased with increasing doping concentration.

Khawla S. Khashan(2013) [23] prepared CuO thin films by spray pyrolysis method using different concentration of $\text{CuCl}_2 \cdot 2\text{H}_2\text{O}$. X-ray diffraction (XRD) and UV-VIS transmission spectroscopy were used to characterize the structure and optical properties of the prepared thin films. XRD patterns show that the films are polycrystalline and monoclinic with $(\bar{1}11)$ and (111) crystalline orientations. The optical band gaps are in the range of (2.05 -2.42) eV, with high absorption coefficient change from $(3 \times 10^5 - 1 \times 10^5) \text{ cm}^{-1}$ at 0.3M concentration. Also, the excitation coefficient varied from (0.85 – 0.7). These constants are found to be oscillatory in nature, which are attributed to the particular structure of films and their doping concentrations.

Abdulhadi kadhim AL-Ogaili et al(2015) [24] were characterized silver nanoparticles that synthesized by pulsed (Q-switched, 1064 and 532nm doubled frequency-Nd: YAG) laser ablation using (Q-

switched, 1064 and 532nm doubled frequency-Nd: YAG) system. The silver metal was immersed in double distilled deionized water DDDW, Without any chemical additives, the optical and antibacterial properties have been studied as a function of both the laser energy and the number of pulses. It has been observed that both the laser energy and number of laser pulses have a control over the size of the nanoparticles. Increasing these parameters resulted in a clear blue shift in the absorption peak of the fabricated nanoparticles indicating that the average size of the particles decreases with increasing laser energy and number of pulses. Also, increasing the period of ablation reduces the average size of nanoparticles.

M. A. Al-Hur (2015) [25] prepared CdS and $Cd_{1-x}SCu_x$ thin films by spray pyrolysis method. The optical band gap of pure and doped CdS were varied from 2.34 to 2.45 eV with increase Cu concentration from (0 -0.1). The X-ray diffraction (XRD) analysis revealed that the films were polycrystalline and exhibited two phases cubic and hexagonal structure and the hexagonal phase was increased with increasing Cu concentration.

Azhar A. Hassan (2015) [26] prepared transparent conducting oxides thin films of copper aluminum oxide ($CuAlO_2$) by spray pyrolysis technique onto glass substrates at (500°C). The precursor solution was prepared by mixing $CuCl_2$ and anhydrous $AlCl_3$ salts at different (Cu:Al) ratio (1:1), (1:2), and (2:1). The XRD results show that the pure delafossite phase of $CoAlO_2$ was dominate at the ratio (1:1). The UV-visible spectrum shows the highest absorption coefficient value in the visible region for the film prepared with (1:1) ratio. The optical allowed direct and indirect band gap of the prepared thin films at (1:1), (1:2) and (2:1) were calculated to be (2.9, 3, 2.6 and 1.2, 1.5, 1.4) eV respectively.

The extinction coefficient was also calculated at different ratios. The authors stated that the effective ratio for photoelectric application is (1:1).

Dunia K. M. Al-Nasrawy(2015) [27] prepared lead silicate glasses at different lead oxide content. The structural, surface morphology and bonds properties were studied by means of X-ray diffraction, AFM, and FTIR. The X-ray diffraction patterns revealed that the strongest peak related to a hexagonal silica dioxide, while other phases related to silica oxide (SiO_2) and lead oxide (PbO). Growth and decay phases in X-ray diffraction patterns have been changing lead oxide content. AFM analysis shows that the film has a homogeneous surface with an average diameter around 100 nm. Infrared spectrum is characterized by the presence of large absorption band between (1200 and 900) cm^{-1} and have its maximum value at 1080 cm^{-1} which is attributed to stretching vibrations of Si–O–Si bonds. Another bands were attributed to Pb–O–Pb, Pb–O–Si, $[\text{AlO}_4]$ -tetrahedron, and Si–O–Al bond.

R.Ramos Barradob (2015) [28] Lead oxides (II) in the form of bulk and thin films as electrodes for rechargeable lithium batteries have been prepared by pyrolysis of aqueous solutions from $\text{Pb}(\text{CH}_3\text{-COO})_2 \cdot 2\text{H}_2\text{O}$ and deposited onto lead substrates at 175 °C. The films heated at 250 °C show well crystallized four-dimensional PbO structure, and it developed to polymorph orthorhombic with further heating for long period. The configuration of different Li_yPb alloys was examined in cells at a current density of 0.25 mA/cm^2 over (0.0-1.0) volt.

Raneen Imad Jibrael et al (2016)[29] were prepared graphene suspension by electrochemical exfoliation of graphite electrodes that immersed in aqueous solution contains sulfuric acid, nitric acid and distilled water ($\text{H}_2\text{SO}_4/\text{HNO}_3/\text{H}_2\text{O}$). A bias voltage of 10 V has been applied, and the resulted grapheme foam was deposited onto glass slide.

The structural and optical properties of graphene was characterized by X-ray diffraction (XRD), scanning electron microscope (SEM), energy dispersive spectroscopy (EDS), optical microscopy (OP) and Uv-Vis spectroscopy. The XRD pattern shows crystalline structure of graphene with sharp peak at 26.59° corresponds to an interlayer distance of 0.334 nm of (002) orientation which matching with the interlayer distance of normal graphite. The SEM image of graphene showed thin layered graphene structures with wrinkled shapes. The compositions of graphene consist of carbon and oxygen with atomic percentages of 82.75% and 12.01%, respectively. The absorbance spectra showed that graphene suspension and graphene film have two transitions included π - π and n - π respectively.

Halal H. Rashed et al(2017) [30] prepared lead oxide nanoparticles by laser ablation of lead target immersed in deionized water using pulsed Nd:YAG laser with laser energy 400 mJ/pulse and different laser pulses. The chemical bonding of lead oxide NPs was investigated by Fourier Transform Infrared (FTIR); surface morphology and optical properties were investigated by Scanning Electron Microscope (SEM) and UV-Visible spectroscopy respectively, and the size effect of lead oxide nanoparticles was studied on its antibacterial action against two types of bacteria Gram-negative (*Escherichia coli*) and Gram-positive (*Staphylococcus aureus*) by diffusion method. The antibacterial property results show that the antibacterial activity of the Lead oxide NPs was inversely proportional to the size of the nanoparticles in both Gram-negative and Gram-positive, and also it has been found that Gram-positive bacteria possess greater sensitivity and less resistance to the lead oxide nanoparticles compared with Gram-negative bacteria

Nawfal Y. Jamil et al (2018) [31] studied the effect of Ag doping concentration (0, 1, 5, 10) % on the optical and structural properties of

CdSe thin films. Measurements of the transmittance, absorption of the prepared CdSe thin films in the wavelength range of (400-750)nm was carried out. The band gap energy for CdSe thin films were calculated with respect to Ag concentration (0, 1, 5, 10) % to be (1.97, 1.92, 1.68, 1.52) eV respectively. X-ray diffraction (XRD) results show that deposited pure CdSe thin film was polycrystalline with hexagonal structure, whereas doped films show cubic structure with [111] direction.

Noha. H. Harb (2018) [32] prepared Ag doped CdO thin films at different Ag ratios (0.1, 0.3, 0.5) % using pulse laser deposition technique (PLD), and the resulted thin films annealed at 300 K. The Nd:YAG laser with the following parameters $\lambda=1064$ nm, energy of 600 mJ , a repetition rate of 6 Hz and 400 pulses was used. The effect of doping content on the structural and optical properties of CdO films was studied. The structural results showed that these films were polycrystalline with a preferred orientation in the (002) direction for Ag. The grain size is proportional with the concentration of CdO. The optical properties of Ag doped CdO thin film included transmittance, absorption coefficient, and the energy gap in the wavelength range of 300-1100 nm were studied. The prepared films show a direct energy gap inversely proportional to the concentration of CdO.

1-4-Aims of the work:

1-This study aims to prepare PbO/Cu and PbO/Ag nanoparticles NPs using the laser ablation technique of colloidal targets that immersed in deionized water.

2 -study the structural , morphological and optical properties of the suspension PbO/Cu and PbO/Ag nanoparticles, which using papered samples in opto – electronic devices field.

.

Chapter tWO

Materials and methods

2.1 Introduction:

This chapter describes the process of laser ablation in liquid, as well as the optical, structural, and morphological properties of PbO/Cu and PbO/Ag nanoparticles. Also the chapter contains a theoretical review along with the relations and scientific explanations that in this study.

2.2 Nano materials

In the last two decades, the term of Nano science has rushed into the scientific vocabulary such as nanomaterial, nanoparticle, nanostructure, Nano colloids and Nano cluster [23].

Nano materials are defined as a solid material characterized by at least one dimension in the nanometer range which can also be classified into Nano crystalline materials and nanoparticles. The Nano crystalline materials are polycrystalline bulk materials with grain sizes in the nanometer range (less than 100 nm), while the nanoparticles refer to ultrafine dispersive particles with diameters below 100 nm. Nanoparticles (NPs) are generally considered as the building blocks of bulk Nano crystalline materials [3]. Exists in different shapes such as spherical, triangular, cubical, pentagonal, rod-shaped, shells, ellipsoidal and so forth. It contains small enough number of constituent atoms or molecules that differ from the properties of their bulk counterparts [22]. The term Nano colloid is a stable liquid phase containing particles in different sizes ranging from nanometers to several hundreds of micrometers. Many colloidal particles can be detected by the scattered light, such as dust particles in air [15]. The term Nano cluster usually refers to small nanoparticles that have well-defined composition and surface structure as finite aggregates of atoms or molecules that bounded by metallic, covalent, ionic or Vander Waals bonds [20].

Nano materials have attracted much attention for their unique and superior characteristics that are unavailable in conventional macroscopic materials. Nanomaterial may have a significantly lower melting point or phase transition temperature and appreciably smaller lattice constants, due to a huge portion of the surface atoms out of the total amount of atoms [17-18]. Also the crystal structures are stable at high temperatures, but in the nanometer sizes they are stable at lower temperature. Therefore, the ferroelectric and ferromagnetic may lose their ferroelectricity and ferromagnetism when the materials are shrunk to the nanometer scale.

The optical properties of nanomaterial are different from bulk materials. For example, the absorption peak of a semiconductor nanoparticle shifts to short wavelength region, due to increase its band gap energy.

The bulk semiconductors become insulators when the characteristic dimension is small. The diameters of the nanoparticles produced by laser ablation are in the range of (5-100) nm [5].

Thus for particles sizes less than 10nm, the quantum confinement effects (discrete electron energy levels resulting from the potential well at the boundary of the nanoparticles) of certain materials appear. This leads to consider laser ablation an attractive method for generating the quantum dot [19].

The Nano materials are widely used in many photoelectronic applications such as: photo-thermal therapy, surface-enhanced Raman Spectroscopy, biochemical sensors, Nan photonics devices, carrier systems for drug delivery, solar cells, optoelectronic device, diabetic

healing, cooling system, antibacterial against, cancer treatment, imaging, and inkjet-printer. [20].

2.3. Classification of Nano materials

According to the order of structural, nanomaterial's can be classified as zero-, one-, two and three dimensional nanostructures.

2.3.1.Zero-dimensional (0-D) nanostructures

Nano materials are materials where in all the dimensions are measured within Nano scale. Also, named as nanoparticles, with all possible geometries, such as spheres, cubes and platelets these nanoparticles could be single crystal, polycrystalline and amorphous particles. If all the nanoparticles are single crystals, they are often referred to as Nano crystals. When the NPs have a dimension even small, and a quantum confinement effects are observed, the common term used to describe such nanoparticles is the quantum dots [33].

2.3.2. One-dimensional (1-D) nanostructures

Nano materials have one dimension that is outside the Nano scale. This type has been called by a variety names such as: whiskers, fibers or fibrils, nanowires and Nano rods. In many cases, one-dimensional systems take into account carbon-based, metal-based or even oxide-based systems. Nanotubes and Nano cables are also considered one-dimensional structures if the extension over one dimension is predominant over the other types [32 -34].

2.3.3 Two-dimensional (2-D) nanostructures

Nano materials are materials in which two of their dimensions are not confined to the Nano scale. They are another important nanostructure

that include many shapes such as nano films, Nano layers, Nano coatings and Nano discs, therefore, they have been a attracted much attention.[32 – 34].

2.3.4. Three dimensions (3-D) system

Nano materials, also known as bulk Nano materials, are relatively difficult to classify. However, it is true to say that bulk Nano materials are materials that are not confined to the Nano scale in any dimension. These materials are thus characterized by having three arbitrarily dimensions above 100 nm

The arrangement of three-dimension Nano system consists of both crystalline and amorphous nanostructures, such as Nano crystals have a very large variety of ordered Nano arranged porous materials. Figure 2.1 explain the relationships among 0-D, 1-D, 2-D and 3-D Nano materials in three dimensions space [32- 34].

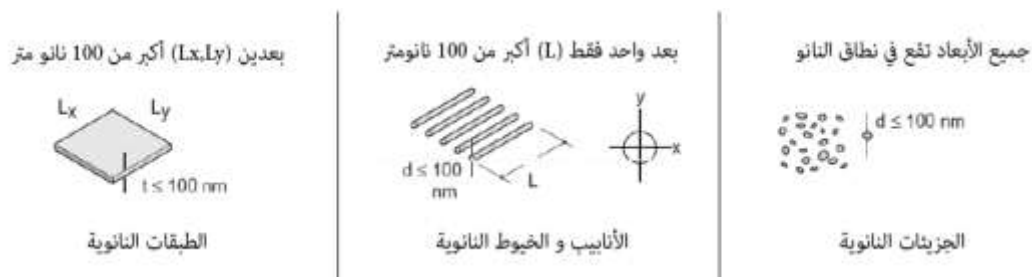


Figure 2.1 Classification of Nano materials according to the order of structural [33].

2.4. Laser Ablation In Liquid:

The ejection of material from a surface under low and high intensities laser pulses are known as pulsed laser ablation (PLAL). The efficiency of this process is described by the ablation rate, which gives the maximum layer thickness ablated during irradiation with a laser pulse [35, 36]. The ablation rate is strongly influenced by the laser such as features and target properties [37, 38].

The surface may be melted into a liquid with a moving solid-liquid interface. The Liquid may be removed from the molten pool as droplets that result in a higher ablation rate. However, a series of events during laser ablation have process could place, and discussed as follows:-

Although many theoretical and experimental studies have been devoted to the interpretation of the physical phenomena occurring during the intense short-pulse laser interaction with materials, some processes like the dissipation of absorbed energy into the lattice and corresponding material removal mechanisms, are still under investigations. Recently, the double-pulse technique, consisting in the application of two time-delayed sequential laser pulses, has been used in order to get a better insight into the temporal characteristics of the different ablation mechanisms [39,40].

Compared to material's ablation in vacuum or in low pressure backgrounds, laser ablation in liquids has attracted significant attention during the last several years, mainly because it allows producing "pure" NPs of a large variety of compounds comprising neither surface-active substances nor counter-ions [41, 42].

Various laser sources can be used for NPs generation using this technique, from IR to UV, while their pulse duration spans from tens of nanoseconds to tens of femto seconds during laser ablation in liquids. The

laser pulse passes through the liquid layer that should be transparent to the laser wavelength and melts the target surface. The thin liquid layer adjacent to the melted surface is heated up to high temperature and expands over the melt providing its ejection into the surrounding liquid. As a result, the dispersed melted material remains in the solvent forming a colloidal of NPs suspensions. Upon ablation of metallic objects, the laser radiation is absorbed by free electrons, and the subsequent surface melting occurs after the thermal excitation of the electrons within the lattice. In that case of metal's ablation with laser pulses, the time of electron-phonon relaxation is on the order of the pulse duration itself, and thus, both melting and expansion of the melt into the surrounding liquid occurs when the laser pulse is already over. If the ablation of a metal target is carried out with two consecutive time-delayed pulses, short delay times, comparable to the relaxation time, may be influence in generating of superior concentration of free electrons which could concurrently transfer their energy to the lattice. At elongated delays can be supposing that NPs production and has the same properties as those generated by two independent laser pulses [43].

2.5. Mechanisms of Laser Ablation Technique and Nanoparticles Formation

2.5.1. General Considerations of Laser Ablation of Materials

The most efficient physical method for nanofabrication is the laser ablation technique because of a number of advantages compared to conventional methods, the advantages of laser ablation method are simplicity of the procedure and the absence of chemical reagents in solution .This method also gives certain flexibility over other techniques as all types of materials can be processed and ablated due to the very high

energy density. Controlling the size of produced NPs by optimizing the process parameters such as laser irradiation time, pulse duration, energy density, laser wavelength...etc. [44].

As mentioned above when a laser pulse reaches to the surface of target, some of this energy is reflected by the surface of target, this reflectivity depends on the material and laser wavelength [45]. The other part of energy absorbed by the sample this absorption energy can be considered as an energy source inside the material, in order to induce any effect on the substrate, however, the source can develop its own dynamics depending on the specific electronics and lattice responses of the material, although it is driven by the incident light beam, i.e. it is transferred from optical photons to electrons and then to the lattice, which then diffuses the energy into the material. Photochemical reactions may occur at extremely high energy pulses which remove atoms and molecules from the surface of material, rapid vaporization process occur when the temperature of heated surface reaches close to the critical temperature. The vaporization resulting in plasma that consists of ionized vaporized atoms. The plasma shielding phenomena occur when the plasma cloud absorbs some of the incident laser energy and thereby only allows a fraction of the laser energy to reach the surface. The plasma expands and heats by photon absorption. Later the vapor cools and aerosol particles begin to form [46].

2.5.2. Laser Ablation Technique

Generally, the product of nanoparticles from laser ablation comes directly from the condensation of the plasma plume which generated by the laser pulse irradiating the surface of the solid target. Therefore there are three basic processes of the plasma plume from laser ablation of

solids. These processes are generation, transformation, and condensation, which play important roles in materials preparation. Figure 2.2, shows a schematic diagram of the physical mechanism of formation NPs [47]. These processes occur starting from electronic absorption of laser optical energy (at 10–15 sec) to particles condensation (at 3–10 sec) after laser pulse duration [20]. Figure 2.2a explains the plasma generation processes; two important parameters determine the natural of process, the laser intensity and pulse duration.

For a nanosecond laser pulse (ns) with intensity less than 10^8 W/cm², the thermal vaporization is a dominant mechanism: phase transition occurs when the temperature of the solid surface increases, the phase transition starting from solid to liquid, liquid to vapor, and ending when vapor transform to plasma. For a picosecond laser pulse (ps) with intensity between 10^{10} – 10^{13} W/cm², both thermal and non-thermal mechanisms occurred. For intensity higher than 10^{13} W/cm² with femtosecond laser pulse (fs), Coulomb explosion is the main bond breaking mechanism [20]. After the plasma generation process, transformation stage begins and it contains plasma expansion as shown in Figure 2.2b. The expansion of plasma occurs at the end of the laser pulse, it will be governed by the initial plasma properties and the expansion medium. After 1 μ s from laser pulse, Plasma will be expansion adiabatic. After that time, there is an energy loss and gradient temperature happened [47].

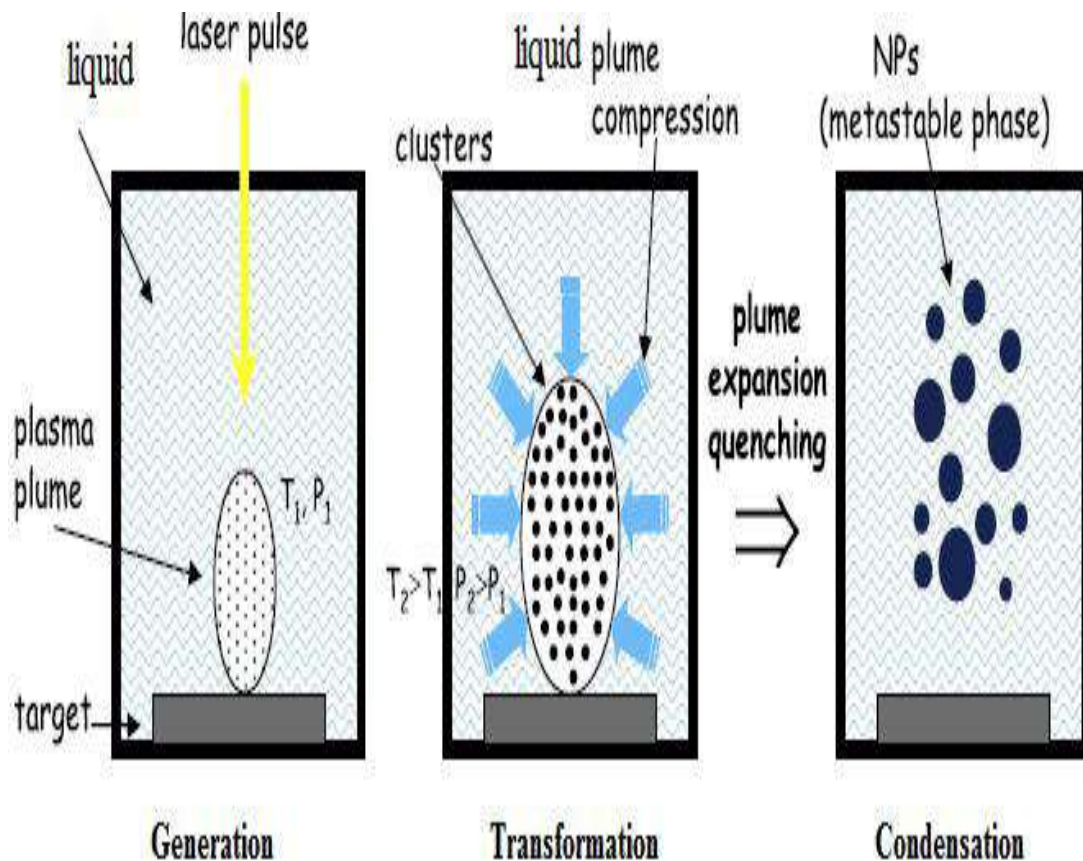


Figure 2.2: A schematic diagram of the physical mechanism of formation NPs.

a- Generation process, b- Transformation process and c - Condensation process [47].

The last process responsible of the generation of nano sized is condensation of the vaporized atoms particles as shown in Figure 2.2c. There are many critical factors effect on the condensation process such as the ambient pressure, gas properties and temperature. Condensation processes were predicted when the plasma temperature decreased to a sufficiently low value related to the vapor number density [45, 50,]. I.e. Condensation starts when the vapor plume temperature reaches the boiling temperature of the material (~ 3000 K) and stops at the condensation temperature of the material (< 2000 K) [20].

Besides the main particle generation mechanisms, Coagulation and agglomerates processes considered the most important minor mechanisms to alter the distribution of particle size or the total particle number concentration, these processes can occur from several nanoseconds to several milliseconds after the laser pulse. These processes increase the final particle size, whereas the particle after forming from laser ablation which collide each other in gas ambient and if the momentum is large enough or participate particle in liquid phase. Particle coalesces to form new large particle this process is called Coagulation process and usually happened in the latter time scale.

Agglomerates are formed as early soon condensation state ,when the Nano size aerosols are form from vapor ,they are strongly charged with electrons existing in the plasma then the charged particles attach to each other by the electronic bond [46].

2.5.3. Mechanisms of Formation NPs

The ablation mechanisms causing the generation of the plasma plume are different for the Nano second and ultra-short, e.g., femtosecond laser pulses, therefore this matter will explain in the following paragraphs [47].

2.5.4. Laser ablation in Nano second Laser Irradiation

For the ablation of the nanosecond laser with irradiances less than 108 W/cm², there is enough time to propagation of thermal wave into the bulk material thereby causing a melting and evaporation.

The dominant mechanisms in the plume absorption are inverse Bremsstrahlung and thermal vaporization. When the vaporization starts, the evaporated material (vapor particle) will expand. Then, this vapor

plume interact with background gas, because of the background gas is pushed further away from the solid target, yielding the confinement of the plume.

Since the temperature in the vapor plume can rise to much high values, therefore a plasma plume will be generated during the front part of the incident laser pulse irradiating of the solid target.

The plasma plume excitation and ionization are mainly a result of the multiphoton absorption, ionization, and inverse Bremsstrahlung in the gaseous phase induced by the laser pulse [20, 47].

Ablation of the nanosecond laser, the plasma plume expands in femtosecond laser without any other heating process, and the plasma plume expansion will fast lose the temperature with short lifetime. Importantly, the ultra-fast duration (e.g., the femtosecond laser) is the shorter time of the mechanical relaxation (expansion) of the absorbing volume, and the laser heating takes place at nearly constant volume conditions, causing the buildup of a high thermoplastic pressure. Then, the photomechanical effects induced by the pressure relaxation start to play an important role in material ejection [48, 49].

The femtosecond ablation has several advantages compared to longer pulse lengths. The main advantage of using femtosecond lasers is the minimal effective thermal load to the material thus no heat affected zone, but in nanosecond laser the heat affected zone is large, Figure (2.3) shows of nanosecond —pulsed laser ablation techniques [50].

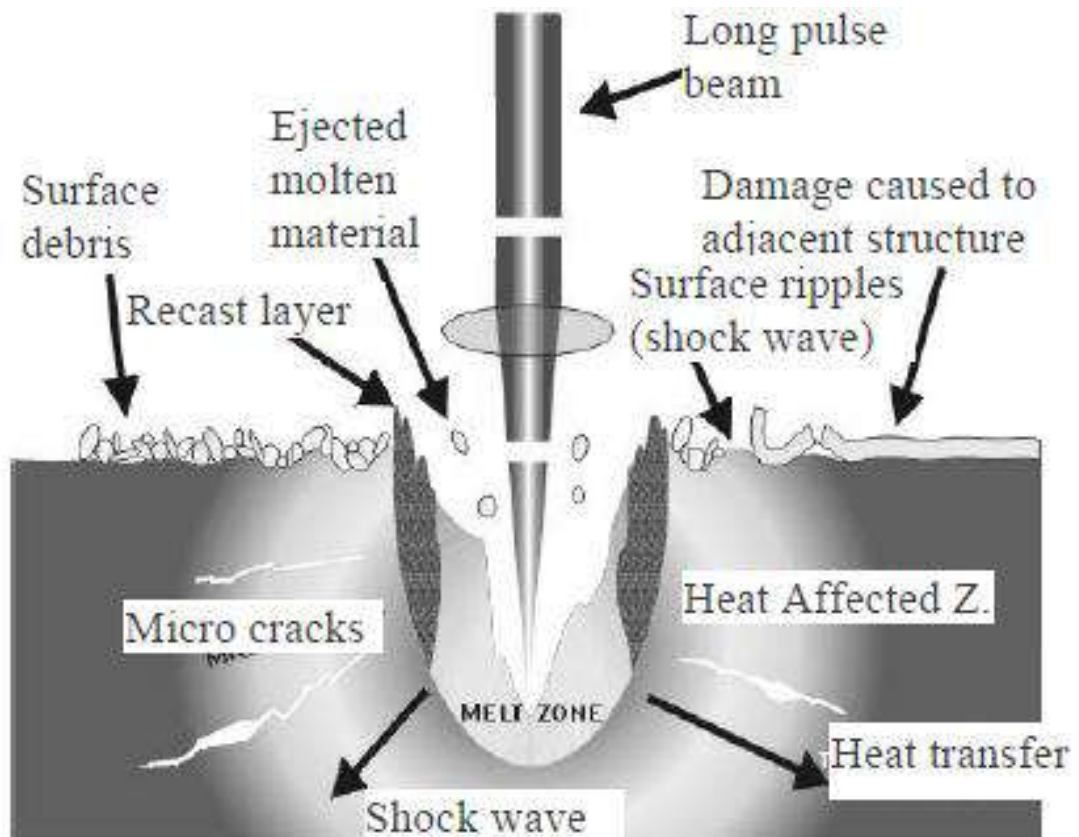


Figure 2.3: Mechanisms of laser ablation techniques in: nanosecond – pulsed laser ablation laser ablation [50].

Another important advantage of femtosecond laser processing is that the peak power is very high, allowing nonlinear absorption within the bulk of transparent materials. Because of nonlinear absorption, it is possible to limit the region of material modification to the area around the laser focus. Any energy absorbed above or below the focus will generally be below the material modification threshold, so no damage is produced [53].

Laser ablation of materials from a solid target occurs either in vacuum or in liquid environment in laser-based materials processing to produce Nano clusters. In the former method the Nano clusters can be deposited on a solid substrate resulting formation of a nanostructured

film [52]. This method has some disadvantages such as the difficulty of controlling the production of NPs.

In the latter method the Nano clusters can be released into the liquid forming a colloidal nanoparticle solution leading for a more effective collection of synthesized particles. The solvent can provide positive physical and chemical effects such as plasma confinement, cooling actions, oxidation or reduction leading to enhancement of ablation efficiency [53].

PLAL is a one-step top-down procedure (dispersion method) strategy of nanoparticles preparation [54, 55]. This technique can also be applied for the preparation of oxides base nanostructures such as oxide nanoparticles and Nano composites, because ablated species with high energy can be easily reacted with water and oxidized, and the formed nuclei can react with the organic molecules in aqueous solution [55, 56].

2.6 Fundamental Mechanisms of PLAL Technique

2.6.1 General Arrangement of PLAL Technique

Figure 2.4a shows the general schematic diagram of a typical experimental setup for PLAL. The setup basically only needs pulsed laser beam delivery optics and a container to hold the target and liquid. The container as well as the target is usually rotating by using magnetic stirrer or rotating stage for examples to ensure no ripple was observed on the surface of the solution and to avoid a deep ablation crater.

The setup may be modified to control the ablation process, but the common features still exist, that is, a laser beam is focused onto a target immersed in liquid, and the ablated materials are dispersed into the liquid [57].

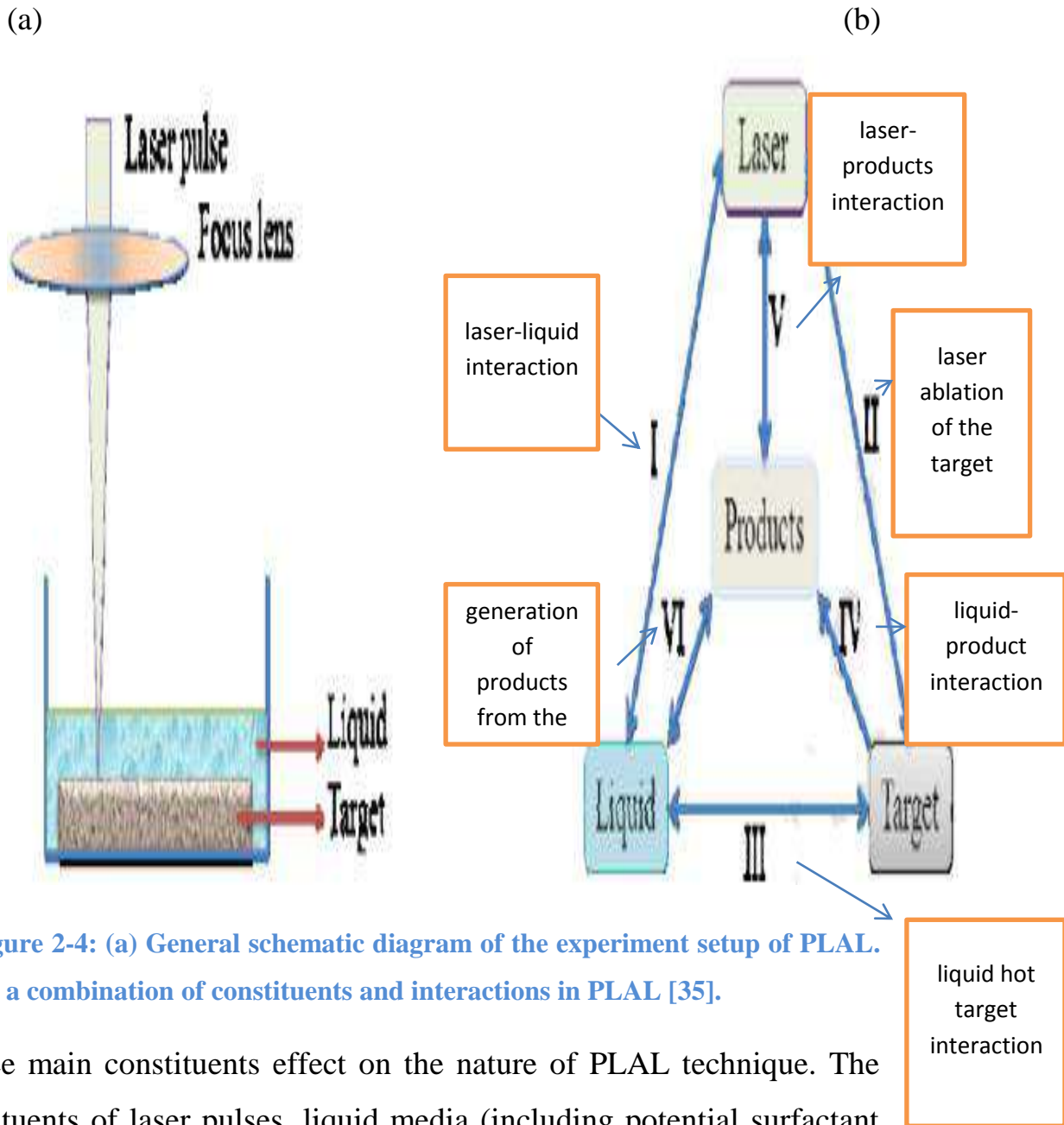


Figure 2-4: (a) General schematic diagram of the experiment setup of PLAL. (b) a combination of constituents and interactions in PLAL [35].

Three main constituents effect on the nature of PLAL technique. The constituents of laser pulses, liquid media (including potential surfactant molecules/ions and electrolyte ions), and solid targets as shown in Figure 2.4b, the ablated products also may be interacted with each other. These interactions occur in the same system and in a short time after the laser pulse, thus are strongly coupled. The coupled interactions may lead to especially unique micro- /nanostructures that might not be envisioned by conventional fabrication techniques [58].

2.7. PLAL Parameters

In general, there are three main factors, which can influence size and composition of nanoparticles/nanostructures produced by PLAL technique these factors corresponding in (laser parameters, liquid properties and ablated material properties). The effect of these parameters will explain in the following paragraphs [68].

2.7.1 Laser Parameters

Laser parameters such as pulse width (pulse duration), laser fluence, laser wavelength influence on nucleation, growth, and aggregation mechanisms, thus these parameters effect on the characteristics of nanoparticles, [60, 61]. All these parameters determine the temperature, density and angular distribution of ejected atoms and particles [69].

The first laser parameter is a width of pulse influences the thermal transport in the material. The short pulse laser ablation has a smaller thermally affected area when it is reduction of heat affected zones has been attributed to suppression of thermal diffusion resulting from the short pulse duration [46].

The second parameter is laser fluence. At low fluences, nanoparticles with relatively small mean size and narrow dispersion were obtained and vice versa. Because the value of laser fluence depend on the laser energy, thus the magnitude of the laser energy changes the mass removal mechanisms from pure vaporization to liquid ejection, and eventually even phase explosion happen when very high energy is involved as well as the increases in energy lead to obtain more micrometers particles from molten layer .Also, the pulse energy has a

strong effect on materials which have high reflectivity and then leads to increase the intensity of absorption peak and then increase the efficiency of ablation because of increasing the stability of NPs [46].

The third parameter is the laser wavelength. The choice wavelength of laser plays an important role on ablation process. The selection of a wavelength with a minimum absorption depth ensures a high energy deposition in a small volume for rapid and complete ablation [71].

The fourth parameter is the pulse repetition rate. If the rate is too low, all of the energy which was not used for ablation will leave the ablation zone allowing cooling. If the residual heat can be retained using a high repetition rate, thus limiting the time for conduction, then ablation will be more efficient. More of the incident energy will go toward ablation and less will be lost to the surrounding work material and the environment [71]. It should be noted that the size of the nanoparticles decreased with an increase of the pulse number. This may be related to self-absorption of laser light provided by the particles.

2.7.2. Target Properties

Many physical and chemical properties of material effects on the produced nanoparticles by PLAL such as the chemical composition of material and its purity also thermal diffusivity influence on this technique.

Whereas the laser pulse irradiates the material, it deposits energy at the focal spot. This creates a temperature gradient and the heat diffuses to a length scale l_{diff} . Given below, resulting in surface cracks and other unwanted damage to the target material. The diffusion length is given by following equation [44]:-

$$d_{diff} = 2(\tau D_{th})^{1/2} \dots\dots\dots (2.1)$$

Where

τ - is the pulse duration (s).

D_{th} - is the thermal diffusivity of the target material (m^2/s).

Also, the thermal relaxation time of material (TRT) plays an important role in comparison this time with pulse duration of laser (τ), Whereas $\tau \ll TRT$ this leads to unthread interaction such as in femtosecond laser and when $\tau > TRT$ this leads to thermal interaction as nanosecond laser.

2.8. Advantages and Disadvantages of PLAL Technique

PLAL has become an increasingly popular top-down approach for producing nanoparticles because it has many advantages compared with other techniques to produce nanoparticles such as pulsed laser deposition, photo-reduction, solve thermal, electrolysis, microwave-induced, glow discharge, aerosol flow reactor, spray pyrolysis and spark discharge [74 , 75]. One of disadvantage PLAL technique that the size distribution of the NPs tend to be broadened due to agglomeration of Nano clusters and to the possible ejection of the relatively large target fragments during the laser ablation process [64].

The main advantages of this technique is its ability to produce various kinds of Nano materials such as metals, noble metals, semiconductors, Nano alloys, oxides, magnetic and core-shell nanostructure [76 , 77]. PLAL do not need vacuum equipment, and nanoparticles stabilize directly by adding the stabilizer to ablation environment because the role of surrounding solvent, as mentioned above has physical effects such as confinement and high cooling rate and

chemical reactions effects such as oxidation or reduction [78]. In addition, the surfactant molecules can control on aggregation and dispersion by preventing the increase of particle size because of their adsorption on the nanoparticles as coating reagents effect [79].

PLAL is considered an alternative and promising method for the controlled fabrication techniques of nanomaterial by rapid reactive quenching of ablated species at the interface between the plasma and liquid with high-quality nanoparticles. The Nano materials produced by PLAL technique have inherent stoichiometry from their mother targets therefore, it has a capability to produce nanomaterial of desired chemical composition and they have surfaces free from chemical contaminations [80].

Beneficial aspects of the PLAL method are the new phase formation involves in liquid -solid interface. Also the phase, size and shape of the synthesized Nano crystals can be readily controlled by tuning laser parameters and by choosing the suitable surfactant solutions to ensure the nanoparticles are relatively free from oxidative effects [81, 79]. The oxidation of the nanoparticles could be easily controlled if the liquid selected in the operation is oxygen-free [82].

Furthermore, the produced NPs in this method can easily be obtained in one-step procedures without subsequent heat-treatments, because of the high energetic state of ablated species [83].

The high purity of the nanomaterial, the material variety, and the dispersion of the nanoparticles in a variety of liquids allowing them safe and stable handling of the colloids [84, 85], Simplicity of the procedure, and it requires minimum amount of chemical species for synthesis NPs

and because of it can generate nanoparticles without counter-ions or surface-active substances [86].

Although these advantages, some of the disadvantages of PLAL method especially under water include: some light is absorbed by water; light may be scattered by the water surface, suspensions, and bubbles; power loss due to water cooling; water photolysis; water vapor hazardous to electronics; and possible corrosion of materials. Also, the liquid could splash out from the container at every laser pulse, requiring the liquid level to be constantly topped-up. That means the experiment had to be stopped on several occasions during an ablation run to refill the liquid [87].

2.9. Characterization of selected materials

2.9.1. Physical properties of lead oxides

[Lead Oxide (PbO), an important industrial material, has been widely applied in gas sensors, pigments and paints [88, 89]. PbO has two polymorphic forms and a wide band gap: red α - PbO, stable at low temperature, and yellow β - PbO, stable at high temperature [90, 91]. Because of its applications, considerable progresses have been made on the synthesis of lead (II) monoxide polymorphs (α - PbO and β - PbO) over the years. Methods such as thermal evaporation [92], sputtering [93], pulsed laser deposition [94], chemical vapor deposition [94], sol-gel, precipitation, solve-thermal and hydrothermal processes have been adopted for the synthesis of PbO[95].

2.9.2. Physical properties of copper

Copper is a member of the first row transition series of elements, which consists of Sc, Ti, V, Cr, Mn, Fe, Co, Ni, Cu and Zn, and belongs

to group II of the periodic table, along with Ag and Au. The element has an atomic number of 29, an atomic mass of 63, two main oxidation states (+1 and +2) and two naturally occurring isotopes (^{63}Cu and ^{65}Cu), with abundances of 69.17% and 30.83% respectively. In spite of a similarity in electronic structure, there are few resemblances between the chemistry of the three elements in group 11, although certain complexes of Cu^{2+} and Ag^{2+} are isomorphs [96, 97]

2.9.3. Physical properties of silver

The silver based electrical contact materials are widely used by electrical and electronics industry representing a significant group of functional materials [98]. Basic properties required for these materials are high electrical and thermal conductivity, high resistance to arcing, high welding resistance, low contact resistance, high hardness and strength. For several decades Ag-CdO has been the material of choice for application in wide range of switching devices [99]. This is due to its superior anti welding properties and wears resistance, suitable hardness that enables good machinability and high electrical conductivity. Taking into consideration toxic nature of cadmium and strict environmental legislation (RoHS, WEEE) numerous materials have been investigated as a possible more environmentally friendly substitutes [100].

2.10. Optical properties of material

2.10.1. Absorbance:

The part of the incident beam that is not reflected by the material is either transmitted through the material or absorbed. The fraction of the beam that is absorbed is related to the material thickness and the way in which the photons interact with the structure of materials. The intensity of the beam after passing through the material is given by: [101]

$$I=I_0e^{-\alpha t} \dots\dots\dots(2-2)$$

Where t: Is sample thickness

I₀: Intensity of light incident on sample

I: Intensity emerging from sample.

α: absorption coefficient .Equation (2-3) is also known as the Beer–Lambert law .The unit of absorption coefficient is (cm⁻¹) , And this parameter varies depend on the wavelength of the incident light and the nature of material [102].

2.10.2. Transmittance:

The fraction of the beam that is not reflected or absorbed is transmitted through the material, Figure (2.6) shows beam that is reflected, absorbed, incident and transmitted. Transmission is the term utilized to describe the operation by which incident radiant flux leaves a medium or surface from a side other than the incident side , usually the cross side. The spectral transmittance T (λ) of a medium is the ratio of the transmitted spectral flux iT to the incident spectral flux I₀ , or

$$T = I_T/ I_0 \dots(2-3)$$

Repeat remove thination.[103].

Absorbance is associated with the permeability by following the relationbelow[104]:

$$A = \text{Log} (1/T) \dots\dots\dots(2 -4)$$

$$T = \exp [-2.303A] \dots\dots(2 -5)$$

Using the following steps, we can determine the fraction of the beam that is transmitted:

1. If the incident intensity is I_0 , then the loss due to reflection at the front face of the material is $\hat{R} I_0$. The fraction of the incident beam that actually enters the material is

$$I_0 - \hat{R} I_0 = (1 - \hat{R})I_0 \quad \dots(2-6)$$

$$I \text{ reflected at front surface} = \hat{R} I_0 \quad \dots(2-7)$$

$$I \text{ after reflection} = (1 - \hat{R})I_0 \quad \dots(2-8)$$

2. A portion of the beam that enters the material is lost by absorption. The intensity of the beam after passing through a material having a thickness x is

$$I \text{ after absorption} = (1 - \hat{R}) I_0 \exp(-\alpha x) \quad (2-9)$$

3. Before the partially absorbed beam exits the material reflection occurs at the back surface. The fraction of the beam that reaches the back surface and is reflected is :

$$I \text{ reflected at back surface} = \hat{R} (1 - \hat{R})I_0 \exp(-\alpha x) \quad (2-10)$$

4. Consequently, the fraction of the beam that is completely transmitted through the material is:

$$I_{\text{transmitted}} = I_{\text{after absorption}} - I_{\text{reflected at back}}$$

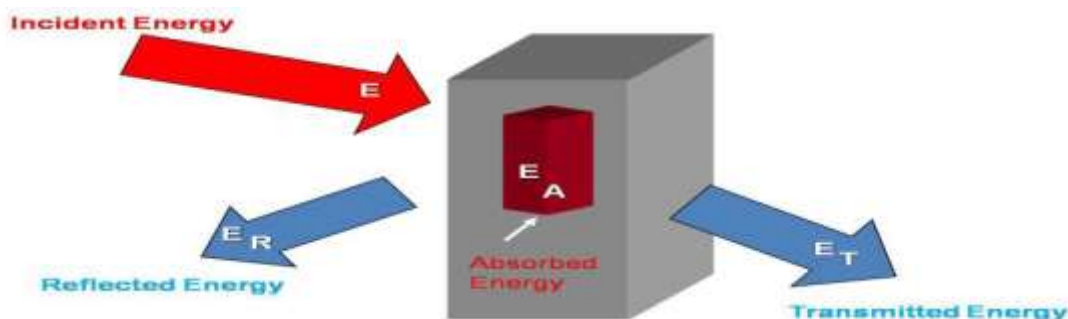


Figure (2-5) Beam that is reflected, absorbed, incident and transmitted [105]

2.11.3 Reflection:

When light radiation come from one medium into another having a various refractive index, some of the light is scattered at the interface between the two sides even if both are transparent .The reflectivity \hat{R} is the part of the incident light that is reflected at the interface [106].

$$\hat{R} = I_R / I_0 \quad \dots(2-11)$$

Where i_0 and $i \hat{R}$ are the intensities of the incident and reflected beams, Respectively.

Reflectance can be obtained from absorption and transmission spectra in accordance with the law of conservation of energy by the relation [107]

$$\hat{R} + T + A = 1 \quad \dots(2-12)$$

2.10.4 Absorption coefficient:

The absorption coefficient (α) is defined as the gradually reduction of the flow of incident ray energy on a unit area along the direction of wave diffusion inside a medium. The absorption coefficient depends on the energy of photon and properties of the semiconductor regarding the gap energy of the semiconductor and the kind of electronic transitions [119].

$$\alpha t = 2.303 \log I/I_0 \dots\dots\dots(2-13)$$

where : $\log I/I_0$ represents the absorbance (A).

The absorption coefficient can be calculated as follows:

$$\alpha = 2.303(A/t) \quad \dots(2-14)$$

2.10.5. Electrical energy gap

The fundamental absorption refers to band-to-band or the transitions in which an electron transfers from the valance band to the conduction band with absorption of photon energy higher from energy of forbidden gap. For materials of high absorption properties within the UV frequencies, Tauc and Menth developed a power law, which identified such optical property by

$$\alpha h\nu = B (h\nu - E_g)^r \quad \dots(2-15)$$

where B is an energy independent constant.

(r) is a constant which determines the type of optical

where α is the absorption coefficient (cm^{-1}), ν is the frequency (sec^{-1}) and (E_g) is the optical energy gap, (r) constant for fixed electronic transition and varies between 1/2, 3/2, 2, and 3. The values of (r) are 1/2 for direct transition, 3/2 for forbidden direct transition, 2, and 3 for indirect transition. By plotting $(\alpha h\nu)^{1/r}$ versus $h\nu$ for fixed r value, the extrapolation of the linear part could be used to define E_g [90].

2.10.6 Extinction coefficient:

Extinction coefficient represents the amount of energy absorbed in a thin film, or more precisely refers to several different measures of the absorption of light in a medium. The extinction coefficient can be represented by the following relation

$$K = \alpha \lambda / 4\pi \quad \dots\dots\dots(2-16)$$

It is noted that the extinction coefficient depends mainly on the wavelength of the incident radiation, and the absorption coefficient, which depends on the type of material [93].

2.11.7 Refractive index:

It is defined as the ratio between the speed of light in a vacuum to the speed in the medium.

$$\dot{R} = ((n-1)^2 + k^2) / ((n+1)^2 + k^2) \quad \dots\dots(2-17)$$

from this equation we can calculate the refractive index:[90]

$$n_o = \left[\left(\frac{1+R}{1-R} \right)^2 - (k_o^2 + 1) \right]^{1/2} + \frac{1+R}{1-R} \dots\dots$$

2.11. Indexing X-Ray Diffraction Patterns

The XRD patterns, the product of XRD experiment, are somewhat like fingerprints in that they are unique to the material that is being examined.

The information in XRD pattern is a direct result of two things:

- (1) The size and shape of the unit cells determine the relative positions of the diffraction peaks;
- (2) Atomic positions within the unit cell determine the relative intensities of the diffraction peaks (remember the structure factor?).

Taking these things into account, we can calculate the size and shape of a unit cell from the positions of the XRD peaks and we can determine the positions of the atoms in the unit cell from the intensities of the diffraction peaks.

Full identification of crystal structures is a multi-step process that consists of:

- (1) Calculation of the size and shape of the unit cell from the XRD peak positions;
- (2) Computation of the number of atoms/unit cell from the size and shape of the cell, chemical composition, and measured density;

- (3) Determination of atom positions from the relative intensities of the XRD peaks

We will only concern ourselves with step (1), calculation of the size and shape of the unit cell from XRD peak positions.

2.12. PROCEDURE FOR INDEXING NON-CUBIC XRD PATTERNS

Index a diffraction pattern, assign the correct Miller indices to each peak (reflection) in the diffraction pattern. An XRD pattern is properly indexed when aLL of the peaks in the diffraction pattern are labeled and no peaks expected for the particular structure are missing. The procedures are standard. They work for any crystal structure regardless of whether the material is a metal, a ceramic, a semiconductor, a zeolite, etc...

The equations will differ slightly from each other due to differences in crystal size and shape (*i.e.*, crystal structure). As was the case for cubic crystals, there are two methods of analysis that involve calculations. The second I will refer to as the analytical method. Both the mathematical and graphical methods require some knowledge of the crystal structure that you are dealing with and the resulting lattice parameter ratios (*e.g.*, c/a , b/a , etc...).

First, consider the plane spacing equations for the crystal structures of interest. Some are shown below:[93]

Tetragonal
$$\frac{1}{d^2} = \frac{h^2 + k^2}{a^2} + \frac{l^2}{c^2} \dots\dots(2-18)$$

which can be rearranged in terms of $\sin^2 \theta$ to:

Tetragonal
$$\sin^2 \theta = \left(\frac{\lambda^2}{4} \right) \left(\frac{h^2 + k^2}{a^2} + \frac{l^2}{c^2} \right) \dots\dots(2-19)$$

Should note that as unlike cubic systems where $\left(\frac{\lambda^2}{4a^2} \right)$ is constant, your results for non-cubic systems will depend upon ratios of lattice parameters (*i.e.*, c/a , b/a , etc.) and your interaxial angles (*i.e.*, α , β , γ). We will illustrate this (“sort of”) below. This is due to the non-equivalence of indices in these systems.

The Rietveld method refines user-selected parameters to minimize the difference between an experimental pattern (observed data) and a model based on the hypothesized crystal structure and instrumental parameters (calculated pattern) Advantages of Rietveld method. Analysis of the whole diffraction pattern – Profile fitting is included – Not only the integrated intensities [93]

- Refinement of the structure parameters from diffraction data
 - Quantitative phase analysis (crystalline and amorphous)
 - Lattice parameters
 - Atomic positions and occupancies
 - Temperature vibrations (isotropic and anisotropic)
- Other information
 - Grain size and micro-strain (isotropic and anisotropic)
 - Stacking and twin faults
 - Magnetic moments (neutrons)
- Not intended for the structure solution
 - The structure model must be known before starting the Rietveld refinement

spectrum is calculated by the classical intensity equation:

$$I_i^{calc} = S_F \sum_{j=1}^{Nphases} \frac{f_j}{V_j^2} \sum_{k=1}^{Mpeaks} L_k |F_{k,j}|^2 S_j(2\theta_i - 2\theta_{k,j}) P_{k,j} A_j + bkg_i$$

Scale Factor

S_F : beam intensity

f_j : volume fraction

V_j : cell volume

Structure Factor

Multiplicity of k-th reflection (m_k)

Temperature factor

Volume absorption

Lorentz--Polarization factor

- Geometry
- monochromator (angle θ)
- Detector
- beam size/sample volume
- sample positioning (angular)

Preferred orientation

i : steps

j : number of phases

k : k^{th} reflection

2.13. Quality of Refinement (Reliability factors):

It is a measure of how well the refined structure predicts the observed data. The value is also sometimes called the **discrepancy index**, as it mathematically describes the difference between the experimental observations and the ideal calculated values [93].

N: number of point , P: number of parameter

The profile R-factor
$$R_p = \frac{\sum_i |y_{io} - y_{ic}|}{\sum_i y_{io}} \dots\dots(2-20)$$

The weighted Rp
$$R_{wp} = \left[\frac{\sum_i w_i (y_{io} - y_{ic})^2}{\sum_i w_i y_{io}^2} \right]^{\frac{1}{2}} \dots\dots(2-21)$$

The Bragg R-factor
$$R_B = \frac{\sum_i |I_{ko} - I_{kc}|}{\sum_i I_{ko}} \dots\dots(2-22)$$

The expected Rf
$$R_{exp} = \left[\frac{N - P}{\sum_i w_i y_{io}^2} \right]^{\frac{1}{2}} \dots\dots(2-23)$$

The goodness of fit
$$GOF = \frac{\sum_i w_i (y_{io} - y_{ic})^2}{N - P} = \left(\frac{R_{wp}}{R} \right)^2 \dots\dots(2-24)$$

2.14. Debye scherrer formula

The broadening of line diffraction profile can be happen due the finite size of crystallite ,strain and defects of deflection from ideal crystallite size can be measured by the equation that produced by debye scherrer. It is used in the determination of size of particles of crystals in the form of powder. The Scherrer equation is limited to [nano](#)-scale particles. It is not applicable to grains larger than about 0.1 to 0.2 μm , which precludes those observed in most [metallographic](#) and [cerographic](#) microstructures [91]

$$D = \frac{K\lambda}{FWHM \cos\theta}$$

K: is a shape factor (0.89)

θ : is the brage angle

λ : is the wave length

D: is the crystallite size

FWHM: full width at half maximum of the intensity

Chapter three

Experimental Work

3.1. Laser Ablation in Deionized System:

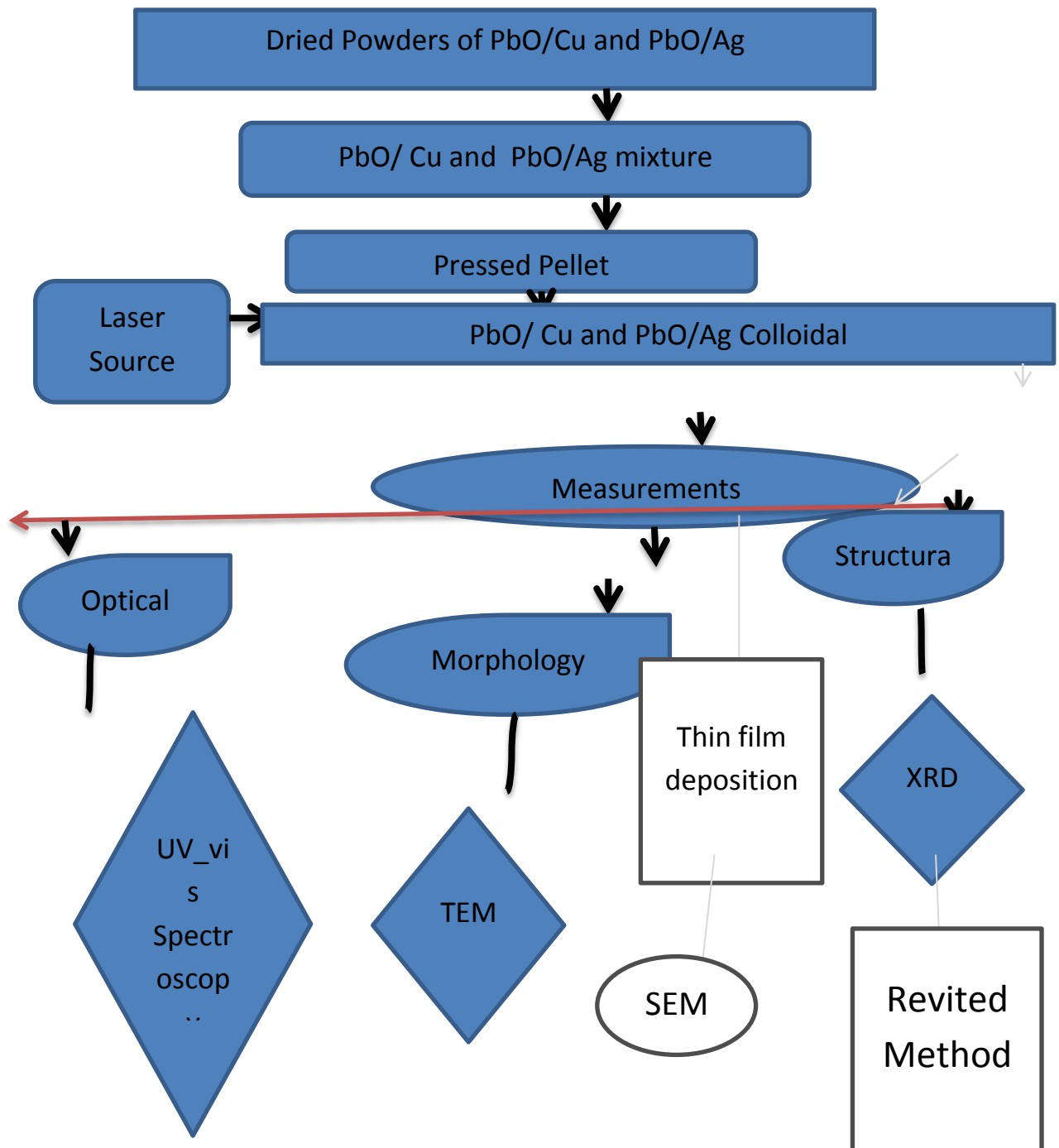


Figure (3.1) this flow chart

3.2. Material Preparations:

3.2.1 Preparation of PbO/Cu and PbO/Ag NPs:

Commercial micro powders of lead oxide (Alherich Sigma Company), copper and silver (BDH Chemicals Ltd England). we have used a mixture of PbO:Cu and PbO:Ag with various concentration of doped noble metal ($x=15,20,30,50,75,85$ wt%) were pressed (4-6 Ton) pellet target (diameter 1.5 cm and thickness with 0.3mm), for synthesis nanoparticles colloidal by employed laser ablation in deionized water (DI). The target was down occupied in 25 ml beaker, the water highiet above the surface of target was kept constant at 10 mm for the duration of ablation laser with the intention of keep the efficiency of laser ablation constant. The pressed targets were vertically irradiated by (Q-switched Nd-YAG laser DIAMOND-288 pattern EPLS), operating at the wavelength (1064 nm), pulse duration of (6ns), 300 number of pulses for 400 mJ of output energy. The laser beam was then focused on the targets using a lens with a focal length of 20 cm. The target and glass container were rotated during the process, to avoid a deep crust due to repeated laser pulses on same spot.



Fig. (3.2) pulsed Laser
ablation in liquid (PLAL)



Fig. (3.3) Images of prepared nanoparticle colloids for (a)PbO/Cu and(b) PbO/Ag.

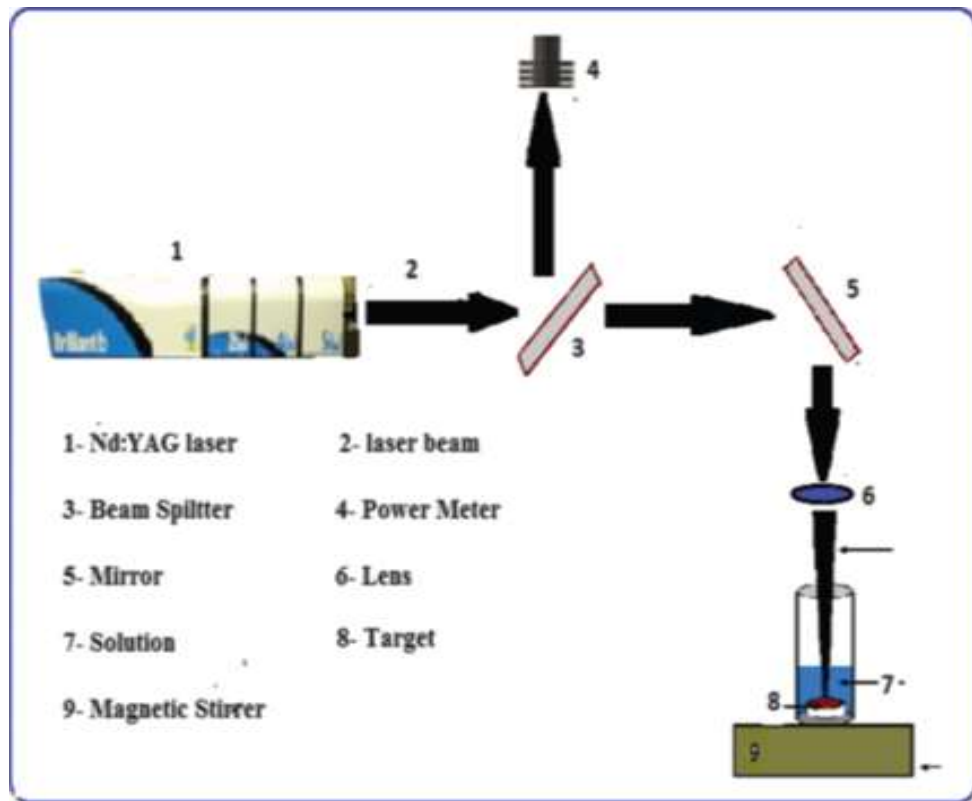


Fig.(3-4).A schematic of experimental setup applied for the synthesis of PbO/Cu and pbO/Ag nanoparticles using pulsed laser ablation in liquid

3.3. Characteristic Of PbO/Cu and PbO/Ag NPs:

3.3.1X-Ray Diffraction Technique

The Structure properties thin films PbO/Cu and PbO/Ag of the nanoparticles solutions of colloidal were prepared for XRD, for structural examinations by drop coating of individual solution onto glass substrate. Dropping was repetitive several times up to a clear film was formed, with consideration of allowed the suspension solutions for 5 min before the deposition. The XRD tests were carried out on a diffract meter provide with a Cu $-K\alpha$ X-ray tube(Shimadzu XRD – 6000), in the angular range $2\theta = 10-80$.

3.3.2 Morphology

Scanning electron microscopy (SEM)

Films of the colloidal solutions were prepared for morphology properties by drop coating of particular solution onto a glass substrate. The dropping was repeated several times until a visible film was formed, with

consideration of the colloidal solutions were sonicated for 5 min before the deposition. As well as, the morphology and calculated size distribution of the produced nanoparticles were examined using an (SEM, FEI Company Inspect S50-Model), scanning electron microscope equipped with an energy-dispersive X-ray spectrometer (EDS, Burker Company- Germany X Flash 6110-Model)). As shown in fig (3.5)



Fig. (3.5) Scanning electron microscopy (SEM)

Transmission Electron Microscopy(TEM).

Drops of the colloidal solutions PbO/Cu and PbO/Ag nano particles (with consideration of the colloidal solutions were solicted for 5 min before the deposition) prepared were dried separately on model copper grid coated with gold (contains about 200 meshes) to characterize their

size and structure using Transmission Electron Microscopy (TEM,Model CM10PW6020,Philips -Germany) as shawn in fig (3.6).



**Fig.(3.6) Ttransmisstion
Electron Microscopy (TEM)**

3.3.3. Optical Analysis

UV-VIS Spectroscopy

Drops of the colloidal solutions (with consideration of the colloidal solutions were solicited for 5 min before the deposition. The optical absorbance of laser synthesized colloidal solutions was recorded in the wavelength range from 190 to 1100 nm using a UV-Vis (Shimadzu-uv-1800, made in Japan) spectrophotometer. The change of color of colloidal solution of NPs indicates that Nano sized colloidal particles have produced; therefore this test is necessary to find the absorption of NPs in UV-Vis. regions. All spectra were measured at room-temperature in a quartz cell with 1 cm optical path. shows the images of prepared suspension for pure PbO, doped Cu and Ag respectively.



Figure (3.7) UV-Visible spectroscopy ometer.

3.4.XRD Characterization of selected materials

3.4.1.XRD of (lead oxide) PbO

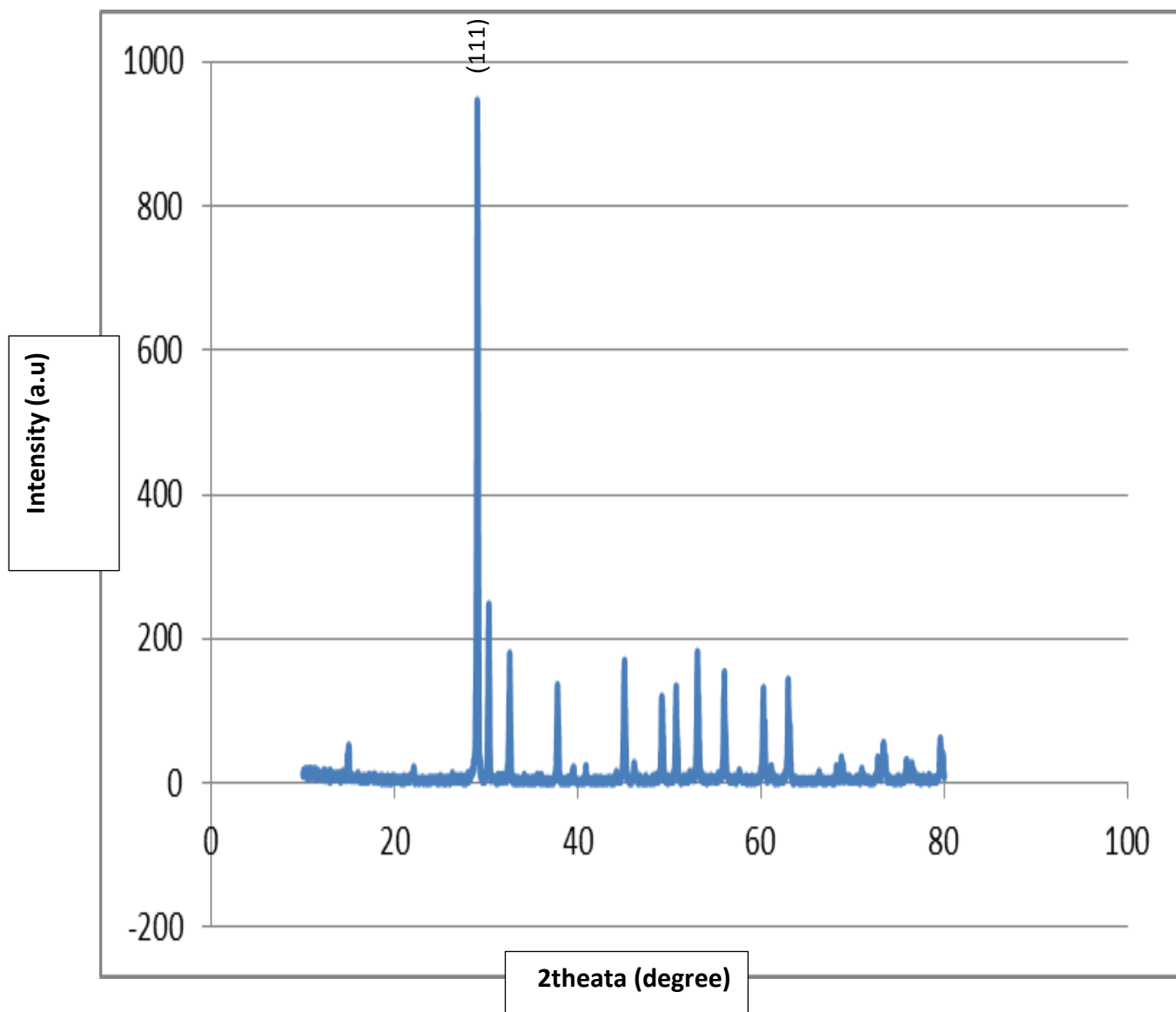


Fig.(3.8) X-ray diffraction pattern for Lead Oxides Chart No(00-038-1477).

PbO

00-038-1477 (Fixed Slit Intensity)					
2θ	d(Å)	I	h	k	l
29.0783	3.068340	100	1	1	1

3.4.2. XRD of copper(Cu)

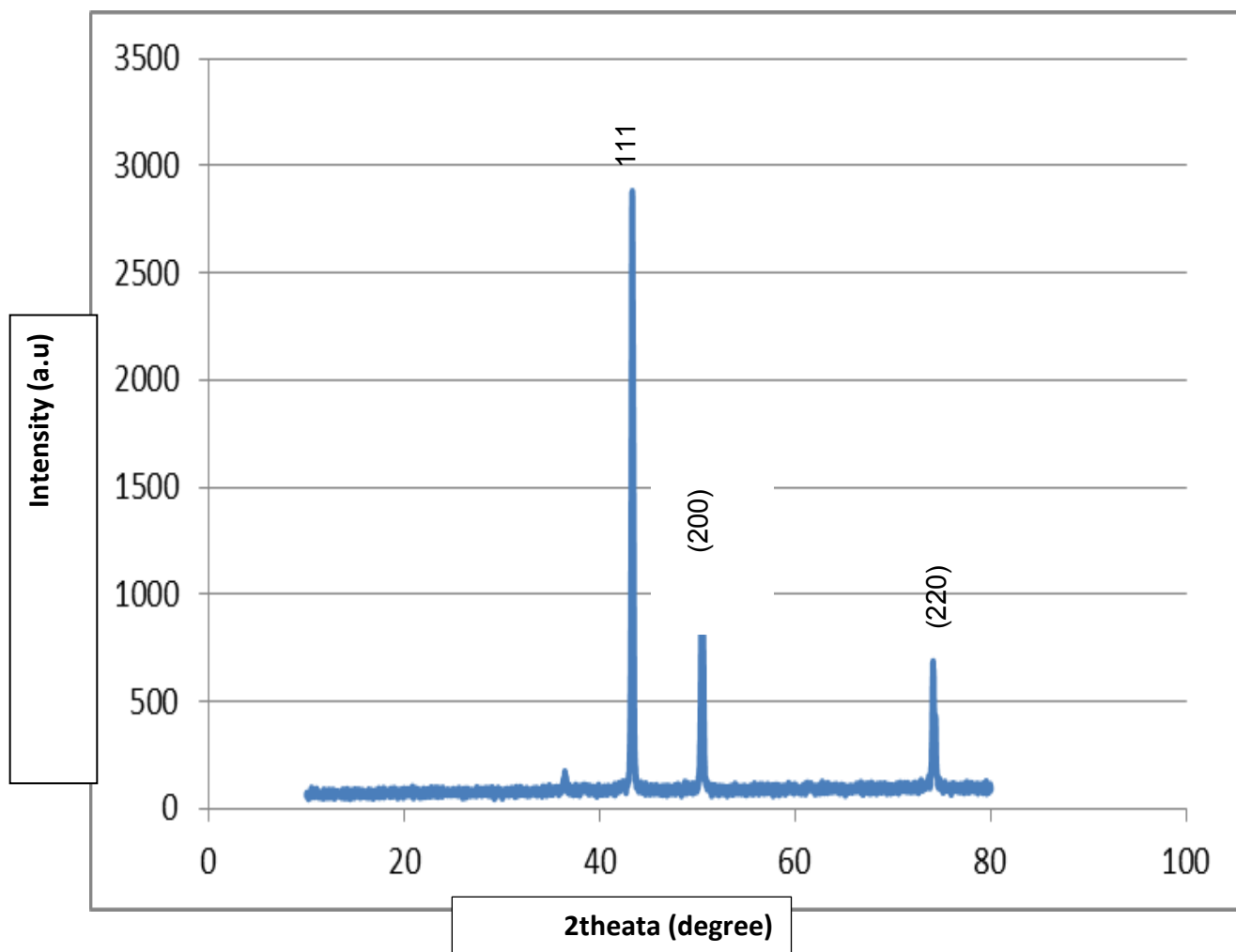


Fig.(3.9) X-ray diffraction pattern for Copper Chart No(00-004-0836).

Cu

00-004-0836 (Fixed Slit Intensity) -

2θ	$d(\text{\AA})$	I	h	k	l
43.2966	2.088000	100	1	1	1
50.4330	1.808000	46	2	0	0
74.1303	1.278000	20	2	2	0

3.4.3. XRD of Silver (Ag)

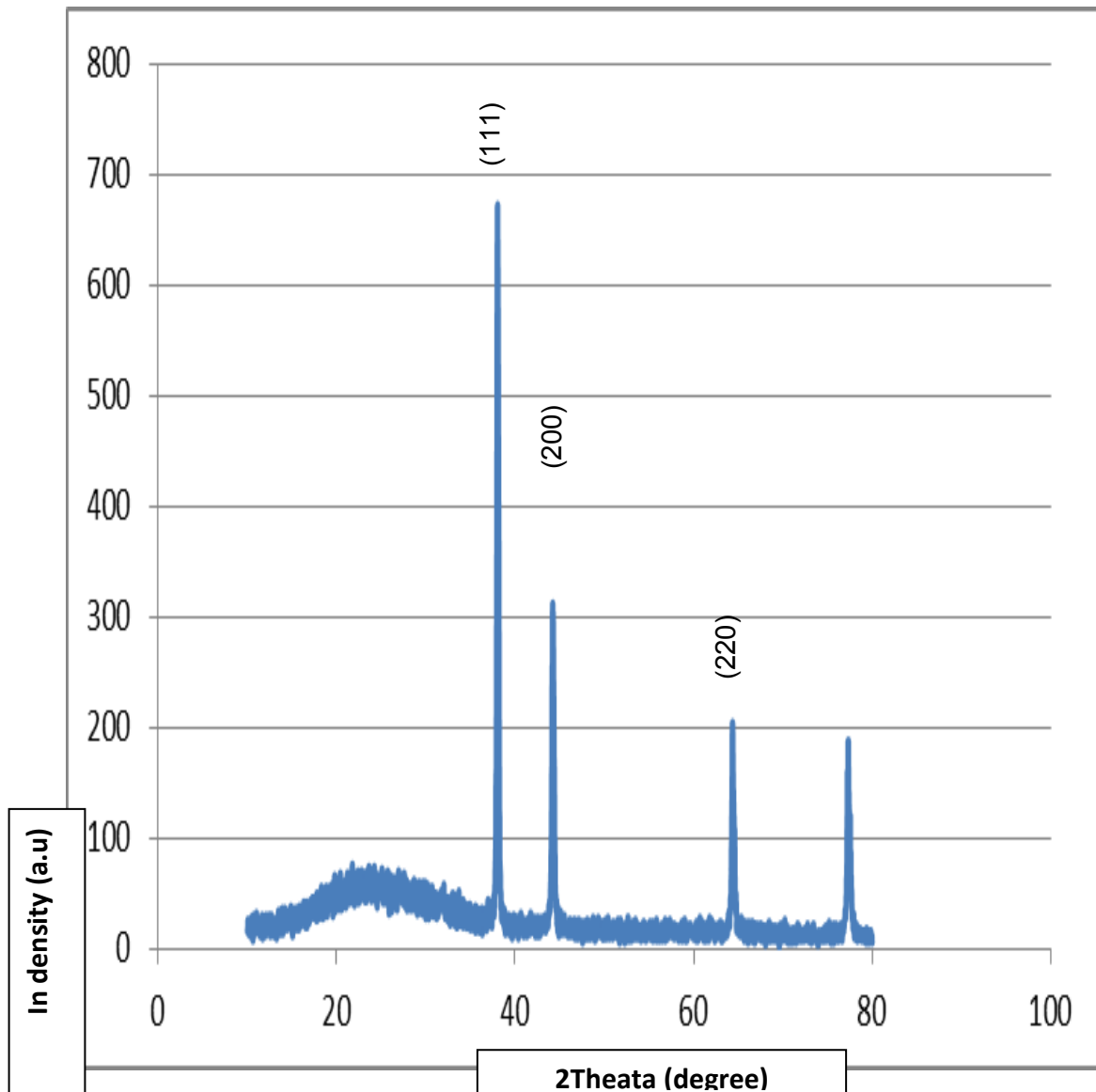


Fig.(3.10) X-ray diffraction pattern for silver Chart No(00-004-0783).

Ag

00-004-0783 (Fixed Slit Intensity) -

2θ	$d(\text{\AA})$	I	h	k	l
38.1164	2.359000	100	1	1	1
44.2773	2.044000	40	2	0	0
64.4257	1.445000	25	2	2	0

Chapter four

*Result and
Discussion*

4.1 Introduction

This chapter includes the results of the structure and optical properties of PbOCu and PbOAg thin films fancied with different Cu and Ag concentration.

4.2. X-ray diffraction of PbO /Cu and PbO/ Ag nanoparticles

The spark of plasma formation emitted light and cracking noise, the started solution was colorless and it changes to yellow within a few minutes, indicates the formation of Nano sized particles with some concentration.

During the preparation of PbO/Cu and PbO/Ag thin films using PLAL, the laser pulse hit the target surface that immersed in liquid, and the plasma plume will appear around the surface of the target.

X-ray diffraction patterns were used to investigate the structural properties of the prepared thin films figure (4.1) show that the prepared films demonstrate as polycrystalline tetragonal structure of PbO₂ (ASTM data card 00-041-1492). Important changes, detected in the X-ray diffraction spectrum, noticeable themselves by increasing of peak intensity in crystal. From fig4.1. The peak positions of the planes attributed to PbO₂ phases were shifted to lower 2θ values with increasing the amounts of Cu content. Compared to pure PbO pattern where the main peaks located at angle 2θ= 34.2569° and 23.6737°, Cu 20% peaks of diffraction were situated at 2θ= 34.1587°, Cu 50% addition the diffraction peaks positioned at 2θ=34.3785° and 22.5861°, with Cu 75% peaks of diffraction were located 2θ=34.0688° and 23.7535°, and for Cu85% diffraction peaks were located at 2θ= 34.1487° and 21.9077°.

Another phases related to Pb(Cu₂O₂) nanoparticles (card number 96-153-5316) were detected at 2θ=16.71°,27.40°,33.67° and 43.93° with reflected planes of (111),(220),(222) and (420)respectively. It can be noticed from fig.1 that there was a in the broaden (full width at half maximum) value with increasing the copper. Concentration For a pure (PbO) thin films the peak located at 2θ= 23.6737° has FWHM

0.32000, Cu 75% at $2\theta=23.7535^\circ$ $2\theta=22.5861^\circ$ FWHM 1.50000. Furthermore, PbO pure nanopartecles at $2\theta=34.2569^\circ$ FWHM 0.77670, Cu 20% $2\theta= 34.1587^\circ$ FWHM 1.32000 and Cu 50% $2\theta=34.3785^\circ$ FWHM 1.04000. This broaden in the FWHM is mainly attributed to the lattice mismatch between the lead oxide and copper metal. Fig.2 represents the XRD pattern of the $PbO_{1-x}Ag_x$ thin films.

The peaks of $2\theta=29.06^\circ$, 34.19° and 48.19° are attributed to Ag_2PbO_2 with relative repletion planes of 121,130 and 12-3 respectively. The Peak positions of PbO_2 shifted to lower 2θ values with increasing the of Ag content. For Ag 15% diffraction peak was located at $2\theta=34.18^\circ$, Ag 20% $2\theta=34.13^\circ$ and Ag 50% $2\theta=34.14^\circ$.

On the other hand, fig.2 revealed the broaden decrease with increasing silver metal addition. At $2\theta=34.18^\circ$ Ag15% FWHM 0.41 and at $2\theta=34.14^\circ$ Ag 2% FWHM 0.37. These results conformity with Adawiya J. Haider[124]. Which that mean the produced crystal composition was affected due to the replacement of the Ag ions (1.28\AA diameter) were substituted into the Pb^{+} (1.23\AA) in the lattice of PbO_2 film. The broadening of Bragg peak is combined of both instrument and tasted sample dependent effects ,i.e, crystal faultiness and distortion for strain induced peak broadening .

It be illustrated from XRD analysis of prepared film there is increase in the peaks intensity (I) at a mainly strongest angle $2\theta\sim 34^\circ$ with decrease Ag concentration (I reached maximum for Ag50% and Ag30%) due to formation scattering factor is depending on atomic number (Z) (atomic number of lead higher than that of silver) also, may be assign to diffraction peaks angles PbO_2 nanoparticles phase identified with phase Ag_2PbO_2 compound nanoparticles in prepared film.

4.3. Indexing of X-ray diffract pattern

There are two methods of indexing structure mathematical and analytical. In this work the produced predominating structure is tetragonal of PbO film with various

concentration of copper and silver. A relative is developed by scrutinizing plane spacing equation and equation of Bragg's law, which deiced the Miller indices of some particular crystal system for a tetragonal system.

Using Match software which depending least square it can be calculated lattice constants a and c for all the samples which are listed in table 1. It can be explain this parameter are decreased with increase in Cu concentration in $PbO_{1-x}Cu_x$ film, These variations may be owing to smaller of ionic radius for Cu^{2+} (0.57\AA) than that of Pb^{2+} (1.23\AA) [9]. Volumes of unit cell for all the samples are also listed in Table 1. ascribable by decreasing tendency of lattice constant parameters ' a ' and ' c ', the volume for the unit cell are similarly decreased with increasing Cu contents, as stated previously [115-117]. Furthermore, table was clarification lattice constants ' a ' and ' c ' for all the prepared samples $PbO_{1-x}Ag_x$ are increased with increase in Ag concentration, which attributed to larger ionic radius of Ag^{2+} than that of Pb^{2+} . Subsequently, volumes of Unit cell of all the samples are also increased with increasing Ag contents. [116]

Table 1 has been obvious behavior of crystallite size, it can be deduced for synthesized $PbO_{1-x}Cu_x$ film the crystallite size decrease with increasing Cu doping with enhanced crystallinity.

A similar trend was previously observed [114]. It was basically due to the replacement of the Cu ions were substituted into the Pb^{2+} in the lattice of PbO_2 film. Moreover, crystallite size increase with increasing Ag doping in $PbO_{1-x}Ag_x$ film, refer to substituted Ag ions larger than that ions Pb^{2+} in the lattice of PbO film.

The Rietved method is a well-known technique for deducing structural details from powder diffraction information [116].

This method was established based on least-squares fit step-scan data of an examined diffraction pattern and a simulated X-ray-diffraction (XRD) pattern. In this study, the crystalline structure of the PbO/Cu and $PbOAg$ tetragonal was scrutinized in

detail by the refinement Rietveld profile process in reflex module (Fig. 3 and 4). Patterns of XRD for these synthesized samples have refined employing the space group $P4n2n$. The refinements of Rietveld method allowable the determination of the parameters of lattice and crystal structural. The profile parametric for the function of pseudo-Voigt were utilized to define the shape of the diffraction peaks and the refinement of structure was carried out by contemplating the PbO structural assumption. In the $P4n2n$ space group of tetragonal structure.

Profile of peaks was defined with the function of (Thompson-Cox-Hasting) for our samples. Fig4.3 and Fig4.4 are give a relationship of the experimental and calculated patterns of XRD for the samples Cu6 and Ag6.

The superior agreement between the calculated and observed profiles was measured by adjusting the of conventional factors. Two sets of index were calculated in FullProf, conferring to the meaning of N integer. The first set N was the whole number for points which used in the process of refinement. In second set merely individuals points where are Bragg donations are taken into account.

χ^2 lesser than 2 was reflected a fine analysis, so we have made a very good analysis for synthesis samples. Several R factors Reliability factors are tabulated in Table4.2. The values of R factors like R_p were found to be high. Similarly, high values of R factors for materials of nanocrystalline have been detected by the other authors [117,118]. This might be due to the high noise to-signal ratio of XRD for nanocrystalline materials.

Nevertheless, It is noted a low value of (goodness of fit) χ^2 which condemn the goodness of analysis refinement. Diffraction data pattern for nanocrystalline materials, diffuse scattering is governing than in individuals for crystalline materials bulk, and it was owing to the large ratio of volume atoms to surface. Diffuse scattering come to be substantial at the nanoscale whereas scattering of Bragg gets reduced which leads to weakening in crystallinity and high R factors.

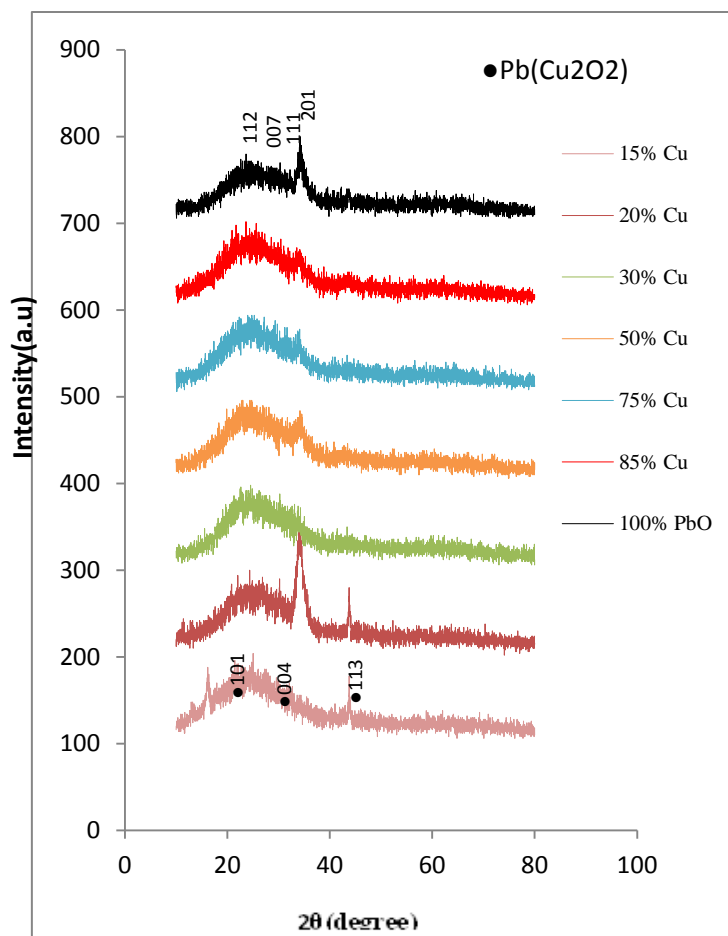


Fig.4. 1 XRD pattern for prepared PbO/Cu film

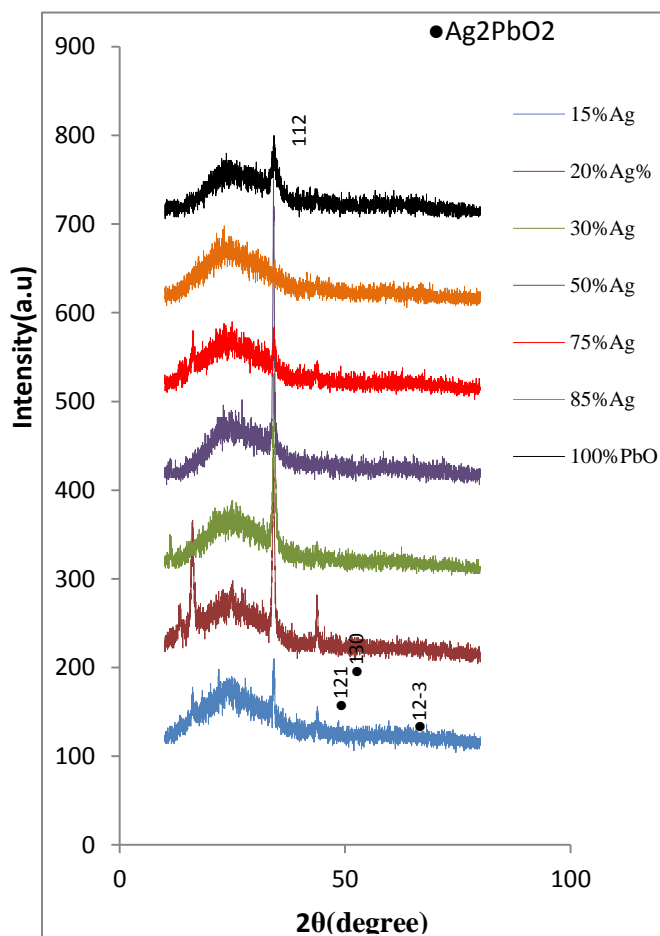


Fig.4. 2 XRD pattern for prepared PbO/Ag film

Table 4.1 structural parameters for the synthesized thin films PbOCu and PbOAg at different Cu and Ag concentration.

sample	Con %	Lattice constants		Volume (Å ³)	crystallite size
		a	c		
PbO	100	3.48760	8.64300	105.128	27.7390
C1	15	4.02738	11.5878	187.952	13.0670
C2	20	3.83678	10.6892	157.350	11.3096
C3	30	3.81565	10.5574	153.707	10.7054
C4	50	3.79751	10.0112	144.372	7.30976
C5	75	3.78023	11.1616	159.500	14.8639
C6	85	3.76614	11.1172	157.684	12.8825
A1	15	5.83331	10.2501	348.785	20.2131
A2	20	5.89770	10.2173	355.387	16.5170
A3	30	6.09760	10.0857	374.993	19.6997
A4	50	6.11211	11.1031	414.787	57.8761
A5	75	5.86600	11.3731	391.348	12.0439
A6	85	5.72496	11.9012	390.063	20.1660

Table 4.2 Reliability factors for PbOCu and PbOAg thin films

Sample	Con %	R _p	R _{wp}	R _{exp}	GoF-index	Phase	Space group
Cu	85	15.1	20.0	17.6	1.1	Tetragonal	-p 4n 2n
Ag	85	16.1	20.4	17.5	1.2	Tetragonal	-p 4n 2n

Table 4.3 Crystallite size of thin films PbOCu and PbOAg of SEM and TEM techniques.

Sample	crystallite size(nm)	crystallite size (nm)
PbO	40.7844	--
C1	39.9627	--
C6	36.4186	12.6339
A1	40.5421	--
A6	37.2877	9.1624

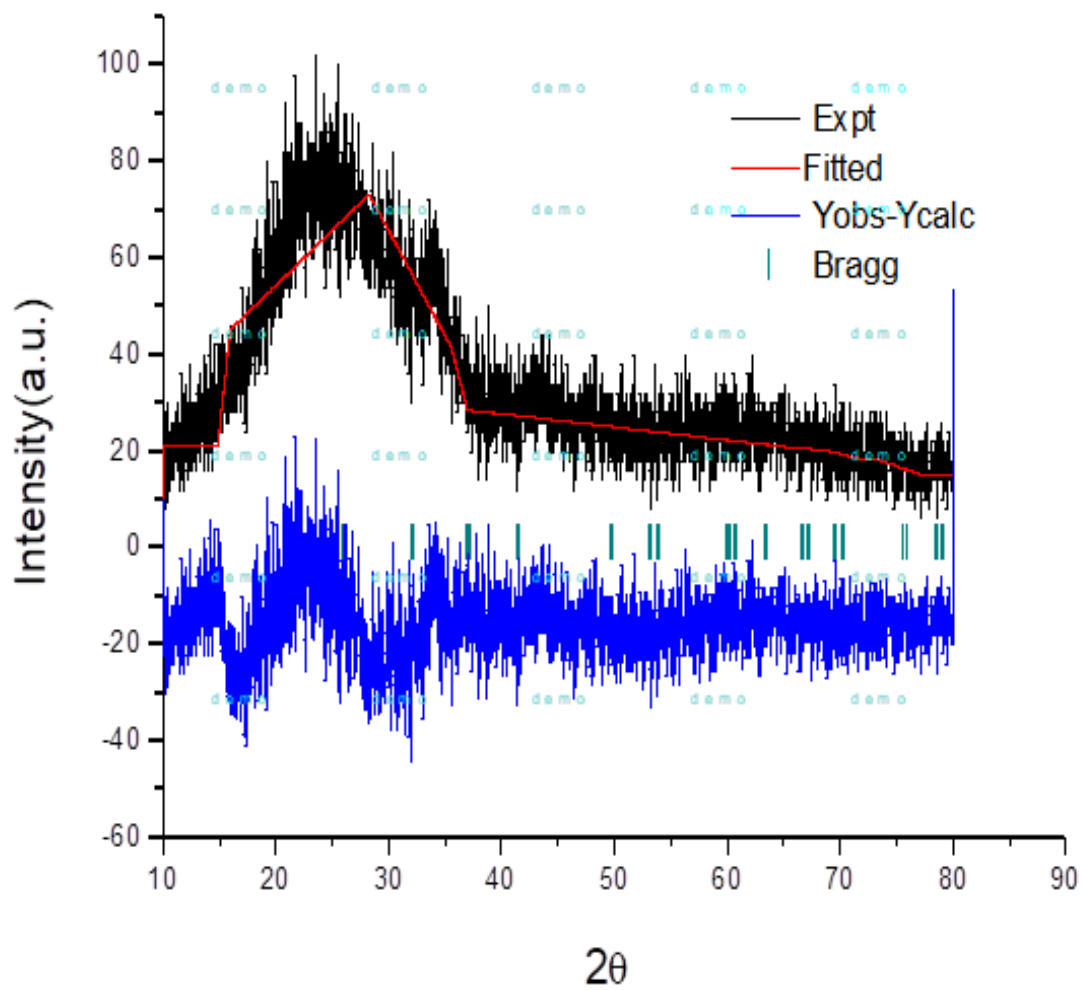


Fig.4.3 Riveted method for pattern of 85% Cu doped PbO thin films XRD.

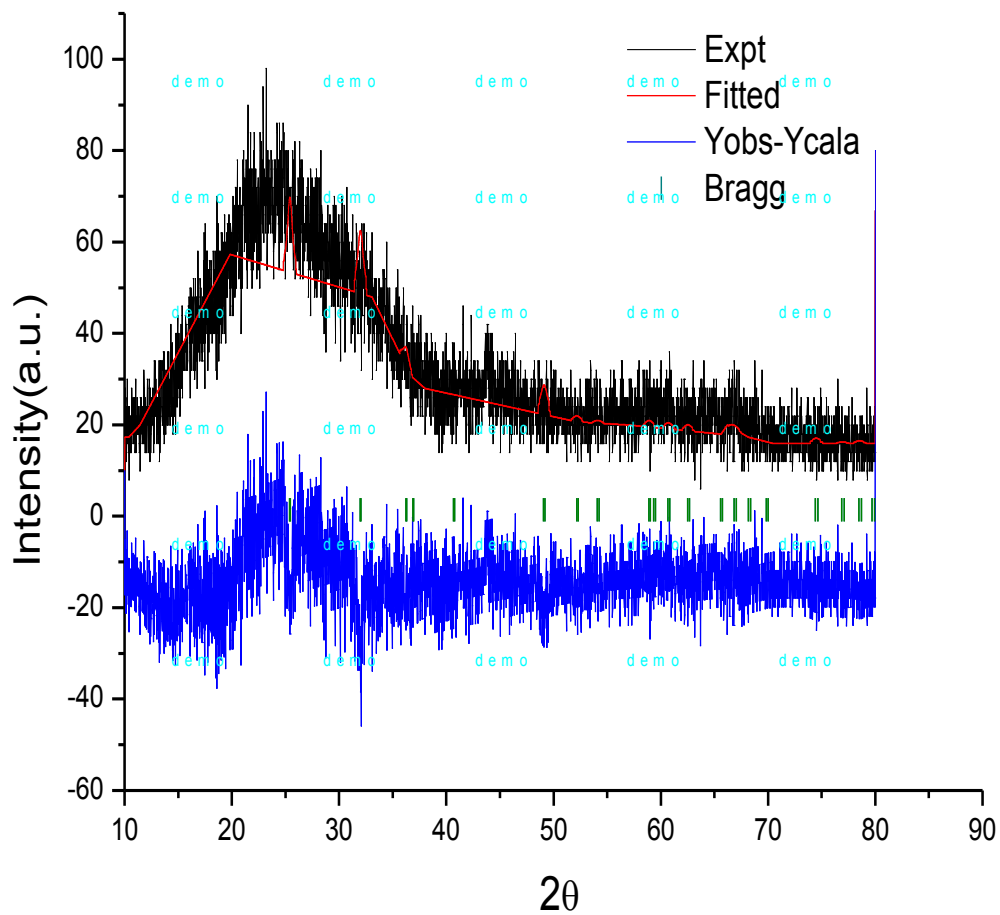


Fig.4.4 Riveted method for pattern of 85% Ag doped PbO thin films XRD

4-4. Morphology of PbO/Cu and PbO/Ag nanoparticles Composites

4-4-1. Scanning electron microscopy (SEM)

SEM Images were employed to define and characterize the influence of the synthesis parameters like, laser pulses number, laser energy, and nature of liquid medium on the morphology of synthesized nanoparticles and their size distribution. Fig4.7 displays the SEM images of deposited samples. The morphology of the samples is homogeneous, with a mesh-like structure of with nanoparticles with spherical shapes. Pure PbO, $\text{PbO}_{1-x}\text{Cu}_x$ and $\text{PbO}_{1-x}\text{Ag}_x$ thin films prepared with various concentrations (15-85wt %), using (PLAL) are designated with dynamical development mechanisms of diffusion or amalgamation processes [115]. Construction of sphere -like (Cu and Ag)-doped PbO nanoparticles may be attributed to two processes describing the nanoparticles growing [113].

First the ions from plasma plume may control the nanoparticles growth .Second the growth of nanoparticles via PLAL is set through the energy of surface for the compose crystals with different orientations which could be resulted in favored formation of nano sphere. Furthermore, temperature and pressure are used may to induce the 2D anisotropic growth in addition to, the high nucleation of temperature.

Size and particle distribution of the deposited films were examined and quantified by visual basic software using several SEM images. Fig4.6 show the histogram figures of area distribution of pure PbO, $\text{PbO}_{1-x}\text{Cu}_x$ and $\text{PbO}_{1-x}\text{Ag}_x$ thin films prepared various concentrations (15-85wt%), It is cleare from fig 6 that the average particle size of Ag NPs is around 37-40 nm, and for Cu NPs is 36-39nm.

Nanoparticles which produced from gaseous phase what is the instance in nanoparticles synthesis procedures by PLAL.

It put on at whatever time particle growth be subject on atoms which diffusion and drift to a growing for nanoparticles. Final dispersal is determined with the obtainable time of growing for nanoparticles. In our study during PLAL the targets were stirring in order to evade drilling and probable effects of heating. Generally, the crater effects the size of particle (volume resembles to number of employed laser pulses).

The dependence of the particle size of particle on the number of laser pulses could be ascribed to heating the target due to increasing the during PLAL. Therefore the threshold energy of the ablation decreases along with the ablation rate and thus ablated species density in phase of gaseous.

. As for the dependency of volumes for craters and intensity of photo absorption on number of functional laser pulses such deduction might not be appear because of volumes and photo absorption will increase exponentially with the pulses number rather than linearly. More-likely situation was that on laser ablation the craters will be larger and deeper. Thus, the ablated material enclosed by its walls and do not have much area to disperse around.

Once laser pulse strike onto a target, a dynamic plasma plume containing atoms, ions and molecules is formed and developed. Formation of particles can be designated with mechanism of dynamic formation [112-116]. From the plume of plasma which contains rapid growth (formation initial stage) of clusters in laser of plasma plume which that are nuclei for additional slow growth (formation of intermediate stage) owing to diffusion of particles in the neighborhood of the clusters. Additional coagulation and coalescence, if growing is not influenced by the surfactants, takes place (formation late stage) conducting to the probable the agglomerations and precipitations. If the growth of particles from phase of gaseous was spatially limited, this increases the probability for the surrounding particles diffusion to the neighborhood of embryologic

particles, which lead to formation of larger nanoparticles at final stage of the growth. In other words, the length of diffusion for gaseous particles (Pb, O, Cu and atoms and ions) to the embryologic particle was smaller. It is expected that larger nano particles were created in deeper craters owing to higher density of gaseous material ablated in spatially limited volume included in nanoparticles growth (higher possibility for growth of larger nanoparticles).

The elemental of composition for the nanoparticles was performed by energy dispersive X-ray spectroscopy (EDS). It was well-known which that ablation of laser in such range of high pulse energy permit for ablation stoichiometric, the stoichiometry for bulk was mirrored into stoichiometry for ablated of plasma for plume (more nanoparticle growing takes place).

It can be noted from the EDX spectrum in fig 4.6 , signals for lead, copper, silver and oxygen are appeared with different percentages which listed in table 4.3 shown in the inset of fig4.5. It show that there is a elevating of the percentage of the oxygen in the prepared samples of deposited films. This might occur for the reason that more oxidization of (Pb, Cu and Ag) as the plasma ion containing excitation energy within laser energy. Another reason can be catching of more atoms oxygen interior increasing of the grain boundary. In other word, there are assigning to chemisorbed of oxygen ions, which matching the results of the study .

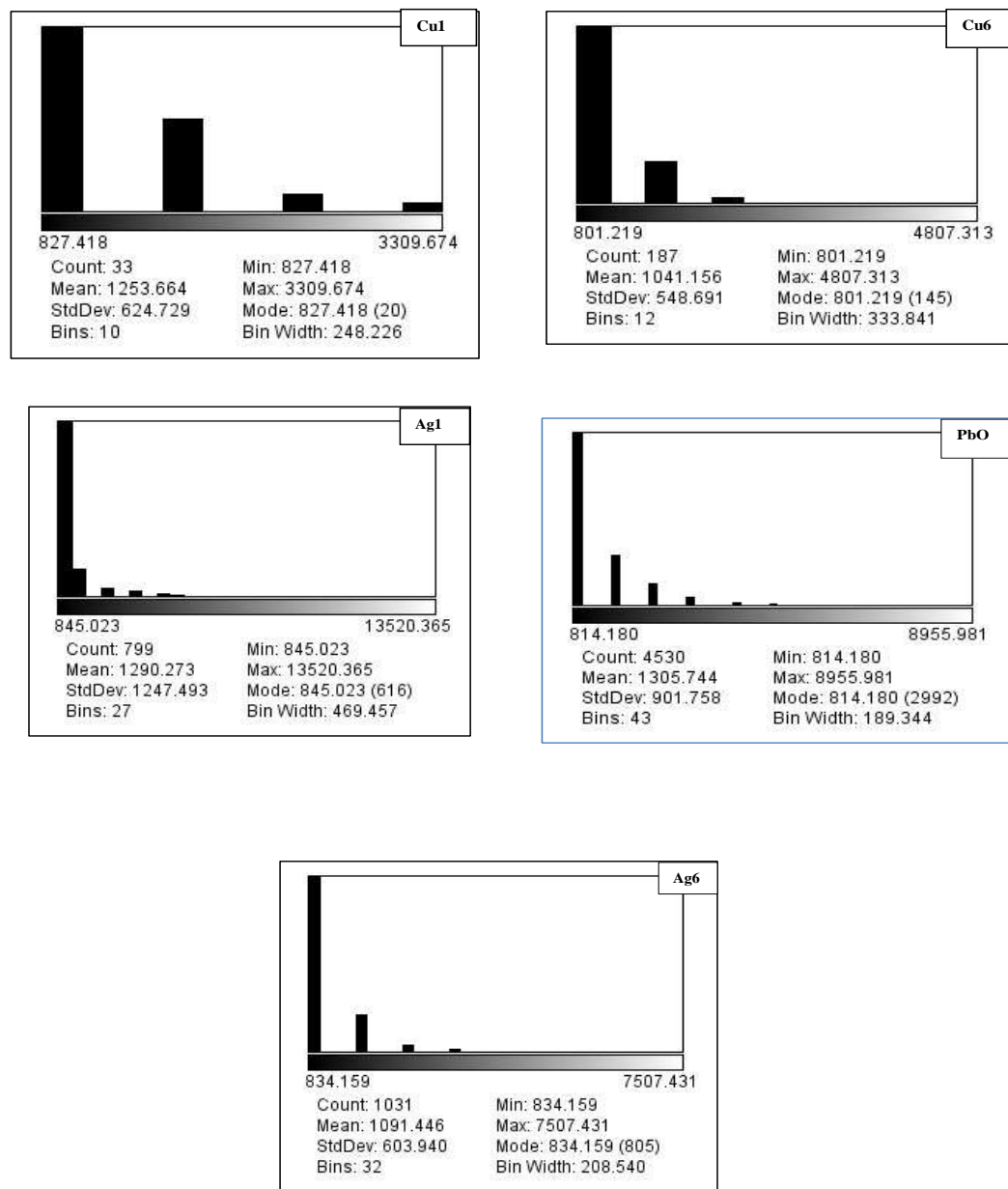
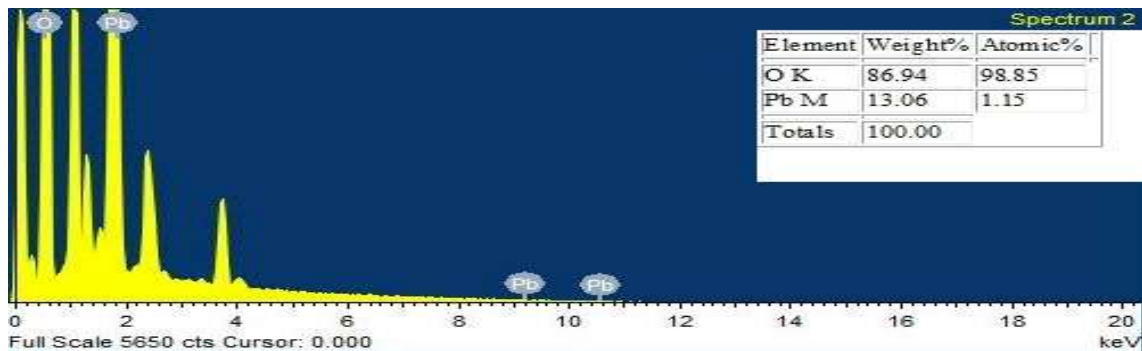
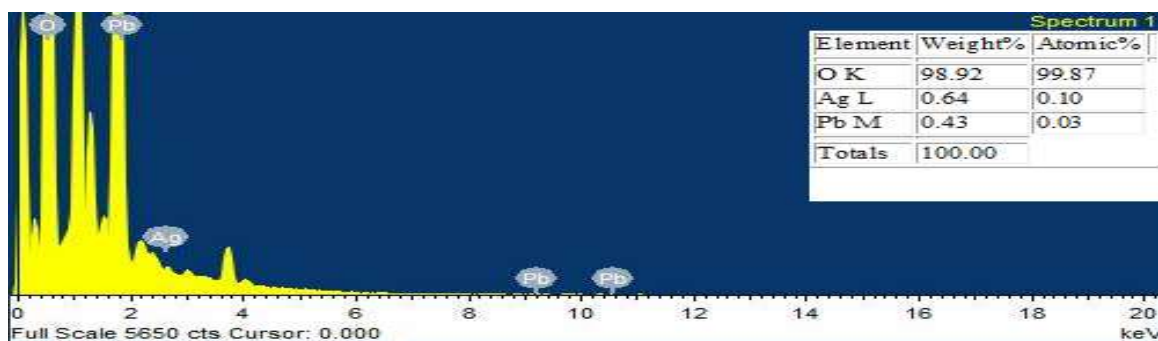


Fig.4.5 Statistical area distribution of synthesized nanoparticales from SEM

(a)



(b)



(c)

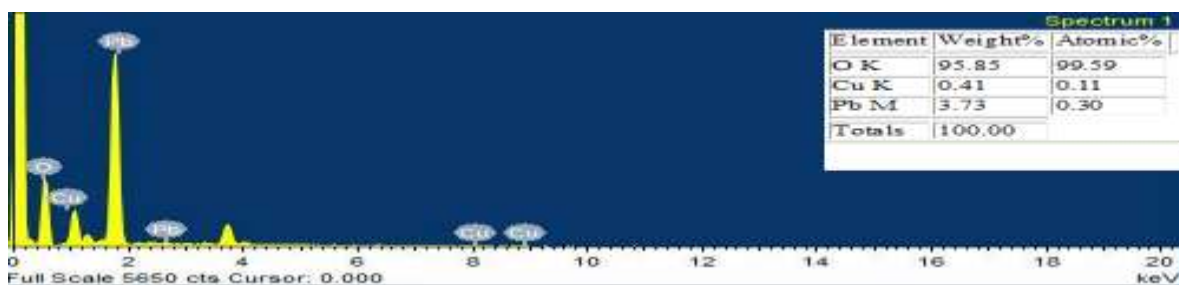


Fig.4.6 EDX spectrums for pure (a)PbO, (b)PbO/Ag and (c)PbO/Cu.

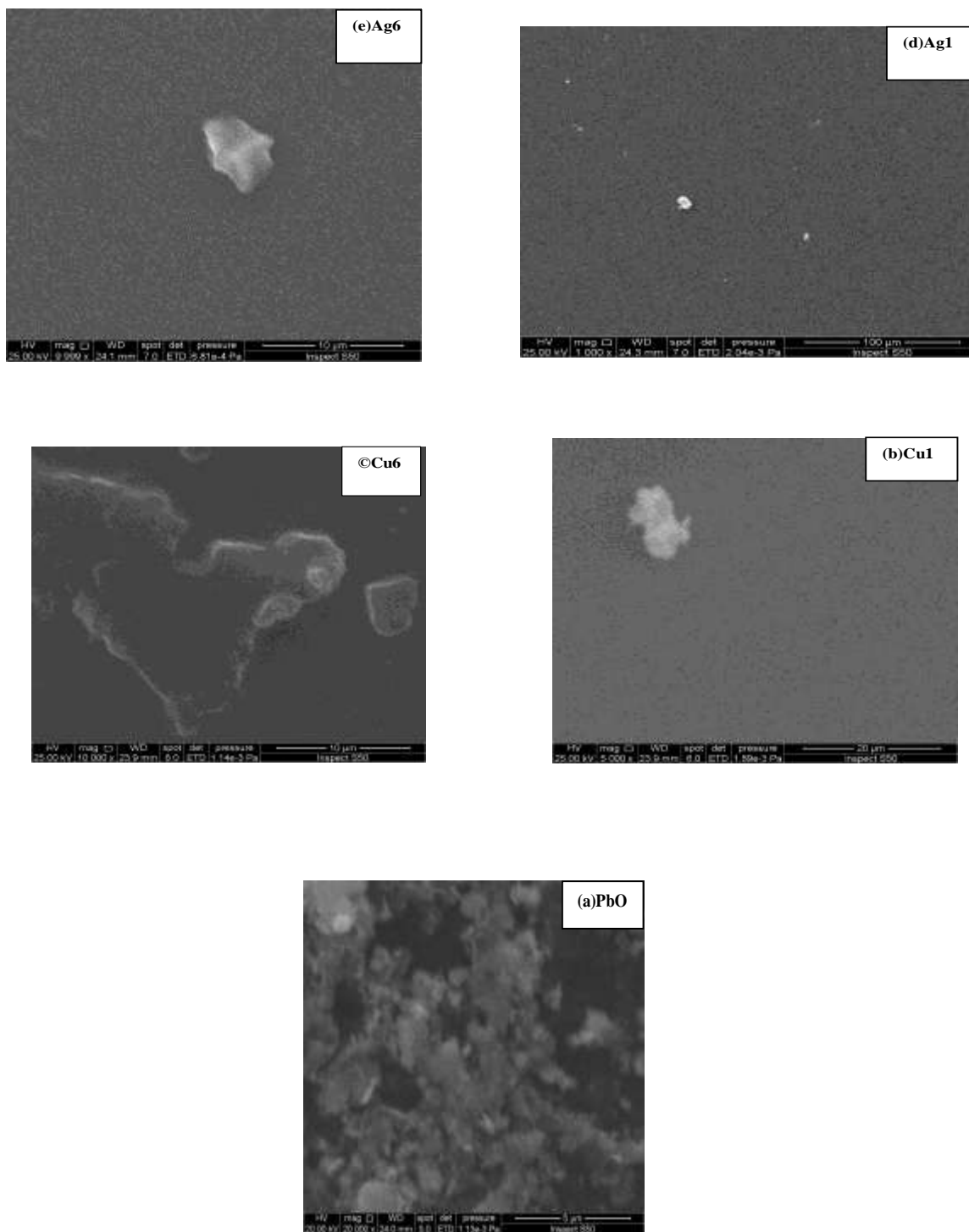


Fig4.7 SEM images for prepared PbO , PbO/Cu and PbO/Ag thin films.

4-4-2. Transmission electron microscopy (TEM)

Fig.10 shows the micrographs of TEM images of the doped suspensions Nano colloidal of PbONPs, doped with a fixed Cu/Ag concentrations ($x=85\%$) obtained by PLAL in DI water. The particle size distribution as shown in fig.4.8 and 4.9 for Ag and Cu doping respectively. From these images, the average particles size for Ag NPs is around 9.163nm, and for Cu NPS is 12.6339nm as listed in table3.

Spherical and small amount of non-uniform shapes of nanoparticles, with homogeneous structure and no agglomeration were detected which may attributed to the ultrasonic process before the analysis. Thermal evaporation is the ablation mechanism related to pulsed laser ablation of prepared target in liquids using a nanosecond pulsed laser. During PLAL pulse laser ablated in medium liquid, the both laser beam wavelength and liquid medium influence the kinetics of nucleation and growth of nanoparticles leading to the formation of nanoparticles with different morphologies, size, and structure. For a given target material and laser parameters, particle were generated depends on the index refractive of the liquid surrounding at given laser wavelength. Lesser reflectivity for laser at the interface of solid - liquid enhances the ablation rate, while absorption of laser by the liquid diminishes the ablation rate. Also, the growth procedures might be influenced by the liquid medium such as physical properties and at that point nanoparticles with dissimilar morphologies, size, and structure can be resulted. It is stated that greatly polar molecules lean towards to form layers of electrical double on the surface nanoparticles, stopping their growth, aggregation and then precipitation. Ablation time and can affect the productivity of nanoparticles and the continuous ablation of nanoparticles in the colloids can end with laser fragmentation to finer nanoparticles or melting of the nanoparticles to bigger ones depending on the energy and ablation wavelength [109-101]. In general, fabrication of nanoparticles depends on laser parameters, target material, and the nature of the liquid.

Polarity, viscosity, and refractive index of the liquid at the ablation laser wavelength are important in determining the final size and size distribution.

The decrease in size at higher ablation time can be due to the effect of continuous irradiation of particles in the colloidal solution at high laser energy fluency].But there was an increase in average size with increase in fluency for all the three liquid media. Increase in energy fluency could result in increase in average size of nanoparticles as reported in many cases [108-110,115].

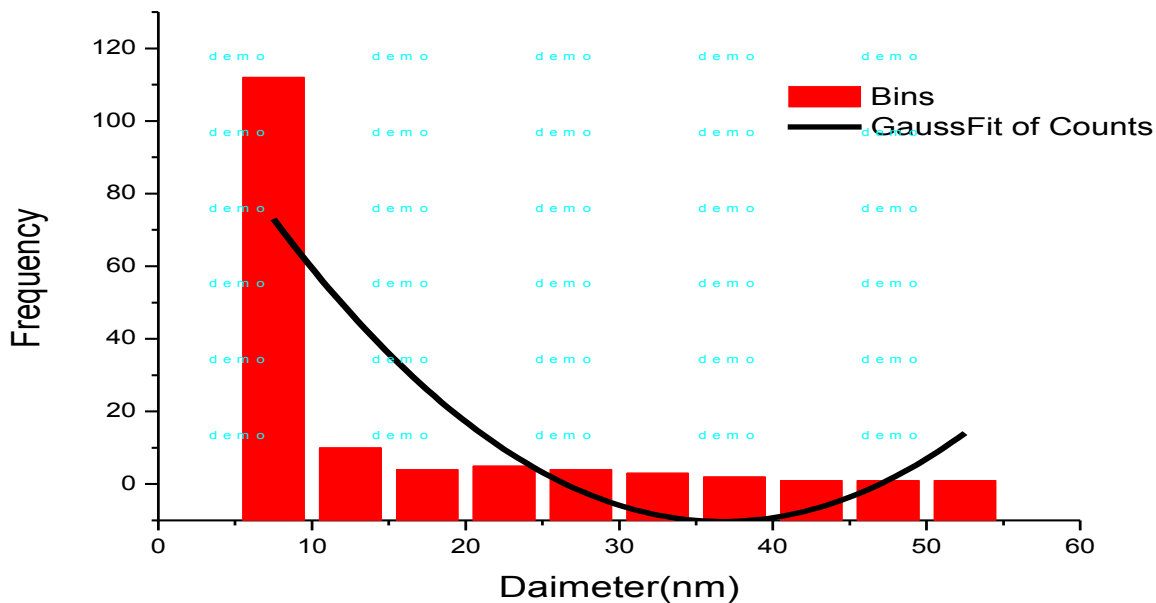


Fig.4.8 A histogram of particle size distribution of 85%Ag doped PbO.

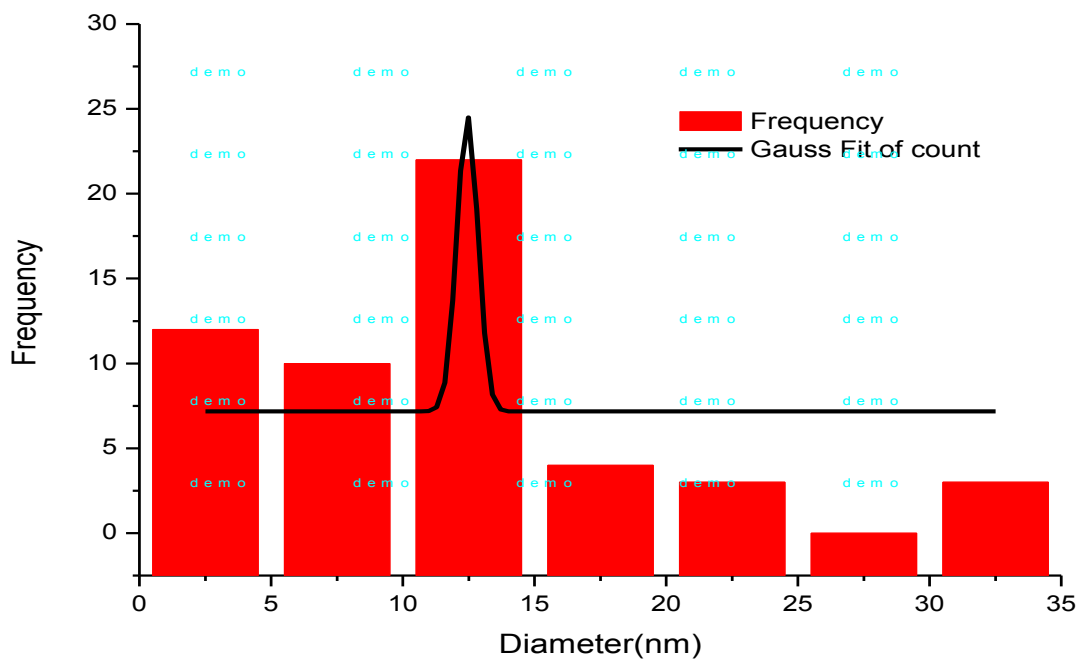


Fig.4.9 A histogram of particle size distribution of 85%Cu doped PbO.

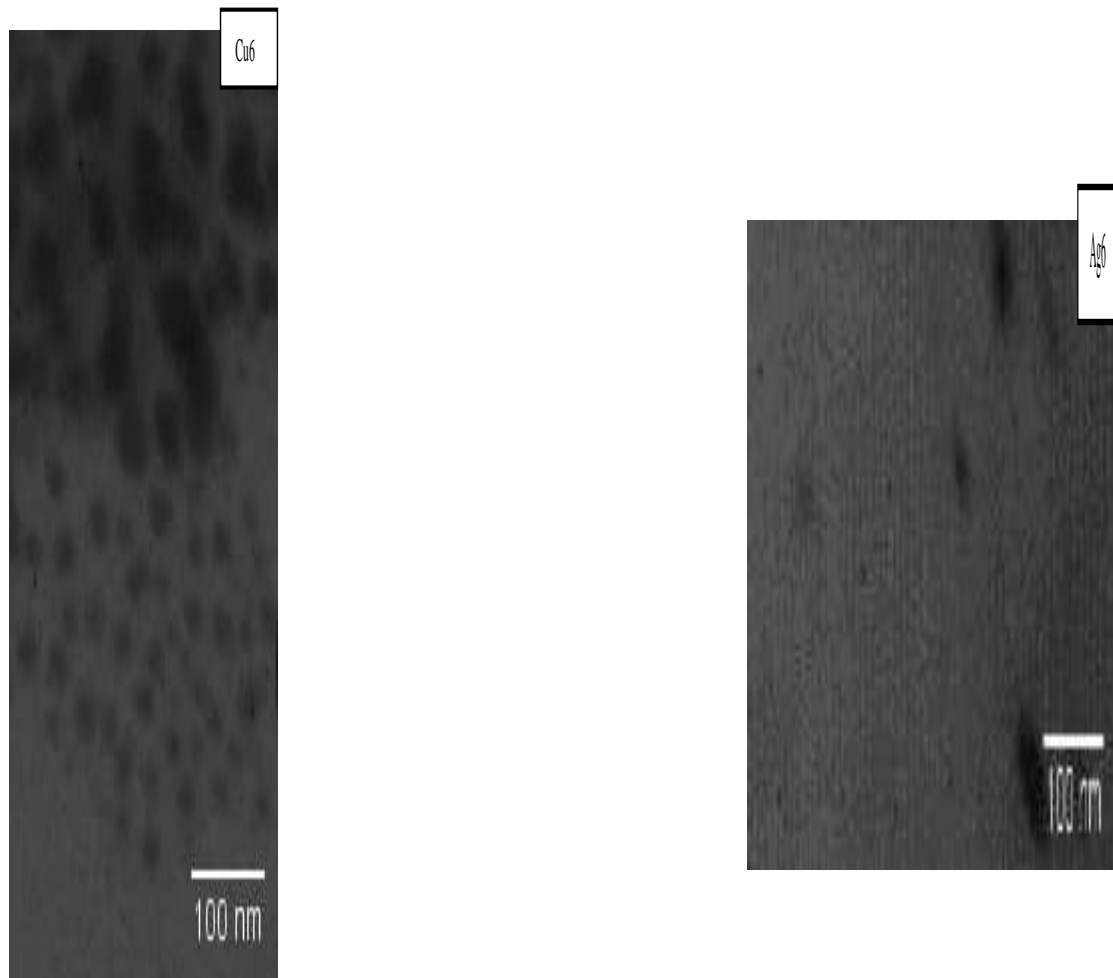


Fig.4.10 TEM images for prepared nanoparticles for PbO/85%Cu and PbO/85%Ag.

4.5. The Optical properties

Fig.11 and 12 show the optical absorption spectrum, of PbO/Cu and PbO/Ag NPs colloidal with different Cu and Ag doping concentration. An average absorption is vary from (0.054-0.96) in the UV-VIS region, that increased as the Cu and Ag content increase. The absorption spectrum reveals low absorbance in the visible and near infrared regions for AgPbO and CuPbO samples. However, absorbance in the ultraviolet region is significantly high and the sample exhibits an obviously enhanced optical absorption around (220-230) nm. This significant increase could be attributed to the Plasmon resonance absorbance of the Ag and Cu nanoparticles, since the noble metals nanoparticles can be photo excited due to their Plasmon resonance. On other word;. all spectra of silver and copper are seemingly made out of a superposition of the original PbO conduction band peaks and a broad peak due to a plasmon band from silver and copper atoms or a cluster of atoms located on the surface of PbO Nano crystals. The Plasmon band formation resulting from fluid like Plasmon oscillations. The results are in good agreement with K S Khashan [120].

This high absorbance in the UV region makes this material important in photovoltaic technology.

On the other hand, the absorption spectrum demonstrates a broad and red-shifted surface Plasmon resonance (SPR) absorption peak for samples. In the range of 240nm for AgPbO and 239nm for CuPbO to 235nm for pure PbO. The appearance of shoulder at arownd 204nm for PbO and around 230nm for AgPbO and 210nm for CuPbO are generally associated with the presence of either oblate spheroid particles or closely aggregated spherical colloids particles that optically behave as oblate spheroids. According to Mie theory[120-122],Thus, the absorption of the nanoparticles is not only simply determined by the nature of the metal itself but also affected by the surrounding

dielectric properties. Generally, the SPR absorption of a pure PbO colloid change as the metal (Ag and Cu) is introduced. The surrounding dielectric properties of PbO thin films change, leading to the observed changes in the SPR frequency of Ag. The tail is may be due to both the scattering of a range of particle sizes and to Urbach effect due to intergrain depletion regions[6]. The extinction coefficient (k) was illustrated in Fig.3 and fig 4 as a function of the wavelength for PbO/Cu and PbO/Ag nanoparticles colloidal with different doping concentration i.e. ($x=15, 20, 30, 50, 75$ and 85% wt%) produced in aqueous solution of DI water respectively.

The extinction coefficient has a red-shift increased in the visible and near infrared regions, while decreased at low wavelength of absorption edge. The extinction coefficient is correlated to the absorption coefficient, when the absorption increased, the, extinction coefficient increased, and it is also increased with Cu and Ag additive. This may be attributed to the extended states (i.e localized states) within both the forbidden energy gap and the conduction band, where the absorption of the photons with long wavelength is increased. At high energies, the absorption is high. This means a high possibility for electron transitions. When the energy of the incident photon is sufficient to move the electron from the valence band to the conduction band.

Fig.14 and 15 show the refractive index (n) for PbOCu and PbOAg thin films prepared with different doping concentration ($x=15, 20, 30, 50, 75$ and 85% wt%) produced in aqueous solution of DI water respectively as a function of wavelength.

The value of the refractive index is increased with decreased photon energy. This indicates that the electromagnetic radiation passing through the material is slow in the low photon energy.

Refractive means bending a beam of light when it enters a material medium. The physical reason for this is that the velocity of light is varied inside the material. The

refractive index is a parameter directly correlated to the density of material. i.e., Less dense of a particular material will have a more open structure and thus a lower (n) value than their denser counterparts. It is obvious from this figure that the refractive index of the synthesized colloidal samples are influenced by increasing the doping percentage, that related to increase the density of structure, Which is a result of increasing the number of atomic refractions due to the increase of the linear polarizability. This is in a good agreement with Lorentz- Lorentz formula [119].

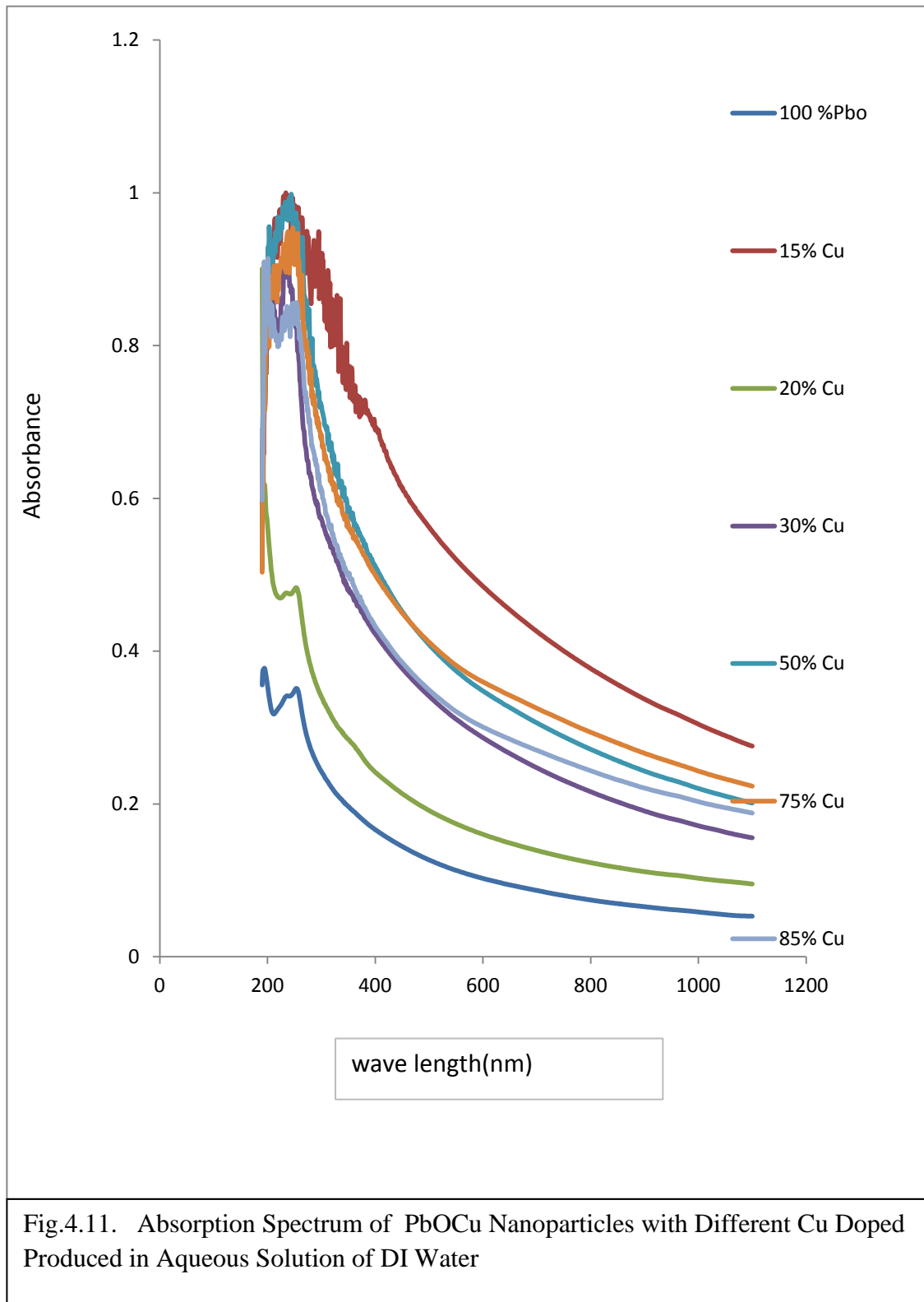
To understand the optical and electrical properties of the thin films manufactured by PLAL method, it is very necessary to study and estimate the average value of the energy gap. This value depends on the films structure and arrangement and the distribution of atoms in the crystal lattice.

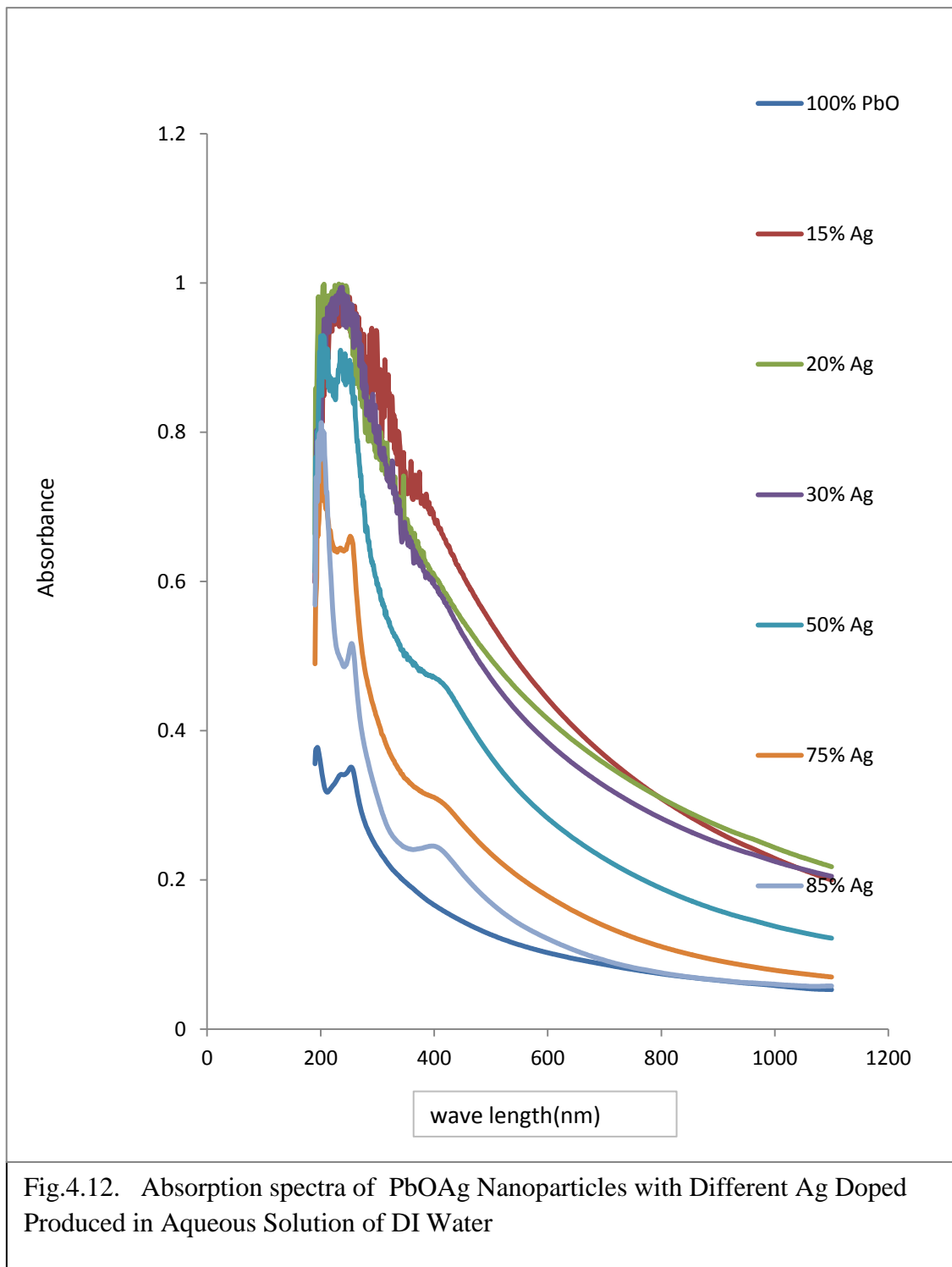
To determine the value of the band gap E_g , the graph of $(\alpha h\nu)^{1/n}$ vs. $h\nu$ has been plotted for different preparation colloidal samples. The optical band gap value represents the point of intersection between the straight line and the axis of the photon energy. E_g band gap of the material and the exponent n depends on the type of the optical transition. For the crystalline semiconductor it is possible for n to be $1/2$, $3/2$, 2 or 3 depending on whether the transitions are direct allowed, direct forbidden, indirect allowed or indirect forbidden respectively. The energy gap depends on the conditions and the nature of the thin film structure and the method of the preparation that affect the crystal structure. The variation in the characteristics of the thin film structure is the reason for these variations in the energy gap.

At high energies with high absorption coefficient values ($\alpha > 10^4 \text{cm}^{-1}$) at high energies we expected direct electronic transitions take place, and the energy and momentum preserve of the electron and photon. At low energies with low values of absorption coefficient is low ($\alpha < 10^4 \text{cm}^{-1}$) at low energies we expected in this case

indirect electronic transition[15].The coefficient absorption for the prepared samples nanoparticles is less than ($\alpha < 10^4 \text{cm}^{-1}$) which indicate indirect electron transitions. The band gap values of the prepared samples are calculated from Tauc plot and listed in Table 1.Lamberts formula was used to estimate the absorption coefficients(α) of the deposited films [120].

Table 3 displays the variation of E_g values with Cu and Ag concentration. It is clear from Table 3 that E_g increases with increasing doping concentration. The red-shift of the obtained band-gaps is likely ascribed to the size and shape of nanoparticles, defects in energy levels, impurities and structural defects. Moreover, UV–Vis spectroscopy showed that doped PbO films exhibit band gap narrowing in both the nano and micro states with respect to the pure PbO films. These results were in good agreement with Chava and Kang and Tang et al.The band gap E_g shifts observed with doping, are due to concentration of majority carriers and changes in nanocrystal electronic structure. With regards to the semiconductor metal transition theory, the E_g reduces when the impurity is higher than the Mott critical density [118]. Hence, doping leads to an obvious narrowing of the band gap. As the doped elements enter the PbO crystal lattices, the localized band edge states form at the doped sites, with a reduction of E_g .[117].





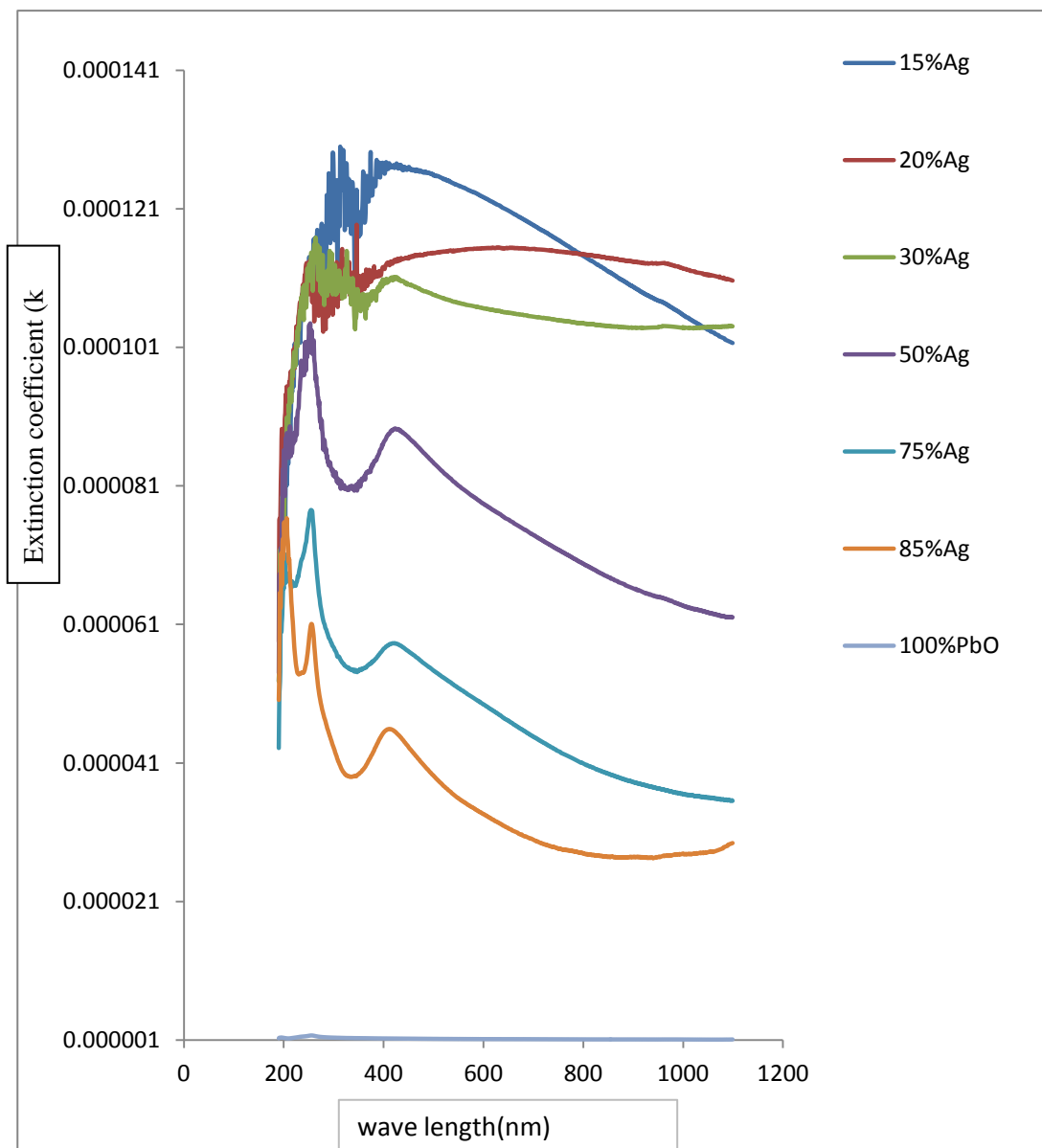


Fig4.13. Extinction Coefficient (k) of PbOAg Nanoparticles with Different Ag Doped in Aqueous Solution of DIW

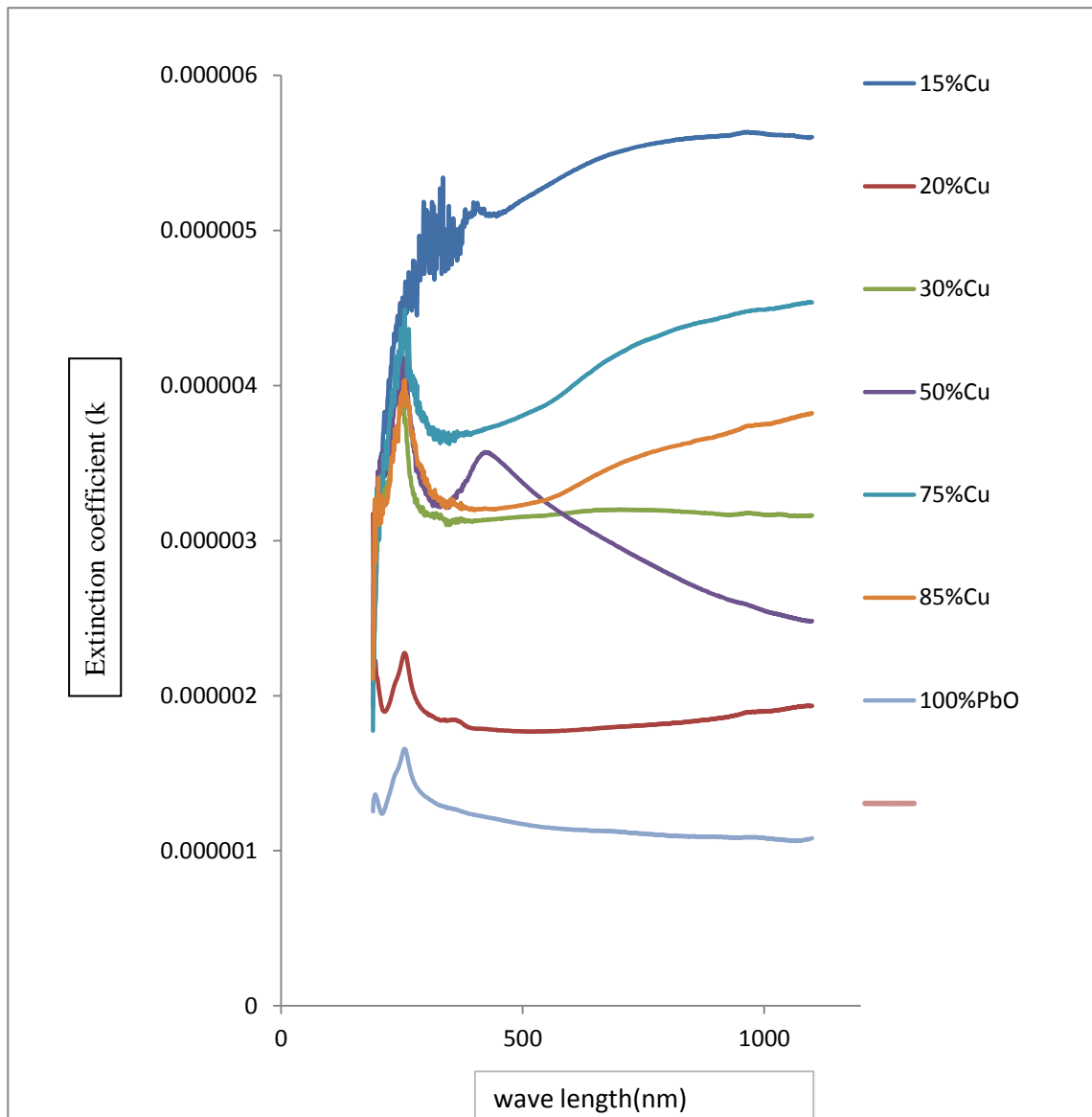


Fig.4.13 Extinction Coefficient (k) of PbOCu Nanoparticles with Different Cu Doped in Aqueous Solution of DIW

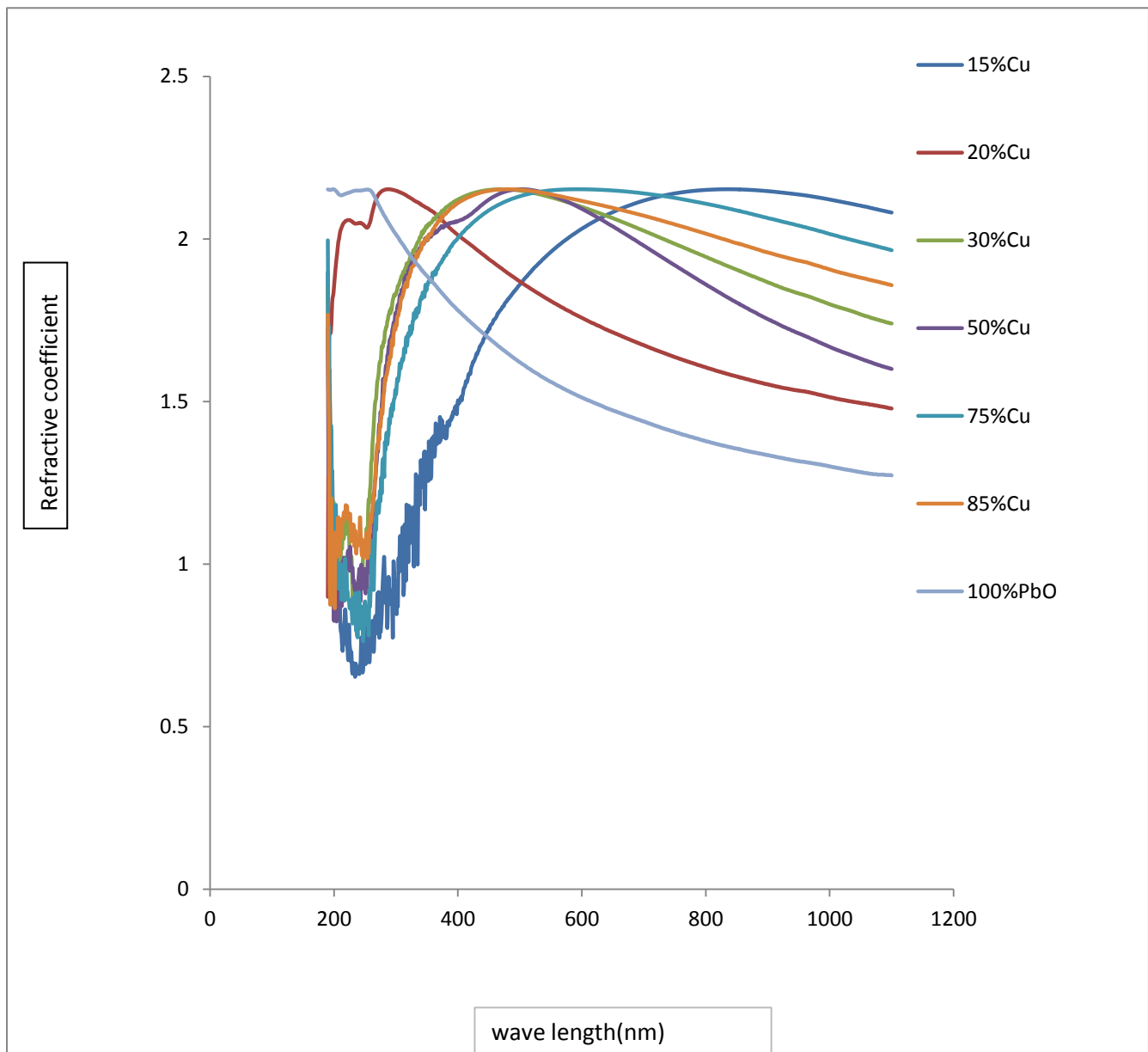


Fig.4.14. Refractive Index (n) of PbOCu Nanoparticles Colloidal with Different Cu Doped Produced in Aqueous Solution of DIW

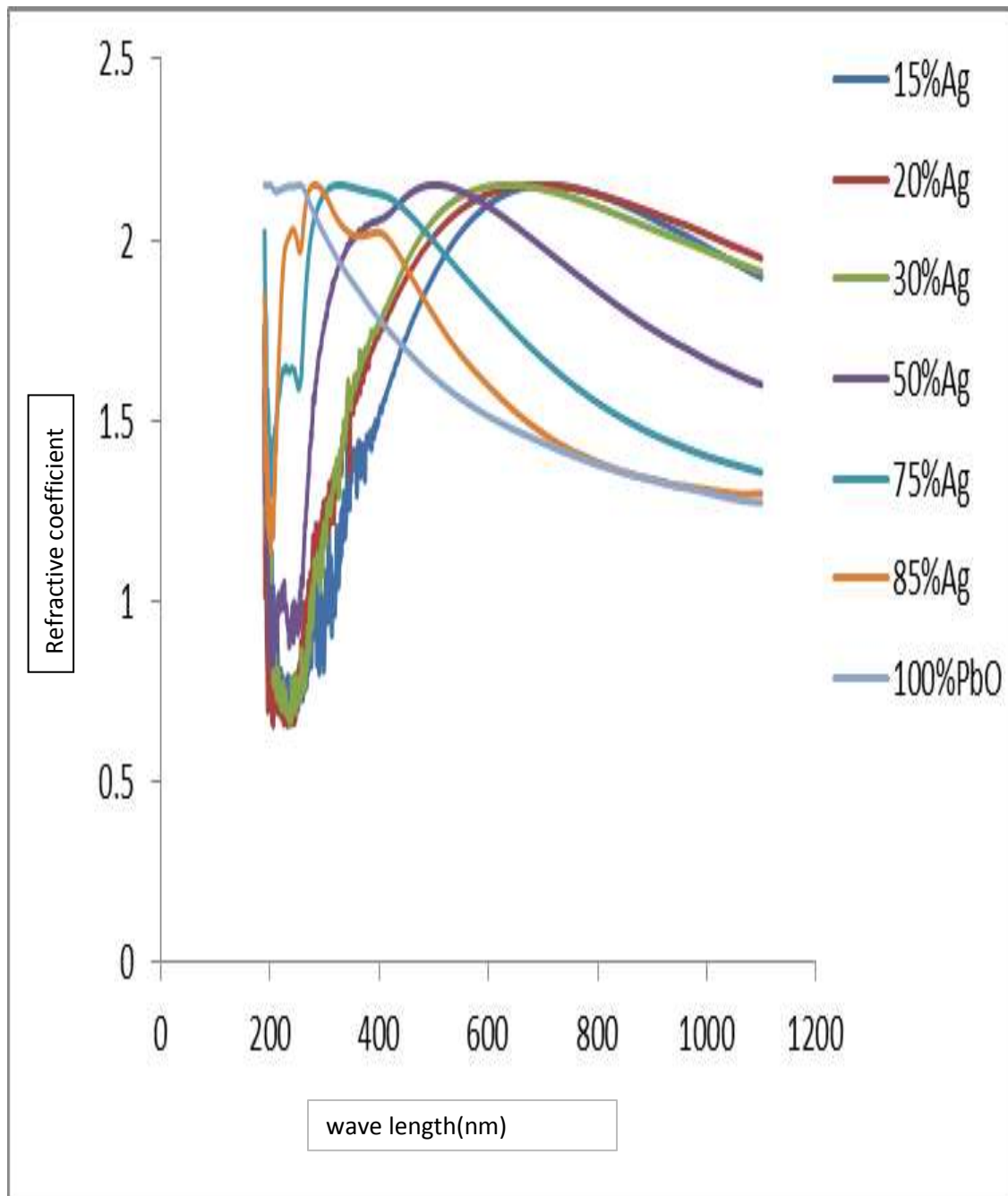


Fig.4.15. Refractive Index(n) of PbOAg Nanoparticles Colloidal with Different Ag Doped Produced in Aqueous Solution of DI Water

Table 4 Allowed direct energy gap E_g (ev) for prepared thin films.

Sample	Allowed energy gap(ev)
100%PbO	3.21
PbO/ Cu 15%	3.11
PbO/ Cu 20%	3.43
PbO/ Cu 30%	3.32
PbO/ Cu 50%	3.27
PbO/ Cu 75%	2.91
PbO/ Cu 85%	3.40
PbO/ Ag15%	2.55
PbO/ Ag20%	2.63
PbO/ Ag30%	3.00
PbO/ Ag50%	3.12
PbO/ Ag75%	3.31
PbO/ Ag85%	4.00

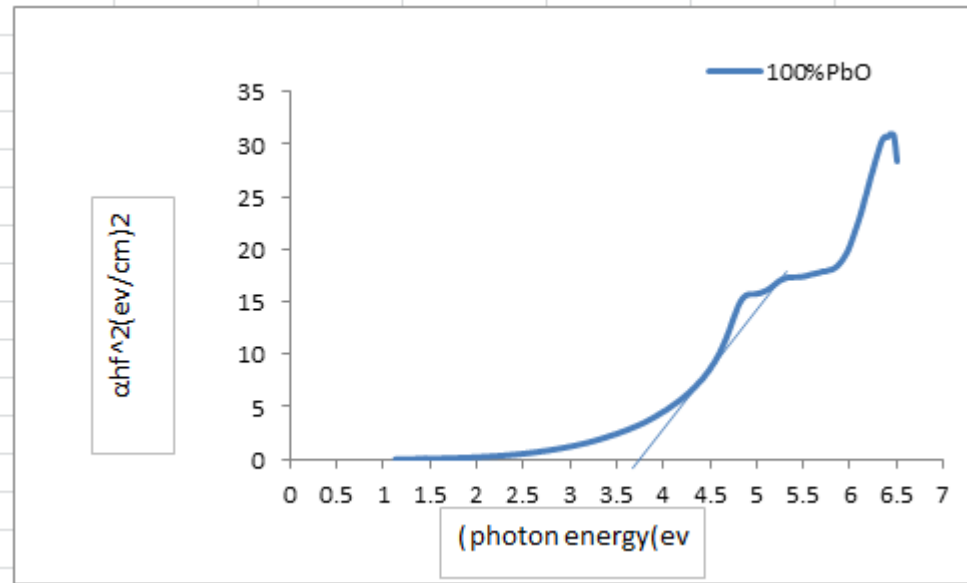


Fig.4.16.shows the allowed transition of the direct energy gap of the of 100% pbO

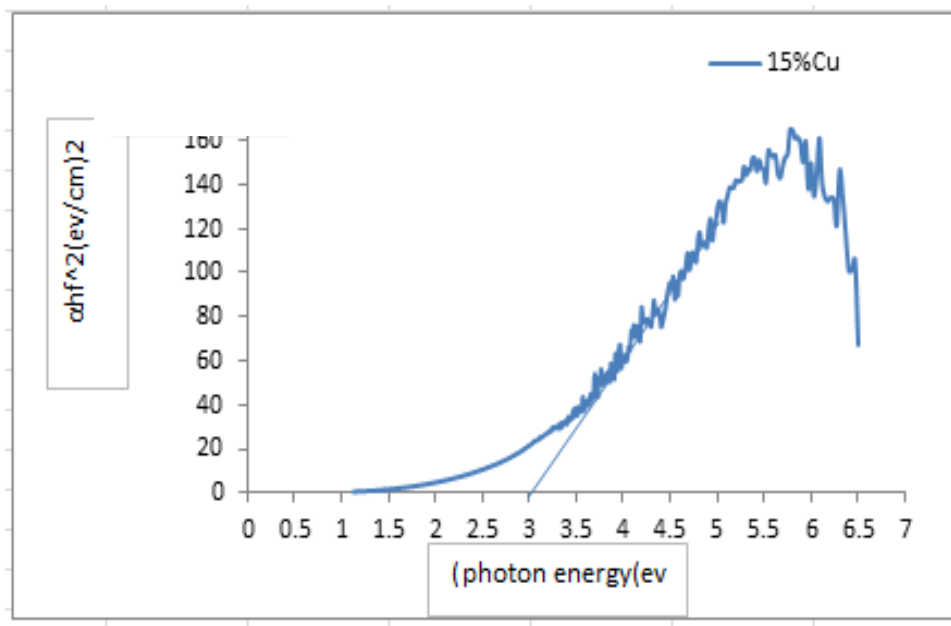


Fig.4.17.shows the allowed transition of the direct energy gap of the of 15% Cu

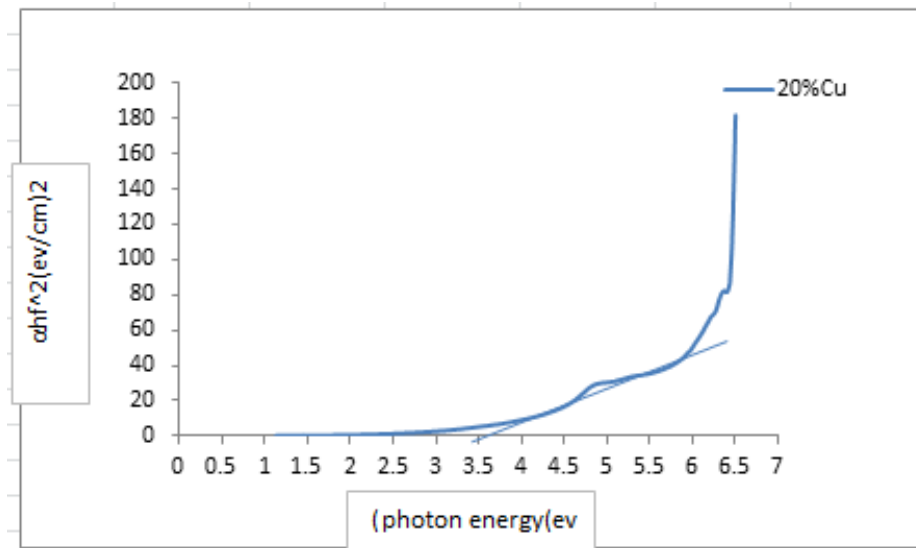


Fig.4.18.shows the allowed transition of the direct energy gap of the of 20% Cu

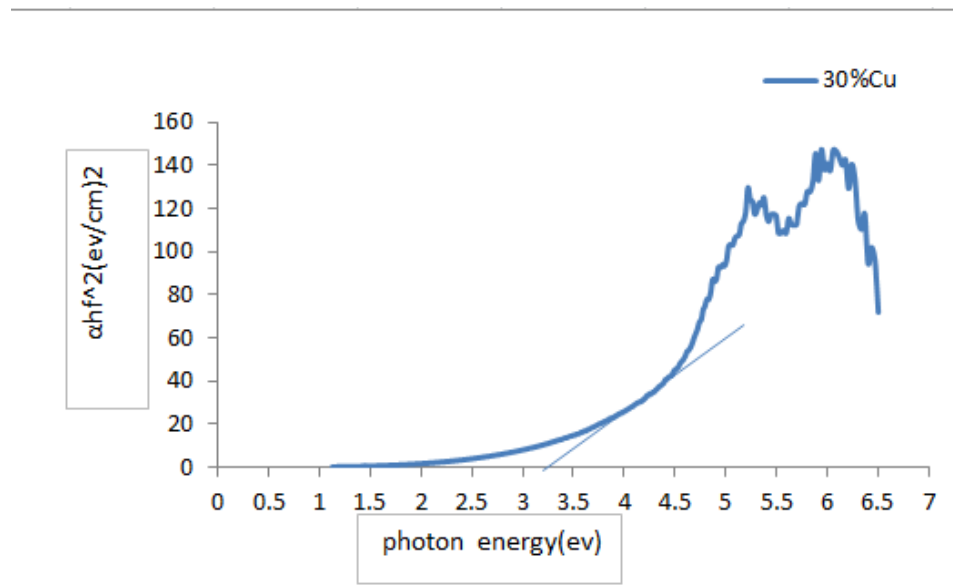


Fig.4.19.shows the allowed transition of the direct energy gap of the of 30% Cu

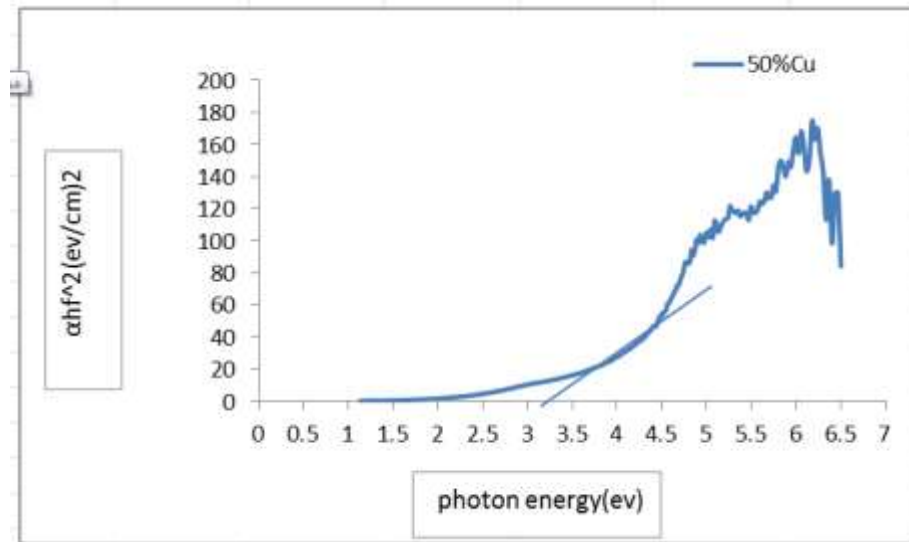


Fig.4.20.shows the allowed transition of the direct energy gap of the of 50% Cu

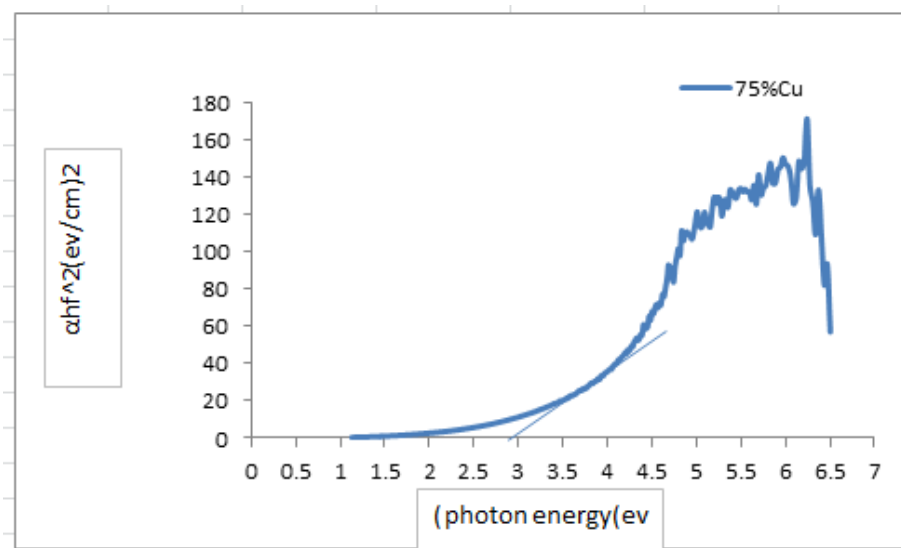


Fig.4.21.shows the allowed transition of the direct energy gap of the of 75% Cu

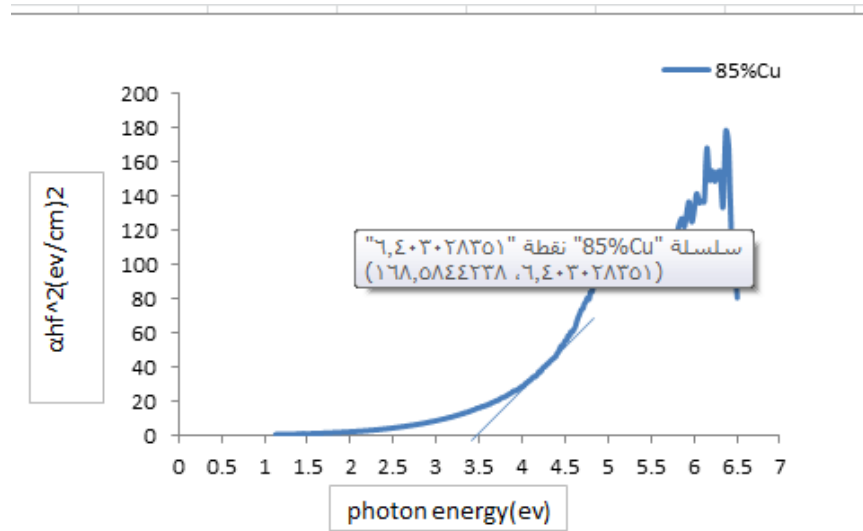


Fig.4.22.shows the allowed transition of the direct energy gap of the of 85% Cu

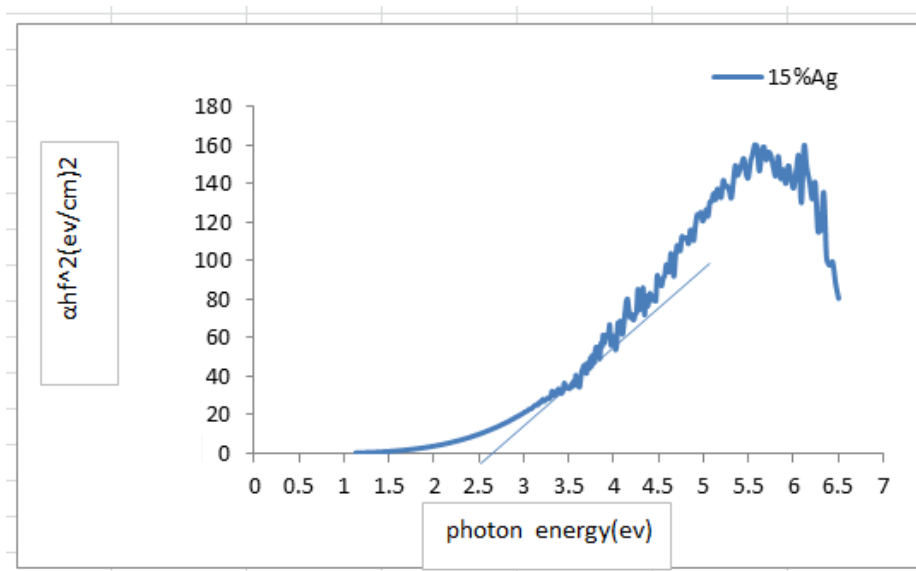


Fig.4.23.shows the allowed transition of the direct energy gap of the of 15% Ag

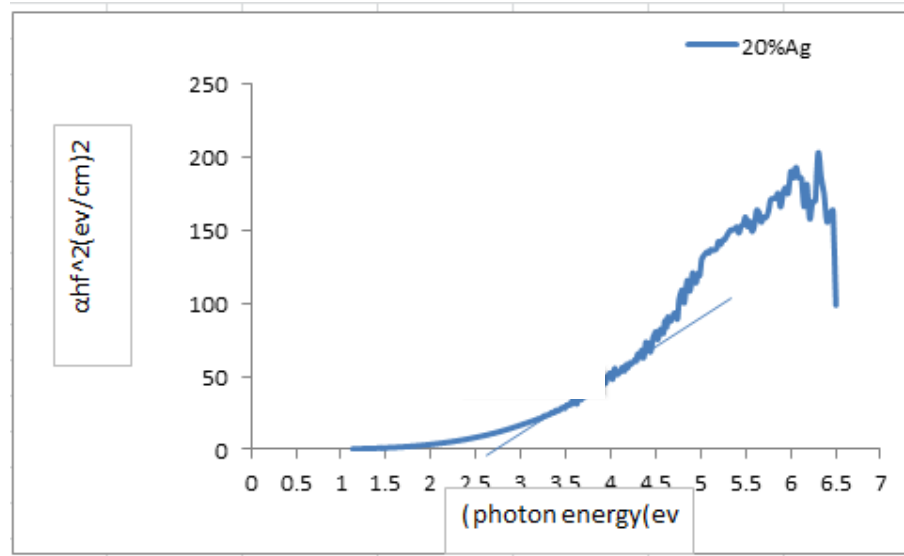


Fig.4.24.shows the allowed transition of the direct energy gap of the of 20% Ag

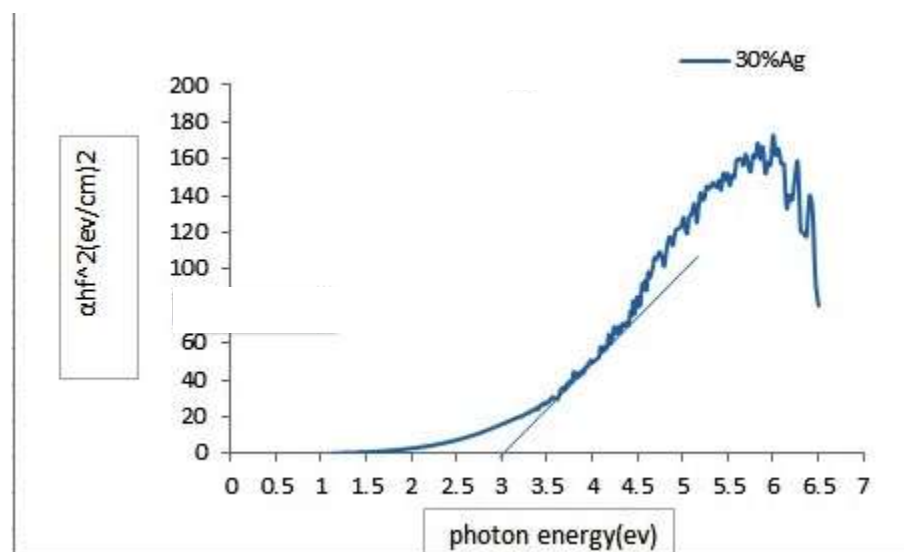


Fig.4.25.shows the allowed transition of the direct energy gap of the of 30% Ag

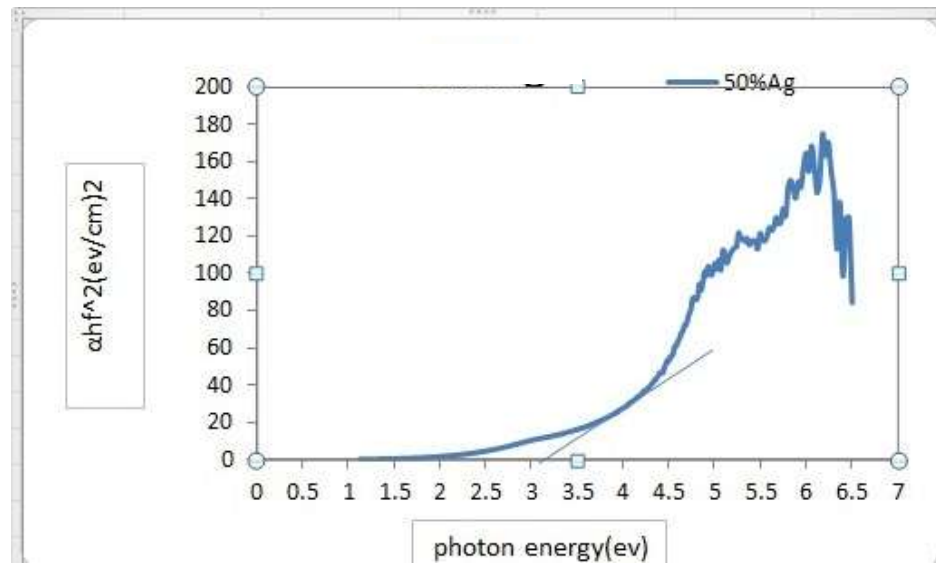


Fig.4.26.shows the allowed transition of the direct energy gap of the of 50% Ag

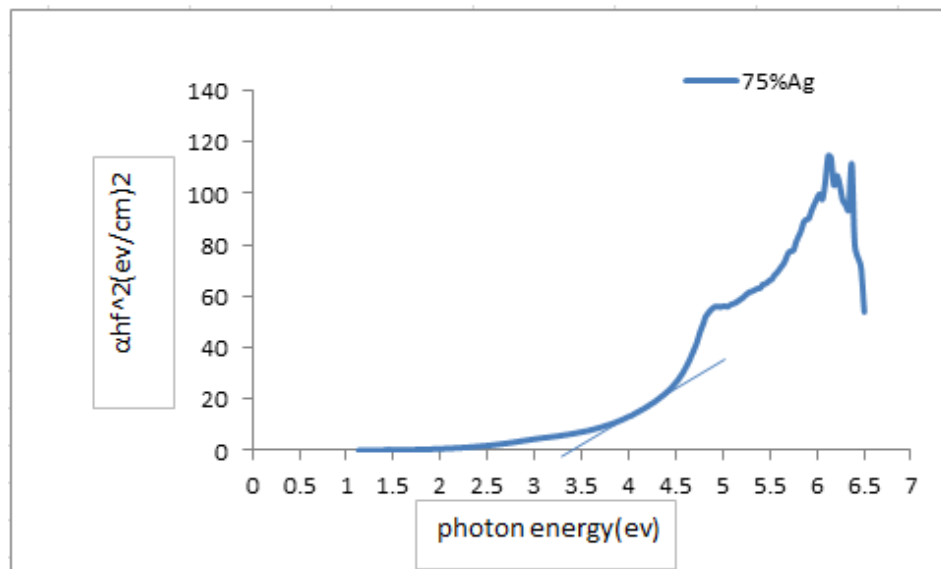


Fig.4.27.shows the allowed transition of the direct energy gap of the of 75% Ag

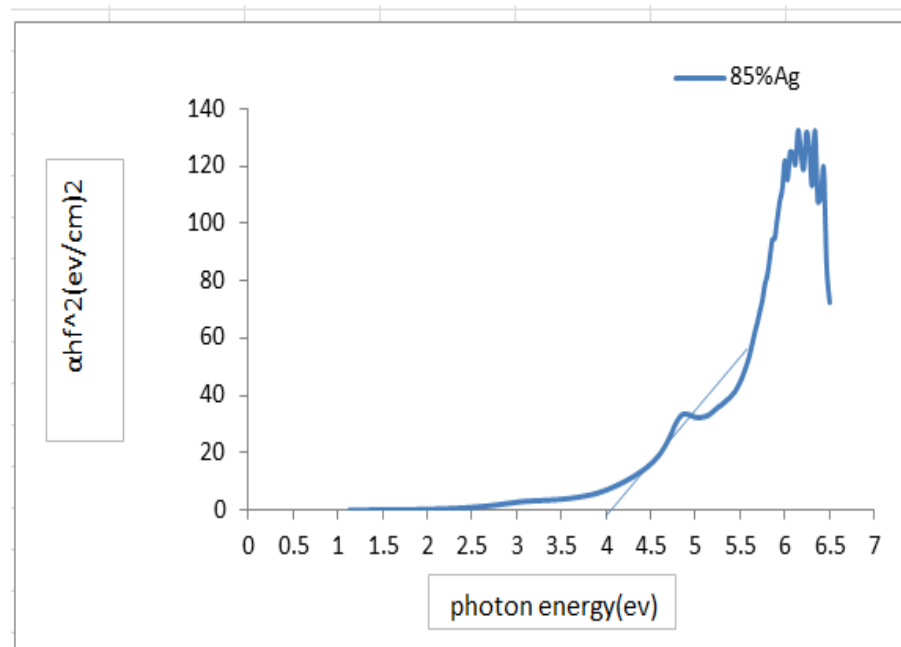


Fig.4.28.shows the allowed transition of the direct energy gap of the of 85% Ag

References

References

References:

- [1] R. Mahfouz, F. J. Cadete, S. Aires, A. Brenier, B. Jacquier and J. C. Bertolini (Synthesis and physico-chemical characteristics of nanosized particles produced by laser ablation of a nickel target in water) *Applied Surface Science* 245, 5181–5190.(2008).
- [2] P. Jain, I. El-Sayed and M. El-Sayed (Ag NPs target cancer) *Nanotoday* 2, 18-29.(2007).
- [3] D. B. Sanchez (The Surface Plasmon Resonance of Supported Noble Metal Nanoparticles: Characterization, Laser Tailoring, and SERS Application), PhD thesis, Madrid University (2007).
- [4] M. Faraday (On the Relation of Gold and Other Metals to Light) *Philos. Trans. R. Soc. London* 147, 145.(1857).
- [5] G. Mie (Beitrage zur Optik Truber Medien, Speziell Kolloidaler Metallosungen) *Ann. Phys.* 25, 377.(1908).
- [6] J. Ba (Nonaqueous Syntheses of Metal Oxide Nanoparticles and Their Assembly into Mesoporous Materials) PhD thesis, University of Potsdam (2006).
- [7] N. Taniguchi (On the Basic Concept of Nano-Technology in International Conference of Product Engineers), Japan Society of Precision Engineering (1974).
- [8] V. Kattumuri (Gold nanoparticles for biomedical applications: synthesis, characterization, in vitro and in vivo studies) PhD thesis, University of Missouri– Columbia (2006).
- [9] M. Z. Spalt (Study of formation of clusters generated by laser ablation using time-offlight mass spectrometry) Doctoral Thesis, Masaryk University (2007).
- [10] M. Raffi, F. Hussain, T. M. Bhatti, J. I. Akhter, A. Hameed and M. M. Hasan(Antibacterial Characterization of Silver Nanoparticles against E: Coli) *J. Mater. Sci. Technol.* 24,192-196. (2008).

References

- [12] H. Cui, P. Liu and G. W. Yang (Noble metal nanoparticle patterning deposition using pulsed-laser deposition in liquid for surface-enhanced Raman scattering) *applied physics letters* 89, 153124.(2006).
- [13] A. V. Kabashin, M. Meunier, C. Kingston and J. T. Luong (Fabrication and Characterization of Gold Nanoparticles by Femtosecond Laser Ablation in an Aqueous Solution of Cyclodextrins) *J. Phys. Chem.* 107, 4527-4531.(2003).
- [14] J. Prikulis, F. Svedberg and M. Kall (Optical Spectroscopy of Single Trapped Metal Nanoparticles in Solution) *Nano Letters* 4 , 115-118.(2004).
- [15] J. L. Elechiguerra, J. L. Burt, J. R. Morones, A. C. Bragado, X. Gao, H. H. Lara and M. J. Yacaman (Interaction of silver nanoparticles with HIV-1) *Journal of Nanobiotechnology* 3, 1-10.(2005).
- [16] M. Arruebo, R. F. Pacheco, M. R. Ibarra, and J. Santamaria (Magnetic nanoparticles for drug delivery) *nanotody* 2, 22-32.(2007).
- [17] S. Petersen, J. Jakobi and S. Barcikowski (In situ bioconjugation- Novel laser based approach to pure nanoparticleconjugates) *App. Surface Science* 255, 5435 5438.(2009).
- [18] S. W. Tong, C. F. Zhang, C. Y. Jiang, G. Liu, Q. D. Ling and E. T. Kan (Improvement in the hole collection of polymer solar cells by utilizing gold nanoparticle buffer layer) *Chemical Physics Letters* 453, 73–76.(2008).
- [19] A.I.Maarroof and G.B.Smith (Effective optical constants of nanostructured thin silver films and impact of an insulator coating) *Thin Solid Films* 485, 198 – 206.(2005)
- [20] M. Mishra, H. Kumar and K. Tripathi (Diabetic delayed wound healing and the role of silver nanoparticles) *Digest Journal of Nanomaterials and Biostructures* 3,49–54.(2008).

References

- [21] Tabor (Nanofluids-Science and Technology) A John Wiley & Sons, INC. Publication (1974).
- [22] Mustafa Amer Hassan (Microfabrication of a new sensorbased on silver and silicon nanomaterials, and its application to the enrichment and detection of bovine serum albumin via surface-enhanced Raman scattering) *Microchim Acta* 164, 157–160.(2012).
- [23] Khawla S. Khashan (Noble Metals on the Nanoscale: Optical and Photothermal Properties and Some Applications in Imaging, Sensing, Biology, and Medicine) American Chemical Society *Acc. Chem. Res.* 41,1578–1586.(2013).
- [24] Abduihadi Kadhim AL Ogaili, M. Burchardt, I. Zawisza, and G. Wittstock (Inkjet- Printed Thiol Self-Assembled Monolayer Structures on Gold: Quality Control and Microarray Electrode Fabrication) *Langmuir* 24, 9110-9117.(2015).
- [25] M.A.AL Hur (Preparation of Cu, Ag, Fe and Al nanoparticles by the exploding wire technique) *Proc. Indian Acad. Sci. (Chem. Sci.)*, 499–508.(2015).
- [26] Azhar A.Hassan Xia (Rapid synthesis of small Copper nanocubes by mediating polyol reduction with a trace amount of sodium sulfide or sodium hydrosulfide) *Chemical Physics Letters* 432, 491–496.(2015).
- [27] Dunia K. M. AL Nasrwy (Massspectrometric investigations of the synthesis of Lead Oxides nanoparticles via optical) *Vacuum* 82, 1088–1093.(2015).
- [28] R.Ramos Barradob (Lead oxides nanoparticles: characterization of their interesting optical properties and the mechanism of their photochemical formation) PHD Thesis, Georgia Institute of Technology (2015).

References

- [29] Raneen Imad Jibrael, S. Krishnamurthy, K. Carney, N. McEvoy and J. G. Lunney (Pulsed laser deposition of nanoparticle films of Ag) *Applied Surface Science* 254, 1303–1360.(2016).
- [30] Halah H.Rashed , Y. Jang, C. H. Kim, C. Hwang , J. Lee , S. Chae , S. Jung and M. Choi (A flame metal combustion method for production of nanoparticles) *Powder Technology* 197, 170–176.(2017).
- [31] Nawfal Y Jamil, X. Qiao, J. Chen, H. Wang, F. Tan and S. Li (A novel chemical route to prepare Ag nanoparticles) *Materials Letters* 60,1828–1832.(2018).
- [32] Noha. H.Harb (Preparation of silver nanoparticles by photo-reduction for surface-enhanced Raman scattering) *Thin Solid Films* 496,281–287.(2018).
- [33] P. Y. Lim, R. S. Liu, P. L. She, C. F. Hung and H. C. Shih(Synthesis of Ag nanospheres particles in ethylene glycol by electrochemical assisted polyol process) *Chemical Physics Letters* 420, 304–308.(2006).
- [34] M.J. Rosemary and T. Pradeep (Solvothermal synthesis of silver nanoparticles from thiolates) *Journal of Colloid and Interface Science* 268, 81–84.(2003).
- [35] H. Huang and X. Yang (Synthesis of polysaccharide-stabilized gold and silver nanoparticles: a green method) *Carbohydrate Research* 339, 2627–2631.(2004).
- [36] J. Gu, W. Fan, A. Shimojima and T. Okubo (Microwave-induced synthesis of highly dispersed gold nanoparticles within the pore channels of mesoporous silica) *Journal of Solid State Chemistry* 181, 957–963.(2008).
- [37] Y.Liu, L.Lin, W.Chiu (Size-Controlled Synthesis of Gold NPs from Bulk Gold Substrates by Sonoelectrochemical Methods)*J. Phys. Chem. B* 108 ,19237-19240.(2004).

References

- [38] H. Eerikainen and E. Kauppinen (Preparation of polymeric nanoparticles containing corticosteroid by a novel aerosol flow reactor method) *International Journal of Pharmaceutics* 263, 69–83.(2003).
- [39] Y. Itoh, M. Abdullah and K. Okuyama (Direct preparation of nonagglomerated indium tin oxide nanoparticles using various spray pyrolysis methods) *J. Mater. Res.* 19,1077-1086.(2004).
- [40] K. L. McGilvray, M. R. Decan, D. Wang and J. Scaiano (Facile photothermal synthesis of unprotected aqueous gold nanoparticles) *J. Amer. Chem. Soc.* 128,15980.(2006).
- [41] M. Duocastella, J. M. Fernandez-Pradas, J. Dominguez, P. Serra and J. L. Morenza (Printing biological solutions through laser-induced forward transfer) *Appl Phys A* 93, 941–945.(2008).
- [42] S. Y. Yang and S. G. Kim, *Powder Technol.* 146, 185–192.(2004).
- [43] N. S. Tabrizi, M. Ullmann, V. A. Vons, U. Lafont and A. Schmidt-Ott (Generation of nanoparticles by spark discharge) *J. Nanopart Res* 11, 315–332.(2009).
- [44] J. Sylvestre, A. V. Kabashin, E. Sacher, M. Meunier and J. T. Luong (Stabilization and Size Control of Gold Nanoparticles during Laser Ablation in Aqueous Cyclodextrins) *J. AM. CHEM. SOC.* 126 , 7176-7177.(2004)
- [45] A. Fojtik, and A. Henglein (Laser Ablation of Films and Suspended Particles in a Solvent - Formation of Cluster and Colloid Solutions) *Ber. Bunsen-Ges. Phys. Chem.* 97 ,252-254.(1993).
- [46] J. Zhang and C. Q. Lan (Nickel and cobalt nanoparticles produced by laser ablation of solids in organic solution) *Materials Letters* 62 ,1521–1524.(2008).
- [47] O.R. Musaev, A.E. Midgley, J.M. Wrobel and M.B. Kruger (Laser ablation of alumina in water) *Chemical Physics Letters* 487. 81–83.(2010).

References

- [48] R. Karimzadeh and N. Mansour (The effect of concentration on the thermo-optical properties of colloidal Ag nanoparticles) *Optics & Laser Technology* 42, 783-789.(2010).
- [49] S. Yang, W. Cai, H. Zhang, X. Xu, and H. Zeng (Size and Structure Control of Si Nanoparticles by Laser Ablation in Different Liquid Media and Further Centrifugation Classification) *J. Phys. Chem. C* 113,19091–19095.(2009).
- [50] N. G. Semaltianos, S. Logothetidis, W. Perrie, S. Romani, R. J. Potter, M. Sharp, G. Dearden, and K. G. Watkins (CdTe nanoparticles synthesized by laser ablation) *Applied physics letters* 95,033302.(2009).
- [51] G. Compagnini, E. Messina, O. Puglisi and V. Nicolosi (Laser synthesis of Au/Ag colloidal nano-alloys: Optical properties,structure and composition) *Applied Surface Science* 254, 1007–1011.(2007).
- [52] C. He, T. Sasaki, Y. Shimizu and N. Koshizaki (Synthesis of ZnO nanoparticles using nanosecond pulsed laser ablation in aqueous media and their self-assembly towards spindle-like ZnO aggregates) *Applied Surface Science* 254, 2196–2202.(2008).
- [53] G. X. Chen, M. H. Hong, B. Lan, Z. B. Wang, Y. F. Lu and T. C. Chong (A convenient way to prepare magnetic colloids by direct Nd:YAG laser ablation) *Applied Surface Science* 228,169–175.(2004).
- [54] M. W. Murphy, P. G. Kim, X. Zhou, J. Zhou, M. Coulliard, G. A. Botton, and T. Sham (Biaxial ZnO-ZnS Nanoribbon Heterostructures) *J. Phys. Chem.* 113, 4755–4757.(2009).
- [55] G. Compagnini, E. Messina , O. Puglisi and R. S. Cataliotti (Spectroscopic evidence of a core–shell structure in the earlier formation stages of Au–Ag nanoparticles by pulsed laser ablation in water) *Chemical Physics Letters* 457,386–390.(2008).

References

- [56] H. Usui, T. Sasaki and N. Koshizaki (Optical Transmittance of Indium Tin Oxide Nanoparticles Prepared by Laser-Induced Fragmentation in Water) *J. Phys. Chem.* 110,12890-12895.(2006).
- [57] T. Sasaki, Y. Shimizu and N. Koshizaki (Preparation of metal oxide-based nanomaterials using nanosecond pulsed laser ablation in liquids) *Journal of Photochemistry and Photobiology A: Chemistry* 182,335–341.(2006).
- [58] P. V. Kazakevich, A. V. Simakin and G. A. Shafeev (Formation of periodic structures by laser ablation of metals in liquids) *Applied Surface Science* 252 ,4457–4461.(2006).
- [59] F. Mafune, J. Kohno, Y. Takeda, T. Kondow (Formation of Stable Platinum Nanoparticles by Laser Ablation in Water) *J. Phys. Chem.* 107, 4218-4223.(2003).
- [60] P. V. Kazakevich, A.V. Simakin, V.V. Voronov and G.A. Shafeev (Laser induced synthesis of nanoparticles in liquids) *Applied Surface Science* 252, 4373–4380.(2006).
- [61] T. Tsuji , K. Iryo , Y. Nishimura and M. Tsuji (Preparation of metal colloids by a laser ablation technique in solution: influence of laser wavelength on the ablation efficiency (II)) *Journal of Photochemistry and Photobiology A: Chemistry* 145, 201–207.(2001).
- [62] S. I. Dolgaev, A. V. Simakin, V. V. Voronov, G. A. Shafeev and F. B. Verduraz (Nanoparticles produced by laser ablation of solid in liquid environment) *Applied surface science* 186, 546-551.(2002).
- [63] T. Tsuji, K. Iryo, N. Watanabe and M. Tsuji (Preparation of silver nanoparticles by laser ablation in solution: influence of laser wavelength on particle size) *Applied Surface Science* 202, 80–85.(2002).
- [64] A. V. Kabashin and M. Meunier (Synthesis of colloidal nanoparticles during femtosecond laser ablation of gold in water) *J. Appl. Phys.* 94, 7941-7943.(2003).

References

- [65] J. P. Sylvestre, S. Poulin, A. V. Kabashin and E. Sacher (Surface Chemistry of Gold Nanoparticles Produced by Laser Ablation in Aqueous Media) *J. Phys. Chem.* 108, 16864-16869.(2004).
- [66] N. V. Tarasenko, A. V. Butsen and E. A. Nevar (Laser-induced modification of metal nanoparticles formed by laser ablation technique in liquids) *Applied Surface Science* 247, 418–422.(2005).
- [67] M. Kawasaki and N. Nishimura (1064-nm laser fragmentation of thin Au and Ag flakes in acetone for highly productive pathway to stable metal nanoparticles) *Applied Surface Science* 253,2208–2216.(2006).
- [68] Y. Zhao, Y. Jiang and Y. Fang (Spectroscopy property of Ag nanoparticles) *Spectrochimica Acta Part A* 65, 1003–1006.(2006).
- [69] X.P. Zhu, T. Suzuki, T. Nakayama, H. Suematsu, W. Jiang and K. Niihara (Underwater laser ablation approach to fabricating monodisperse metallic nanoparticles) *Chemical Physics Letters* 427, 127–131. (2006).
- [70] V. Amendola, S. Polizzi, M. Meneghetti (Laser Ablation Synthesis of Gold Nanoparticles in Organic Solvents) *J. Phys. Chem.* 110 , 7232-7237.(2006).
- [71] K. Yamada, Y. Tokumoto, T. Nagata, and F. Mafune (Mechanism of Laser-induced Size-reduction of Gold Nanoparticles as Studied by Nanosecond Transient Absorption Spectroscopy) *J. Phys. Chem. B* 110, 11751-11756.(2006).
- [72] X. Zheng, W. Xu, C. Corredor, S. Xu and J. An (Laser-Induced Growth of Monodisperse Silver Nanoparticles with Tunable Surface Plasmon Resonance Properties and a Wavelength Self-Limiting Effect) *J. Phys. Chem.* 111, 14962-14967.(2007).
- [73] H. Muto, K. Yamada, K. Miyajima and F. Mafune (Estimation of Surface Oxide on Surfactant-Free Gold Nanoparticles Laser-Ablated in Water) *J. Phys. Chem.* 111, 17221-17226.(2007).

References

- [74] D. Kim and D. Jang (Synthesis of nanoparticles and suspensions by pulsed laser ablation of microparticles in liquid) *Applied Surface Science* 253, 8045–8049.(2007).
- [75] A. Giusti, E. Giorgetti, S. Laza, P. Marsili, and F. Giammanco (Multiphoton Fragmentation of PAMAM G5-Capped Gold Nanoparticles Induced by Picosecond Laser Irradiation at 532 nm) *J. Phys. Chem.* 111,14984-14991.(2007).
- [76] D. Werner, S. Hashimoto, T. Tomita, S. Matsuo, and Y. Makita (Examination of Silver Nanoparticle Fabrication by Pulsed-Laser Ablation of Flakes in Primary Alcohols) *J. Phys. Chem. C* 112,1321-132.(2008).
- [77] S. Yang, W. Cai, G. Liu, and H. Zeng (From Nanoparticles to Nanoplates:Preferential Oriented Connection of Ag Colloids during Electrophoretic Deposition) *J. Phys. Chem. C* 113, 7692–7696.(2009).
- [78] A. M. Manjon, B. N. Chichkov, and S. Barcikowski (Influence of WaterTemperature on the Hydrodynamic Diameter of silver Nanoparticles from Laser Ablation) *J. Phys. Chem. C* 114, 2499–2504.(2010).
- [79] A. Pyatenko, M. Yamaguchi, and M. Suzuki (Mechanisms of Size Reduction of Colloidal Silver and Gold Nanoparticles Irradiated by Nd:YAG Laser) *J. Phys. Chem. C* 113, 9078–9085.(2011).
- [80] S. Petersen, J. Jakobi and S. Barcikowski (In situ bioconjugation- Novel laser based approach to pure nanoparticleconjugates) *App. Surface Science* 255, 5435 5438.(2012).
- [81] K.Sivaranjani and M.Meenakshisundaram (silver nanoparticles using ocimum basillicum le af extract and their antimicrobial activity)issn 2230 –8407.(2013).

References

- [82] C. Liu (A study of particle generation during laser ablation with applications) Doctoral Thesis, University of California, Berkeley, 1-189.(2005).
- [83] Q. Xia and S. Y. Chou (Applications of excimer laser in nanofabrication) *Appl Phys A* 98, 9–59.(2010).
- [84] L. V. Zhigilei, Z. Lin and D. S. Ivanov (Atomistic Modeling of Short Pulse Laser Ablation of Metals: Connections between Melting, Spallation, and Phase Explosion) *J.Phys. Chem. C* 113, 11892–11906.(2009).
- [85] T. Ctvrtnickova, L. Cabalin, J. Laserna, V. Kanicky and G. Nicolas (Laser ablation of powdered samples and analysis by means of laser-induced breakdown spectroscopy) *Applied Surface Science* 255, 5329–5333.(2009).
- [86] K. Gouriet, M. Sentis and T. E. Itina (Molecular Dynamics Study of Nanoparticle Evaporation and Condensation in a Gas) *J. Phys. Chem. C* 113,18462–18467.(2009).
- [87] Y. T. Li, J. Zhang, H. Teng, K. Li, X. Y. Peng, Z. Jin, X. Lu, Z. Y. Zheng, and Q. Z. Yu (Blast waves produced by interactions of femtosecond laser pulses with water)*PHYSICAL REVIEW E* 67, 056403(2003).
- [88] P. Veluchamy, M. Sharon, M. Shimizu, H. Minoura, *J. Electroanal. Chem.* **365**, 179, (1994).
- [89] S. Ghasemi, M.F. Mousavi, M. Shamsipur, H. Karami, *Ultrason. Sonochem.* **15**, 448, (2008).
- [90] L. Zhang, F. Guo, X. Liu, J. Cui, Y.T. Qian, *J. Cryst. Growth.* **280**, 575 (2005).
- [91] T. B. Light, J. M. Eldridge, J. W. Matthews, J. H. Greiner, *J. Appl. Phys.* **46**, 1489 (1975).

References

- [92] Y. Pauleau, E. Harry, *J. Vac. Sci. Technol. A.* **14**, 2006 (1996).
- [93] M. Baleva, V. Tuncheva, *J. Mater. Sci. Lett.* **13**, 4 (1994).
- [94] L. D. Madsen, *J. Am. Ceram. Soc.* **81**, 988 (1998).
- [95] Z. Liping, F. Guo, X. Liu, J. Cui, Y. Qian, *J. Cryst. Growth.* **280**, 575 (2005).
- [96] L. C. Courrol, F. R. Silva and L. Gomesc (A simple method to synthesize silver nanoparticles by photo-reduction) *Colloids and Surfaces A: Physicochem. Eng. Aspects* 305, 54–57.(2007).
- [97] G. Compagnini, A. A. Scalisi and O. Puglisi (Synthesis of gold colloids by laser ablation in thiol-alkane solutions) *J. Mater. Res.* 19, 2795-2798.(2004).
- [98] R. Holm, *Electrical Contacts - Theory and applications*, Springer, 4th Ed., 2000.
- [99] P.G. Slade, ed., *Electrical Contacts: Principles and Applications*, CRC Press, (1999)
- [100] N. Talijan, V. Čosović, J. Stajić-Trošić, A.Grujić, D. Živković, E. Romhanji, J. *Min. Metall. Sect. B-Metall.* 43 (2) B (2007) 171-176.
- [101] A. Haes (Localized Surface Plasmon Resonance Spectroscopy for Fundamental Studies of Nanoparticle Optics and Applications to Biosensors) Doctoral thesis, Northwestern University (2004).
- [102] R. L. Lee (Mie theory, Airy theory, and the natural rainbow) *Applied Optics* 37 1506,1519.(1998)
- [103] D. Werner, S. Hashimoto, T. Tomita, S. Matsuo, and Y. Makita (In-Situ Spectroscopic Measurements of Laser Ablation-Induced Splitting

References

- and Agglomeration of Metal Nanoparticles in Solution) *J. Phys. Chem. C* 112, 16801–16808.(2008)
- [104] F. Mafune, J. Kohno, Y. Takeda and T. Kondow (Dissociation and Aggregation of Ag Nanoparticles under Laser Irradiation) *J. Phys. Chem.* 105 , 9050-9056.(2001).
- [105] S. Link, C. Burda, B. Nikoobakht, and M. A. El-Sayed (Laser-Induced Shape Changes of Colloidal Gold Nanorods Using Femtosecond and Nanosecond Laser Pulses) *J. Phys. Chem. B* 104, 6152-6163.(2000).
- [106] M. H. Mahdih, M. Nikbakht, Z. E. Moghadam and M. Sobhani (Crater geometry characterization of Al targets irradiated by single pulse and pulse trains of Nd:YAG laser in ambient air and water) *Applied Surface Science* 256,1778–1783.(2010).
- [107] C. Liang, T. Sasaki, Y. Shimizu and N. Koshizaki (Pulsed-laser ablation of Mg in liquids: surfactant-directing nanoparticle assembly for magnesium hydroxide nanostructure) *Chemical Physics Letters* 389 , 58–63.(2004).
- [108] Jacobsson ,T. J. and Edvinsson ,T., "Absorption and fluorescence spectroscopy of growing ZnO quantum dots: Size and band gap correlation and evidence of mobile trap states" *Inorg. Chem*, 50(19): 9578–9586 (2011).
- [109] Chaudhuri,R. G. and Paria, S., "Core/shell nanoparticles: Classes, properties, synthesis mechanisms, characterization, and applications", *Chem. Rev*, 112(4) : 2373 (2012).
- [110] Mahanti, M. and Basak, D., "Highly enhanced UV emission due to surface plasmon resonance in Ag–ZnO nanorods," *Chem.Phys. Lett*, 542(4): 110–116 (2012).
- [111] Amendola, V. and Meneghetti, M., "What controls the composition and the structure of nanomaterials generated by laser ablation in liquid solution" *Phys. Chem. Chem. Phys*, 15(9): 3027–3046 (2013).

References

- [112] Haider, A. J. , Shaker, S .S. and Asma H.M." A study of morphological, optical and gas sensing properties for pure and Ag doped SnO₂ prepared by pulsed laser deposition (PLD) "*Energy Procedia*, 36:776–787(2013).
- [113] Zeng, H. B., Du, X. W. Singh, S. C. et al., “Nanomaterials via laser ablation/irradiation in liquid: A review,” *Adv. Funct. Mater*, 22(7): 1333–1353 (2012).
- [114].X. Wang, Y.M. Lu, D.Z. Shen, Z.Z. Zhang, B.H. Li, B. Yao, J.Y. Zhang, D.X. Zhao, X.W. Fan, Growth and photoluminescence for undoped and N-doped ZnO grown on 6H-SiC substrate, *J. Lumin.* 122–123 (2007) 165–167.
- [115].Morales AE, Zaldivar MH, Pal U (2006) Indium doping in nanostructured ZnO through low-temperature hydrothermal process. *Opt Mater* 29(1):100–104
- [116].Wander A, Schedin F, Steadman P, Norris A, McGrath R, Turner TS, Thornton G, Harrison NM (2001) Stability of polar oxide surfaces. *Phys Rev Lett* 86(17):3811
- [117] Y.-S. Cho, Y.-D. Huh, C.R. Park, Y.R. Do, Preparation with laser ablation and photoluminescence of Y₃Al₅O₁₂: Ce nanophosphors, *Electron. Mater. Lett.* 10 (2014) 461–465.
- [118]. T. Donnelly, S. Krishnamurthy, K. Carney, N. McEvoy and J. G. Lunney (Pulsed laser deposition of nanoparticle films of Au) *Applied Surface Science* 254, 1303–1360.(2007).
- [119].lorenz.lorenz T, Shimizu Y, Koshizaki N (2006)
Preparation of metal oxidebased

References

nanomaterials using nanosecond pulsed laser ablation in liquids. *J Photochem Photobiol A: Chem* 182:335

[120]. Khashan K S, Sulaiman G M and Mahdi R 2017 Preparation of iron oxide nanoparticles-decorated carbon nanotube using laser ablation in liquid and their antimicrobial activity *Artificial Cells Nanomedicine and Biotechnology* pp 1-11

الخلاصة:-

تم تحضير غرواني متجانس يتكون من PbO / Cu و PbO / Ag تقنية تدرية الليزر النبضية (PLAL) ، من خلال تحضير مخاليط $Pb: Cu$ و $Pb: Ag$ بتركيز مختلف (15،20،30،50،75 و 85 wt.%). تم الضغط على المساحيق الناتجة كحبيبات ذات أبعاد (6) استخدمت أهدافاً. الليزر النبضي ND-YAG ذي الطول الموجي (1064) ومدة النبضة 6 نترات في حالة 300 نبضة مرتبطة بالطاقة 400J. وتعرضت المساحيق الناتجة عن PbO / Cu و PbO / Ag لتقنيات XRD و UV-vis لدراسة كل من الهيكلية والبصرية تم استخدام تقنيات TEM و SEM لدراسة حجم وشكل ومورفولوجيا المساحيق المعدة. تم العثور على زيادة الامتصاصية واتخاذ أقصى القيم في الطول الموجي (220-230) نانومتر بسبب صدى Plasmon السطح من كل الغروية. تم العثور على قمم الامتصاصية تميل إلى التحول الأحمر بالقرب من منطقة الأشعة تحت الحمراء. بالإضافة إلى ذلك ، زاد عرض معامل الانقراض والقيمة المحسنة مع زيادة تركيز المنشطات لكل من Cu و Ag أيضاً. تعاني فجوة الطاقة من بعض الانخفاضات ووصلت إلى (32.91 فولت) مقابل 75% بالوزن من النحاس مع PbO و (2.63ev) مقابل 20 wt.% Ag مع PbO



جمهورية العراق
وزارة التعليم العالي والبحث العلمي
جامعة بغداد
كلية التربية للعلوم الصرفة / ابن الهيثم
قسم الفيزياء

المزايا التركيبية والبصرية للمواد النانوية PbO/Cu

وPbO/Ag

رسالة مقدمة الى مجلس كلية التربية-ابن الهيثم-جامعة بغداد

وهي جزء من متطلبات نيل شهادة الماجستير في الفيزياء

من قبل

محمد احمد كريم

بكلوريوس / جامعة بغداد (2016)

بأشراف

أ.م.د رغد صبحي الخفاجي